NUREG/CR-3228
MEA-2051
Vol. 2

Structural Integrity of Water Reactor Pressure Boundary Components

Annual Report for 1983

Edited by F. J. Loss

Materials Engineering Associates, Inc.

Prepared for
U.S. Nuclear Regulatory Commission

GPO Printed copy price: $5.50

NUREG/CR-3228
MEA-2051
Vol. 2
RF, R5

Structural Integrity of Water Reactor Pressure Boundary Components

Annual Report for 1983

Manuscript Completed: August 1984
Date Published: September 1984

Edited by
F. J. Loss

Materials Engineering Associates, Inc.
9700-B George Palmer Highway
Lanham, MD 20706

Prepared for
Division of Engineering Technology
Office of Nuclear Regulatory Research
U.S. Nuclear Regulatory Commission
Washington, D.C. 20555
NRC FIN B8900

ABSTRACT

The objective of this research program is to characterize materials behavior in relation to structural safety and reliability of pressure boundary components for light water reactors. Specific objectives include developing an understanding of elastic-plastic fracture and environmentally-assisted crack propagation phenomena in terms of continuum mechanics, metallurgical variables, and neutron irradiation. Emphasis is placed on identifying metallurgical factors responsible for radiation embrittlement of steels and on developing procedures for embrittlement relief, including guidelines for radiation-resistant steels. The underlying goal is the interpretation of material properties performance to establish engineering criteria for structural reliability and long-term operation. Current work is organized into three major tasks: (1) fracture mechanics investigations, (2) environmentally-assisted crack growth in high temperature, primary reactor water and (3) radiation sensitivity and postirradiation properties recovery. Research progress in these tasks for 1983 is summarized here.

The work is being performed by Materials Engineering Associates, Inc., under the direction of F. J. Loss. NRC funding is provided by the Office of Nuclear Regulatory Research, Materials Engineering Branch, M. Vagins, project manager.

CONTENTS

LIST OF FIGURES

LIST OF TABLES

SUMMARY

1.0 FRACTURE MECHANICS INVESTIGATIONS

1.1 Fracture Toughness Characterization of Irradiated, Low Upper Shelf Welds

With irradiation, the A 533 and A 508 submerged-arc weld deposits (made with Linde 80 flux) in certain U. S. commercial reactor pressure vessels are expected to exhibit a low upper shelf behavior, that is, a Charpy-V Notch (C_v) energy below 68 J (50 ft-lb). In connection with Generic Safety Issue A-11 on Reactor Vessel Materials Toughness, it was necessary to characterize the elastic-plastic fracture toughness of these steels. Seven weld deposits representative of those contained in some U. S. reactor vessels were irradiated to fluences up to 1.5×10^{19} n/cm^2 E > 1 MeV in the Heavy Section Steel Technology (HSST) Program. The J-R curve behavior of these materials has been investigated in the current program in which four different size specimens were used: 0.5T-, 0.8T-, 1.6T- and 4T-CT. This data base will be used in conjunction with safety analyses of reactor pressure vessels in terms of the tearing instability concept of Paris.

The majority of the tests were conducted at an upper shelf temperature of 200°C. These data show that J_{Ic} is reduced by ~ 23% with irradiation whereas a larger change (~ 53%) is exhibited by the average value of the tearing modulus, T_{avg}. A modest size effect was observed for the unirradiated condition, where larger specimen size resulted in higher J-R curve level. The J-R curves exhibit decreasing level with increasing temperature, in contrast to C_v upper shelf behavior which generally is invariant with temperature.

These results generally confirm a previous correlation by the authors of J_{Ic} and T_{avg} with the C_v upper shelf energy. These correlations provide added structural significance to the results of C_v specimens from reactor surveillance programs. Additionally, the J-R curve data have been expressed in terms of a plot of J vs. T. This formulation provides a direct correspondence with the data required for a tearing instability analysis.

1.2 Piping Fracture Mechanics Data Base

To facilitate integrity analyses of nuclear plant piping systems, a computerized fracture toughness data base from typical constituent materials is being established for the NRC. Data collected from other researchers, plus new data developed by MEA, will provide the basis for the data base.

Initial testing of an A 106-C pipe material shows that the L-R orientation is tougher than the C-R orientation. Each orientation shows variations in J-R curve level with temperature, with the lowest R curves observed at 232°C.

1.3 Elastic-Plastic Fracture Toughness Characterization of HSST Intermediate Test Vessel Material

The elastic-plastic fracture toughness (J-R curve) of A 533-B plate and A 508-2 forging from HSST intermediate pressure vessel materials

was characterized. The data are applicable to performing a tearing instability analysis on the failure of three specific vessels: V1, V7 and V7A. Two compact tension specimen orientations, ASTM E 399 designation CL and CR, were used to characterize the material behavior in the directions of crack propagation in the vessels. Properties were essentially uniform with respect to specimen location and orientation. The mean initiation toughness (J_{Ic}) was greater than 190 kJ/m^2 for both materials and the tearing modulus was above 150.

1.4 HSST 4th Irradiation Program

The objective of the HSST 4th Irradiation Program is to statistically characterize the elastic-plastic fracture toughness of welds representative of current commercial welding practice. The materials being investigated include four A 533-B welds; the HSST 02 plate material was included for reference. All materials contain relatively low, but varying, amounts of copper and nickel. Specimen testing is being performed jointly by MEA and ORNL to establish a basis for interlaboratory comparisons.

A direct connection between the copper and nickel content and the level of irradiation damage has been observed. When both copper and nickel were reduced below 0.04 and 0.13 wt-percent, respectively, the material became irradiation insensitive with regard to both temperature shift of the brittle-to-ductile transition and lowering of upper shelf toughness. The upper shelf level, however, was essentially insensitive for all of these materials. This is believed to result from the relatively low copper/nickel percentage contained in even the HSST 02 plate material which had the greatest amount of both elements, 0.14% copper and 0.67% nickel.

The fracture toughness data obtained to date indicate the possibility of a change in shape of the brittle-to-ductile transition curve occurring with irradiation-induced shifts to higher temperature. At present, it appears the transition curve rises less sharply as the curve is shifted to higher and higher temperatures. This observation is tentative and requires support from additional testing.

2.0 ENVIRONMENTALLY-ASSISTED CRACK GROWTH IN LWR MATERIALS

2.1 Temperature Dependence of Fatigue Crack Growth in Irradiated A 508 Forging

During the previous year, results of fatigue crack growth rates for A 508-2 steel in LWR environments as a function of temperature (93°C to 288°C) were published. This year growth rates for irradiated specimens of the same heat of steel were determined over the range of 200°C to 288°C. Growth rates are highest at 288°C, but the rates are still on or below the ASME Section XI reference lines for all the temperatures. These growth rates compare almost exactly with those for the unirradiated specimens tested over this temperature range. This behavior indicates that irradiation does not affect the growth rates and suggests that the temperature/environment micromechanistic reactions are the same for both the unirradiated and irradiated materials.

2.2 Influence of Sulfur Content on Fatigue Crack Growth

A series of tests was conducted to determine the effect of sulfur composition on the fatigue growth rates of pressure vessel steels. This program was carried out with four steels having sulfur compositions ranging from 0.004% to 0.025%. The specimens were of the same design and were precracked in the same way. Since the tests were conducted simultaneously in a multispecimen autoclave, the water chemistry and loading history of all the specimens were the same and the results can be compared directly. The growth rates increase as the sulfur content of the steels increases, although there is an apparent saturation of this effect at about 0.013% S.

2.3 Fatigue Crack Growth in A 351-CF8A Cast Stainless Steel

A project to determine the temperature dependence of fatigue crack growth rates of A 351-CF8A stainless steel was completed. A significant environmental contribution was defined. Fractographic research on these steels showed that the fatigue fracture morphology was ve y similar to that from stress corrosion cracking tests on these materials. The basic characteristics are a very brittle-appearing surface, with a variety of well-defined striation forms: brittle striations on fan-shaped facets at low ΔK values, ductile striations on fan-shaped facets at intermediate ΔK values, and fully ductile striations at higher ΔK values.

2.4 Fatigue Crack Growth in Low-Carbon Piping Steels

Fatigue crack growth rates in low-carbon piping steels have been determined over a large temperature range. There appears to be virtually no orientation dependence for the heat of A 106 steel which was tested at a load ratio of 0.2, but there is a measurable decrease in growth rates in going from 288°C to 338°C. Additional tests are being conducted at higher load ratios. A study of fatigue crack growth rates in A 516 steel showed a measurable orientation dependence. A study of fractography and manganese sulfide inclusion morphology shows that the inclusions play a significant role in crack growth behavior.

3.0 RADIATION SENSITIVITY AND POSTIRRADIATION PROPERTIES RECOVERY

3.1 Assessment of Postirradiation Heat Treatment As a Method for Alleviating Radiation-Induced Embrittlement

A series of capsule irradiations were performed to explore the general reembrittlement path which follows 399°C postirradiation annealing of steels and the potential for weld-to-weld variability in reirradiation sensitivity. Materials employed were two high copper, high nickel content submerged-arc welds made with the same lot of filler wire, but with different welding flux types (Linde 80 and Linde 0091). Charpy-V (C_V) specimen sets of each weld were irradiated at 288°C, annealed at 399°C for 168 hours, and reirradiated at 288°C to a total reirradiation (IAR) fluence of 1.0×10^{19} n/cm^2, E > 1 MeV. Reirradiation properties were established at fluence intervals of about

0.25×10^{19} n/cm^2 and are compared to properties of the as-irradiated (I) condition established at 1.0, 1.5 and 2.0×10^{19} n/cm^2. Fracture toughness properties for I vs. IAR conditions at a fluence of 1.5×10^{19} n/cm^2 were also established, using 0.5T-CT specimens.

Relatively rapid reembrittlement of the welds after annealing was observed. A fluence of only 0.25×10^{19} n/cm^2 mitigated a large portion of the annealing benefit. However, the reembrittlement level observed for a reirradiation fluence of 0.75×10^{19} n/cm^2 (total fluence of 1.75×10^{19} n/cm^2) was not more than the reembrittlement level induced by the first cycle of irradiation to 1.0×10^{19} n/cm^2. Data trends for one weld (Linde 80 flux) are suggestive of an embrittlement plateau, which if verified, could have a major impact on annealing decisions. Other differences in weld behavior, attributable to welding flux type, were not observed.

An exploratory assessment of 399°C vs. 454°C heat treatment benefits is also reported.

3.2 Impurity Element-Alloy Element Interactions in Radiation Embrittlement Sensitivity

A series of laboratory melts of A 302-B and A 533-B steels with statistical variations in impurity element and alloying element contents are being irradiated at 288°C to study composition interactions in radiation sensitivity development. Radiation sensitivity is judged from relative change in notch ductility produced by a fluence of $\sim 2 \times 10^{19}$ n/cm^2.

In 1983, A 533-B plates depicting variations in copper, phosphorus, tin and arsenic content were evaluated. Data comparisons revealed that the phosphorus contribution to radiation sensitivity is heavily dependent on copper content. The detrimental effect of increasing phosphorus level (from 0.003 to 0.025% P) is greatest when the copper content is low. The inverse dependence explains why recent computer treatments of irradiation data banks (predominantly high copper steels) failed to identify a phosphorus effect. More importantly, the experimental findings show a clear need for including of a phosphorus term in radiation embrittlement projection equations when applied to the newer (improved, low copper) steels.

Other comparisons suggest that the level of the phosphorus contribution is not dependent on nickel content. A relationship between arsenic content and apparent radiation sensitivity was not observed. However, a possible dependence of C_v upper shelf retention on tin content was indicated by some data sets.

3.3 Studies of Neutron Exposure Rate Effects on Reactor Vessel Steels

The significance of high vs. low neutron exposure rates to the magnitude of mechanical property change produced by a given fluence at 288°C is being investigated experimentally. The tests are designed to resolve the base issue of the level of representation afforded by test reactor irradiation assessments of materials to the power reactor

service case. The approach involves the exposure of four reference materials (two plates, two welds) produced commercially to fluxes of 7-8 x 10^{10}, 4-5 x 10^{11}, and 7-8 x 10^{12} n/cm^2-sec^{-1} and to fluences as high as 2 x 10^{19} n/cm^2. Facilities in a water-cooled test reactor (UBR) were selected for the irraditions because of the high degree of control possible over specimen exposure conditions.

Four experimental assemblies, each containing C_v, fatigue precracked C_v, tensile and compact tension specimens, were loaded into the reactor early in 1983. Irradiations were still in progress at years end. The exposure to one assembly was approximately 75% complete at that time. Three assemblies depicting intermediate flux tests, are located in facilities at the edge of the fuel lattice; the fourth assembly for low flux testing, is being irradiated in a reflector facility. Initial test results in qualification of dose rate effects are expected in early 1985.

3.4 Mechanical Properties Determinations for PSF Simulated Surveillance and Through-Wall Specimen Capsules

The Light Water Reactor Pressure Vessel Surveillance Dosimetry Improvement Program of the Nuclear Regulatory Commission (NRC) has irradiated mechanical property test specimens of several steels in a pressure vessel wall/thermal shield mock-up facility. The investigation is part of a broad NRC effort to develop key neutron physics-dosimetry-metallurgy correlations for making highly accurate projections of radiation-induced embrittlement to reactor vessels. The steels studied represent a wide range of radiation embrittlement sensitivities and included plates, forgings and submerged-arc weld deposits (two each). MEA was assigned the development and analysis of mechanical properties data for the materials, including notch ductility, fracture toughness and tensile strength assessments.

Specimens irradiated at 288°C by ORNL in five capsules in simulated surveillance and through-wall locations were tested. The postirradiation toughness gradient between vessel surface and midwall locations, indexed to the C_v 41 J temperature, was found to be small (31°C or less) for five of the six materials investigated. Simulated surveillance capsule irradiations reproduced reasonably well the embrittlement at vessel inner surface and quarter-wall thickness positions. The exception to both trends was provided by a 0.23% Cu, 1.58% Ni weld deposit.

Fracture toughness data, corrected for lack of test specimen constraint (β_{Ic} correction) in most cases described a 100 MPa$\sqrt{m}$ transition temperature elevation smaller than the C_v 41 J temperature elevation. The adjustment of the ASME lower bound K_{IR} toughness curve by the irradiation-induced elevation of the C_v 41 J temperature or the elevation of the CT specimen 100 MPa$\sqrt{m}$ temperature, was conservative when compared against static toughness measurements.

STRUCTURAL INTEGRITY OF WATER REACTOR PRESSURE BOUNDARY COMPONENTS ANNUAL REPORT FOR 1983

1.0 FRACTURE MECHANICS INVESTIGATIONS

1.1 Fracture Toughness Characterization of Irradiated, Low Upper Shelf Welds

A. L. Hiser, Jr., F. J. Loss and B. H. Menke

1.1.1 Background

Previous studies have shown that, after irradiation, steels used in the beltline region of commercial, light water reactor pressure vessels can show both a significant increase in the temperature of the brittle-to-ductile transition region and a reduction in Charpy-V (C_v) upper shelf energy level. Certain A 533-B and A 508 submerged arc weld deposits containing a high copper impurity level can exhibit C_v upper shelf energy levels below 68 J (50 ft-lb). For vessels which attain such low toughness, Federal Regulations (10 CFR Part 50) require, as an option, the performance of a fracture mechanics analysis that conservatively demonstrates the existence of adequate margins of safety for continued operation. In the upper shelf region, the vessel material is assumed to exhibit elastic-plastic behavior so that a linear elastic fracture mechanics approach is inappropriate. The question of what is a suitable approach is addressed through Generic Safety Issue A-11 on Reactor Vessel Materials Toughness (Ref. 1). In resolving this issue, the NRC has suggested that under elastic-plastic conditions the vessel can be properly evaluated in terms of the tearing instability concept of Paris and others (Ref. 2). This concept is being verified through intermediate vessel tests at Oak Ridge National Laboratory (ORNL) under the Heavy Section Steel Technology (HSST) Program.

The fracture toughness property required for a tearing instability analysis is the J-R curve. The NRC is therefore establishing a data base of J-R curve trends for irradiated pressure vessel steels of low upper shelf toughness. Of primary interest are A 508 and A 533-B submerged arc weld deposits made with Linde 80 flux and containing a high copper impurity level. The high sensitivity to irradiation associated with the copper impurity, coupled with a low preirradiation toughness associated with the Linde 80 flux, can result in a low upper shelf behavior. Seven welds (61W-67W) of this type were irradiated in the HSST Program. All of the welds are essentially identical to those in operating plants in which the material may exhibit a low upper shelf behavior. Experimental capsules containing compact toughness (CT) specimens of several sizes (e.g., 0.5T-, 0.8T-, 1.6T-, and 4T-CT) as well as C_v and tensile specimens were irradiated to fluence levels of 0.6 to 1.5 x 10^{19} n/cm^2 E > 1 MeV to produce C_v upper shelf levels of 58 to 80 J (40 to 60 ft-lb). The J-R curve characterization of these welds was undertaken by the Naval Research Laboratory (NRL); this work was subsequently transferred to Materials Engineering

Associates (MEA) where the program was completed. A more detailed discussion of this program can be found in the NUREG report summarizing the findings (Ref. 3).

1.1.2 Materials and Irradiations

Seven submerged-arc welds were tested as a part of this program. Weld code 61W, provided by Westinghouse Corporation, was composed of A 533-B base metal which was welded with Linde 80 flux, while weld codes 62W-67W, supplied by Babcock & Wilcox, were composed of A 508 base metal welded with Linde 80 flux. These welds were made from single lots of weld wire, except for weld code 62W which was made using two weld wire lots.

Irradiation of the specimens was conducted by ORNL under the Second and Third HSST 4T-CT Irradiation Series at the Bulk Shielding Reactor (BSR). The target fast-neutron fluence was ~ 1 x 10^{19} n/cm^2 (E > 1 MeV) at a nominal irradiation temperature of 288°C (550°F). Temperature control of the capsules was concentrated on the 4T-CT specimens, and as a result the temperatures of the other specimens had greater deviations from 288°C. These specimens also received a fluence which typically differed from that of the 4T-CT specimens.

All C_v and tensile specimen testing was conducted by ORNL. An example C_v curve is illustrated in Fig. 1.1. This figure shows the flat C_v upper shelf which typically characterizes these materials. The upper shelf levels ranged from 76 to 108 J for the unirradiated condition, and from 58 to 80 J for the irradiated condition.

1.1.3 J-R Curve Results

To assure ductile upper shelf behavior from these materials, tests of the irradiated specimens were conducted predominantly at temperatures of 200°C and 288°C. Additionally, the unirradiated tests were conducted at various temperatures on the Charpy energy upper shelf. As a result, only one test failed by fast fracture (cleavage micromode).

Several of these specimens had non-uniform precracks, probably due to residual stresses associated with the welds. These precracks do violate the crack-front straightness requirements of Reference 4.

To facilitate comparison of results from different size specimens, tests were conducted under similar conditions for different size specimens of each weld code; with the irradiated specimens, attempts were made to match irradiation conditions (fluence and irradiation temperature) for the specimens to be compared. In this section, the J-R curves are viewed with the intent of identifying any bias due to specimen size.

Since the CT specimens were of an ASTM E 399 type design (in terms of pin hole spacing) with only slightly modified notches, all of the specimens had to be remachined to allow placement of razor edges (for mounting of the clip gages) on the load line. Because of the small size of the 0.5T- and 0.8T-CT specimens, these specimens could not be

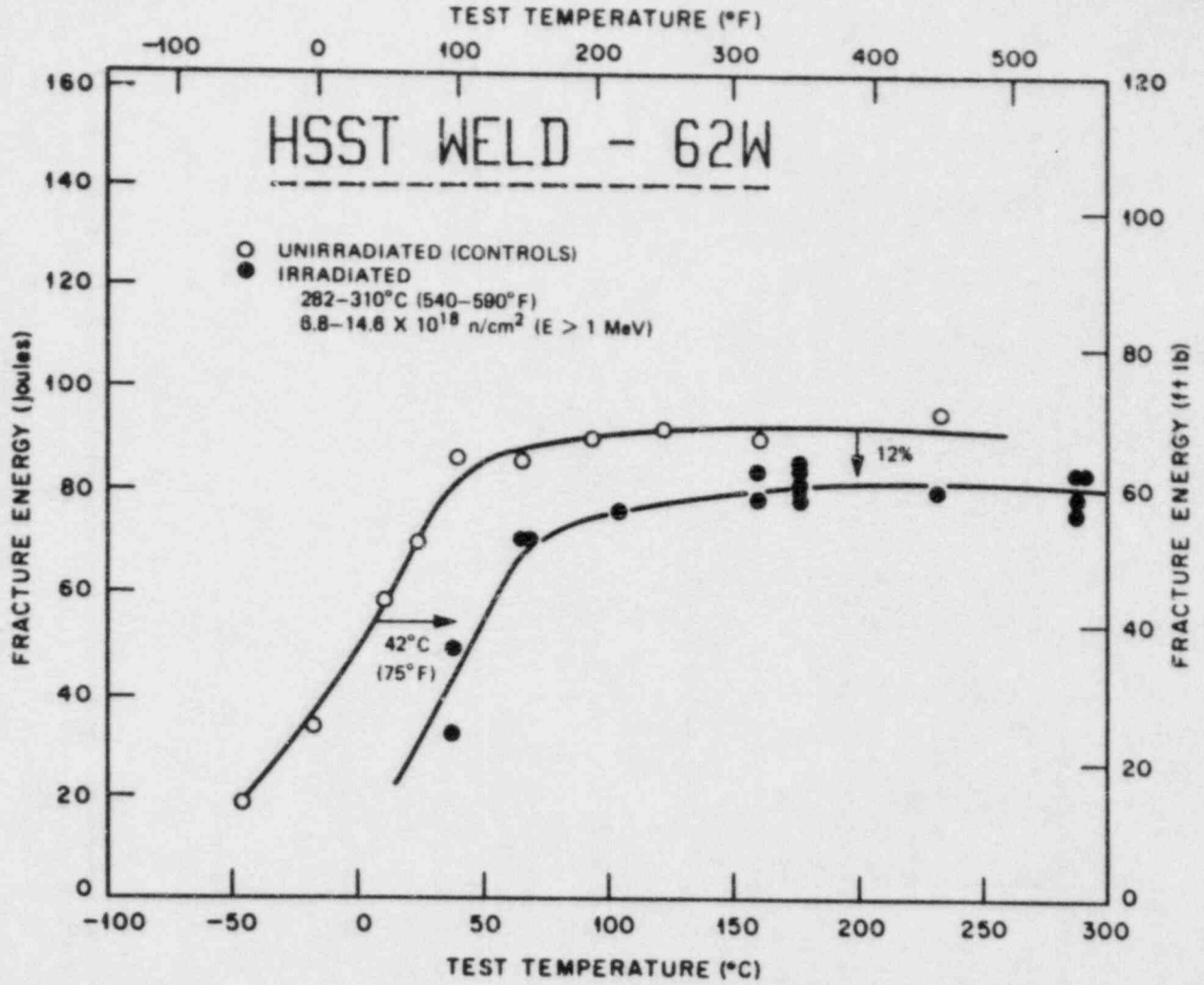

Figure 1.1 Variations of Charpy energy with temperature for HSST weld 61W (ORNL data).

modified in this way. Instead, two clip gages were used in testing these specimens, one at the crack mouth (for compliance determinations) and the other on the load line at the specimen outer surfaces (for J determinations). This procedure, termed the "double clip gage technique," was validated through a multilaboratory round robin (Ref. 5).

1.1.3.1 Results at 200°C

A summary of the 4T-CT results at 200°C is presented in Fig. 1.2. One would expect approximate "layering" according to C_v upper shelf energy (C_v USE); this behavior is not observed for the unirradiated data, as 62W (only at a median level of 93 J) has the highest J-R curve level, while the highest C_v energy material (65W at 108 J) has virtually the lowest J-R curve. Data scatter associated with weld metals, combined with the relatively small C_v USE range, probably masks this correspondence. With the irradiated 4T-CT J-R curves (Fig. 1.2 bottom), excellent agreement between C_v USE and J-R curve level is seen. Duplicate tests here are for welds 61W, 64W and 67W. On average, J_{Ic} (the initiation value of J) decreased by 31% and T_{avg} (the average value of tearing modulus) decreased by 59% due to irradiation, indicating that T_{avg} is a more sensitive indicator of irradiation degradation for these materials.

With the unirradiated 0.5T-CT R-curves (Fig. 1.3 top), many of the data lie below the trend band established for the unirradiated 4T-CT data. Both T_{avg} and J_{Ic} are ~ 26% lower than the 4T-CT values on average, indicating a possible size effect. However, the irradiated 0.5T-CT data lie well within the irradiated 4T-CT data (Fig. 1.3 bottom). The lone exception is the J-R curve from a 61W specimen with only 10% side grooves (insufficient to induce straight crack growth), which probably would have been within the band if it had been grooved by 20%, since crack tunneling is typically associated with higher J-R curves. On average, the irradiated 0.5T-CT data have J_{Ic} values 13% higher and T_{avg} values 13% lower than the corresponding 4T-CT averages.

Table 1.1 summarizes the average values (for all seven welds) of J_{Ic} and T_{avg} at 200°C for each condition. In general for J_{Ic}, no size dependence is observed for either the unirradiated or the irradiated conditions. However, T_{avg} shows a trend of increasing value with increasing specimen size for both conditions. This observation takes into account the several irradiated 0.5T-CT and 0.8T-CT specimens with 10% side grooves, yielding artificially high T_{avg} and J_{Ic} values. The size dependence is more noticable for the unirradiated condition (T_{avg} 27% lower for the 0.5T-CT specimens as compared to the 4T-CT specimens) than for the irradiated condition (T_{avg} 11% lower for the 0.5T-CT specimens).

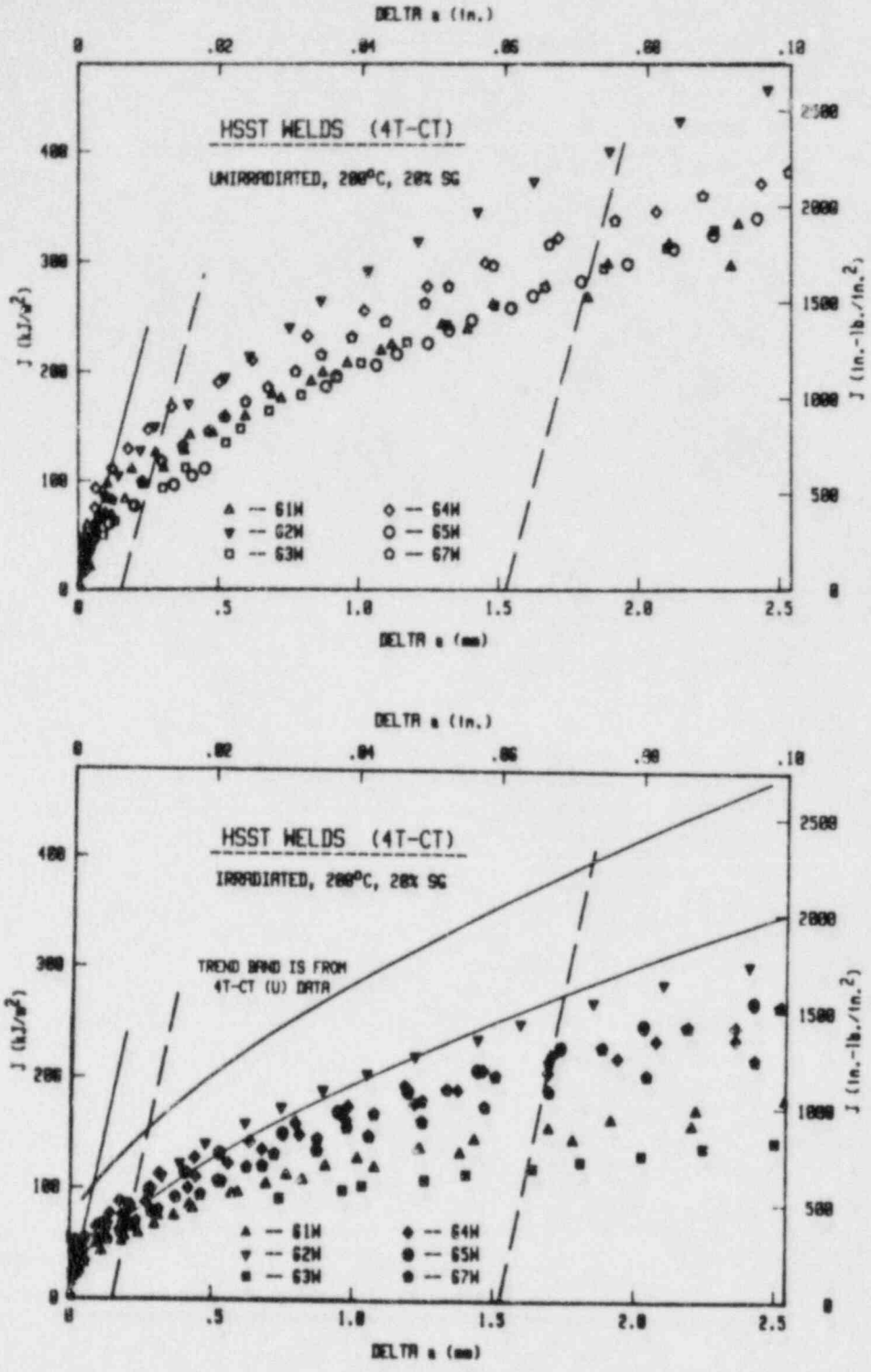

Figure 1.2 A comparison of the 4T-CT J-R curves developed at 200°C, illustrating unirradiated data (top) and irradiated data (bottom).

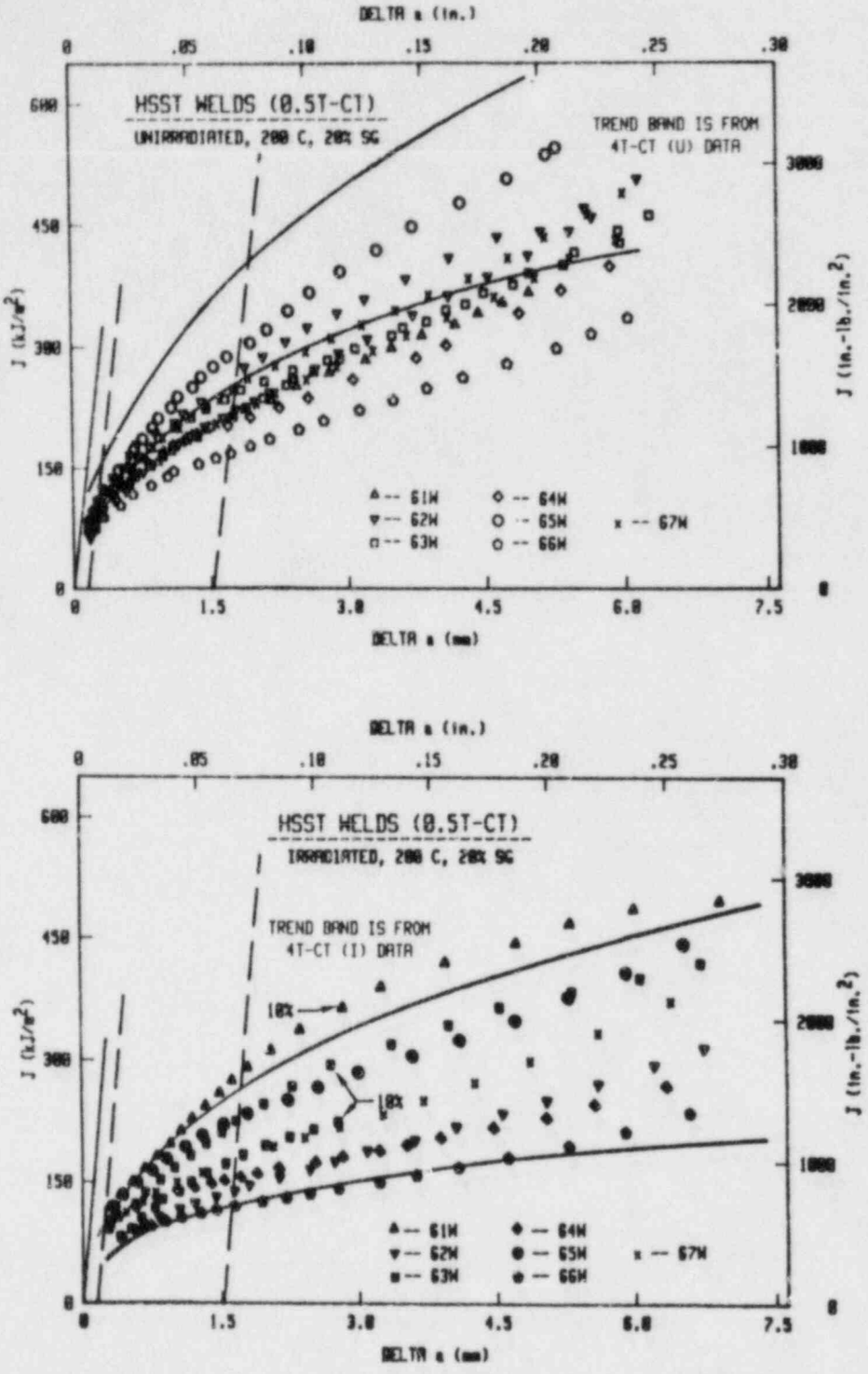

Figure 1.3 The full J-R curves for the 0.5T-CT specimens at 200°C. The trend bands illustrated are from the 4T-CT data of Fig. 1.2.

Table 1.1. Average Values at 200°C

	J_{Ic} (kJ/m^2)		T_{avg}	
	U	I	U	I
4T	115	77	96	40
1.6T	94	73	85	39
0.8T	120	87	71	37
0.5T	96	86	70	36

1.1.3.2 Results at 288°C

Fewer tests were conducted at 288°C than at 200°C. In addition, no irradiated 4T- or 1.6T-CT specimens were tested at this temperature. Due to a problem with the load-line clip gage, the irradiated 0.5T- and 0.8T-CT tests were conducted using the crack-mouth clip gage only. Displacements recorded by this gage were corrected to approximate load-line values by the factor 0.740 for calculation of area under the load-displacement curve (Ref. 5).

Five unirradiated 4T-CT tests were conducted at 288°C (Fig. 1.4). No irradiated 4T-CT tests were conducted at this temperature. Both J_{Ic} and T_{avg} decreased by ~ 17% on average between 200°C and 288°C. In fact, these R-curves have dropped to the point that J_{Ic} and dJ/da are only ~ 10% greater than their counterparts from the irradiated results at 200°C.

A summary of the J-R curves from the 0.5T-CT specimens tested at 288°C is given in Fig. 1.5. The average values of J_{Ic} and T_{avg} are the lowest of any of the specimen sizes at this temperature for the unirradiated condition. For the irradiated 0.5T-CT results, the average J_{Ic} value is ~ 19% greater than the 0.8T-CT average value, with T_{avg} ~ 17% higher. With 0.5T-CT specimens, the decreases due to irradiation are ~ 23% for J_{Ic} and ~ 59% for T_{avg}.

Average values of J_{Ic} and T_{avg} are listed in Table 1.2 for each specimen size. For the unirradiated data, J_{Ic} shows a slight increase with increasing size. A similar trend is exhibited by T_{avg}, except for the 1.6T-CT average value which is slightly greater than the 4T-CT average value. With the irradiated data, both J_{Ic} and T_{avg} are somewhat higher for the 0.5T-CT specimens than for the 0.8T-CT specimens.

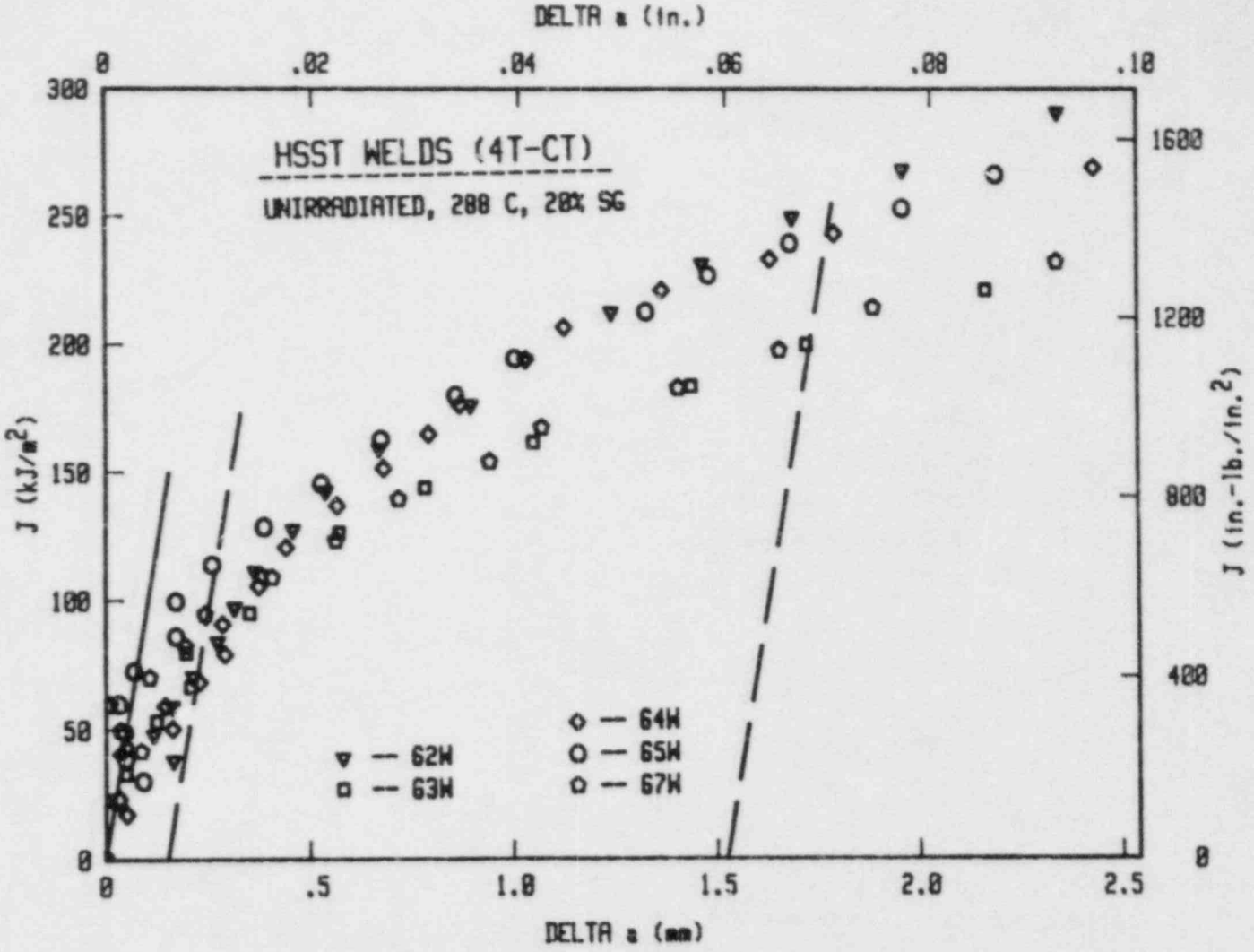

Figure 1.4 Unirradiated 4T-CT J-R curves at 288°C.

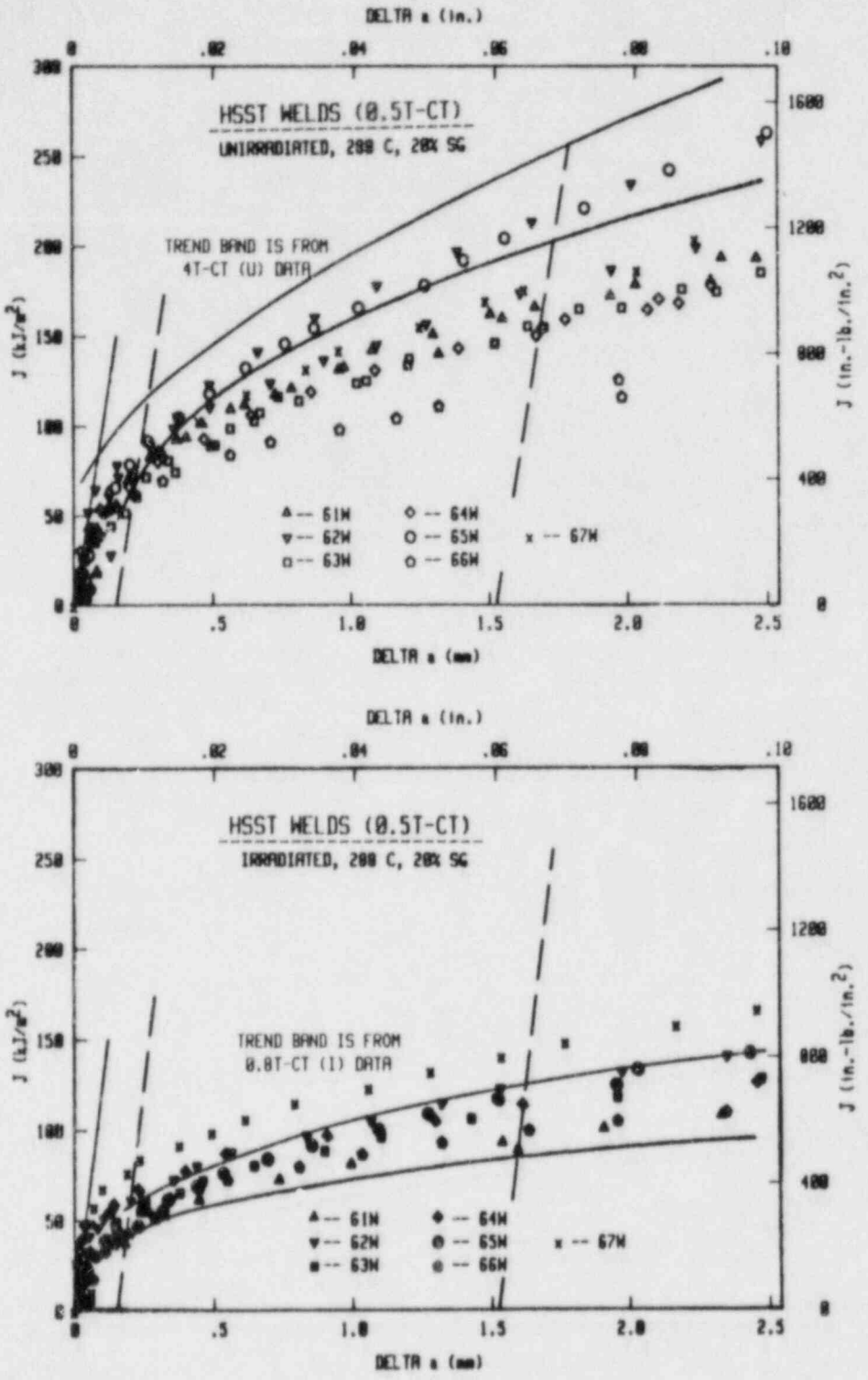

Figure 1.5 The 0.5T-CT J-R curves at 288°C.

Table 1.2. Average Values at 288°C

	J_{Ic} (kJ/m^2)		T_{avg}	
	U	I	U	I
4T	87	--	70	--
1.6T	75	--	74	--
0.8T	74	48	54	18
0.5T	74	57	51	21

1.1.3.3 Effects of Irradiation and Temperature

The degrading effect of irradiation on the fracture resistance of steels has long been established. From Table 1.3, the average decrease in J_{Ic} due to irradiation varies from ~ 24% at 200°C to ~ 31% at 288°C, while the decrease in T_{avg} is approximately double, from ~ 52% at 200°C to ~ 68% at 288°C. As for the effect of temperature, the Charpy-V upper shelf is often characterized with a horizontal line, i.e., the C_v USE does not vary with temperature. However, the J-R curve parameters, J_{Ic} and T_{avg}, typically show an inverse relationship with temperature on the upper shelf.

Table 1.3. Decrease in J_{Ic} and T_{avg} Due to Irradiation

	J_{Ic} (kJ/m^2)			T_{avg}		
	U	I	% Decrease	U	I	% Decrease
200°C	106	81	24	81	38	53
288°C	79	53	33	62	20	68

Clear examples of the effect of temperature on the J-R curve are given in Fig. 1.6. The top graph shows 0.5T-CT data from weld code 61W, over a range of temperatures from 75°C to 288°C. Duplicate tests at 288°C are shown, with little scatter evident. As depicted, the level of the R-curve decreases with increasing temperature. The decrease in both J_{Ic} and T_{avg} is ~ 50%. The same effect of decreasing J-R curve with increasing temperature is seen for irradiated 0.5T-CT specimens from weld code 64W (Fig. 1.6 bottom). Here the range of temperature is one-half of that for the unirradiated 0.5T-CT data from weld 61W, but still T_{avg} decreases by ~ 50% and J_{Ic} by ~ 42%.

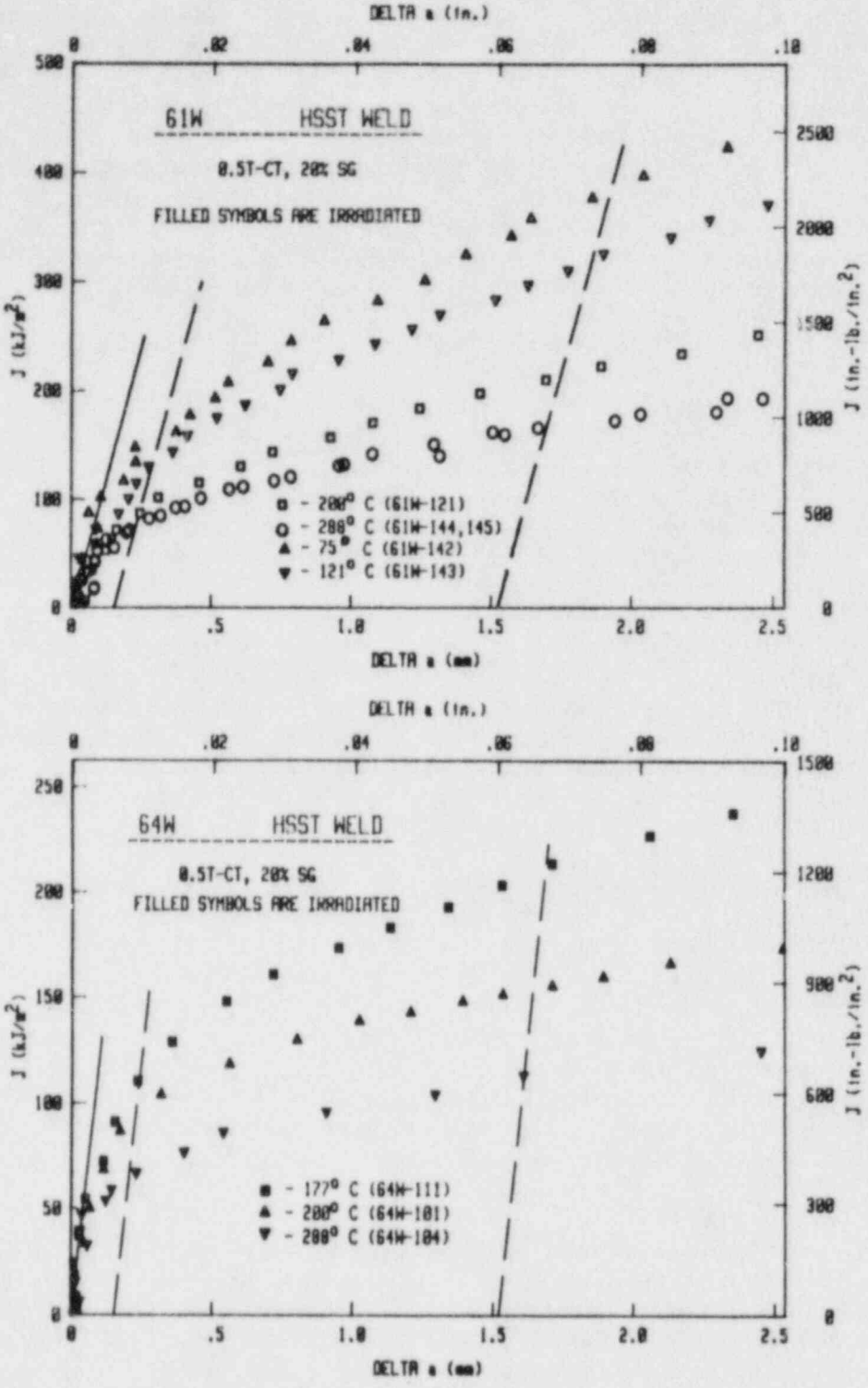

Figure 1.6 Effect of temperature on J-R curves. Data are from 61W unirradiated 0.5T-CT specimens (top) and from 64W irradiated 0.5T-CT specimens (bottom).

A typical summary of J_{Ic} and T_{avg} vs. temperature behavior is shown in Fig. 1.7 for weld code 62W. As shown, J_{Ic} and T_{avg} decrease linearly with temperature for both irradiated and unirradiated conditions, even up to 288°C. An apparent size effect in this material is seen for both conditions in Fig. 1.7 (bottom), where the T_{avg} data for the 0.5T-CT and 0.8T-CT specimens lie almost exclusively below the trend lines, while the 4T- and 1.6T-CT data lie above the least-square trend lines. The effect of irradiation is much easier to discern with the T_{avg} comparison than the J_{Ic} comparison; with the latter, some of the unirradiated data fall below irradiated data. T_{avg} is therefore seen to be a more discriminating indicator of irradiation effects.

1.1.4 Tearing Instability Concept

Within the ductile upper shelf, crack growth in a test specimen or a structure is often characterized by ductile tearing (dimpled rupture mechanisms on a microscale), which proceeds only under rising load. Under certain conditions this stable growth can become unstable, in what is called a tearing instability. The latter can be as catastrophic as a cleavage instability if the structure cannot bring the unstable crack growth under control.

An example of the effect of temperature on the J-T curves is seen in Fig. 1.8. These are the same J-R curves shown in Fig. 1.6 (top). As expected, the inverse relationship of the J-R curve with temperature translates to higher J-T curves at lower temperatures. The individual points on each curve were evaluated as indicated. The maximum value chosen was at 2 mm, because the power-law fit to the data typically deteriorates thereafter.

Figure 1.9 (left) represents a summary of the 4T-CT data obtained at 200°C in terms of a J-T plot. The applied loading line shown is for a flawed cylinder, with a slope of 8.8 kJ/m^2 (50 in.-lb/$in.^2$). This loading line was suggested by the NRC select committee that drafted a resolution to Generic Issue A-11 (Ref. 1). This line has been constructed with a slope that is a factor of 10 less than that expected in an actual vessel containing an axial flaw (1/4T deep) in the beltline region. The numbers in parentheses indicate the C_v upper shelf energy associated with that weld code. The general trend exhibited by these data is increasing J-T curve with increasing C_v energy.

All of the 288°C results are summarized in a J-T format in Fig. 1.9 (right). These data represent a significant decrease in level from 200°C. To illustrate the structural significance of these J-R curves, the applied J levels were computed assuming linear elastic conditions and a 1/4T semielliptic, axial surface flaw under loadings of design pressure (2500 psi) and twice design pressure (5000 psi), arrows A and B, respectively. While the latter represents a hypothetical faulted condition that may never occur, it serves to illustrate the magnitude of the pressure transient that would be required to exceed the margin of safety provided by the indicated loading line for the subject low shelf steels in the irradiated condition.

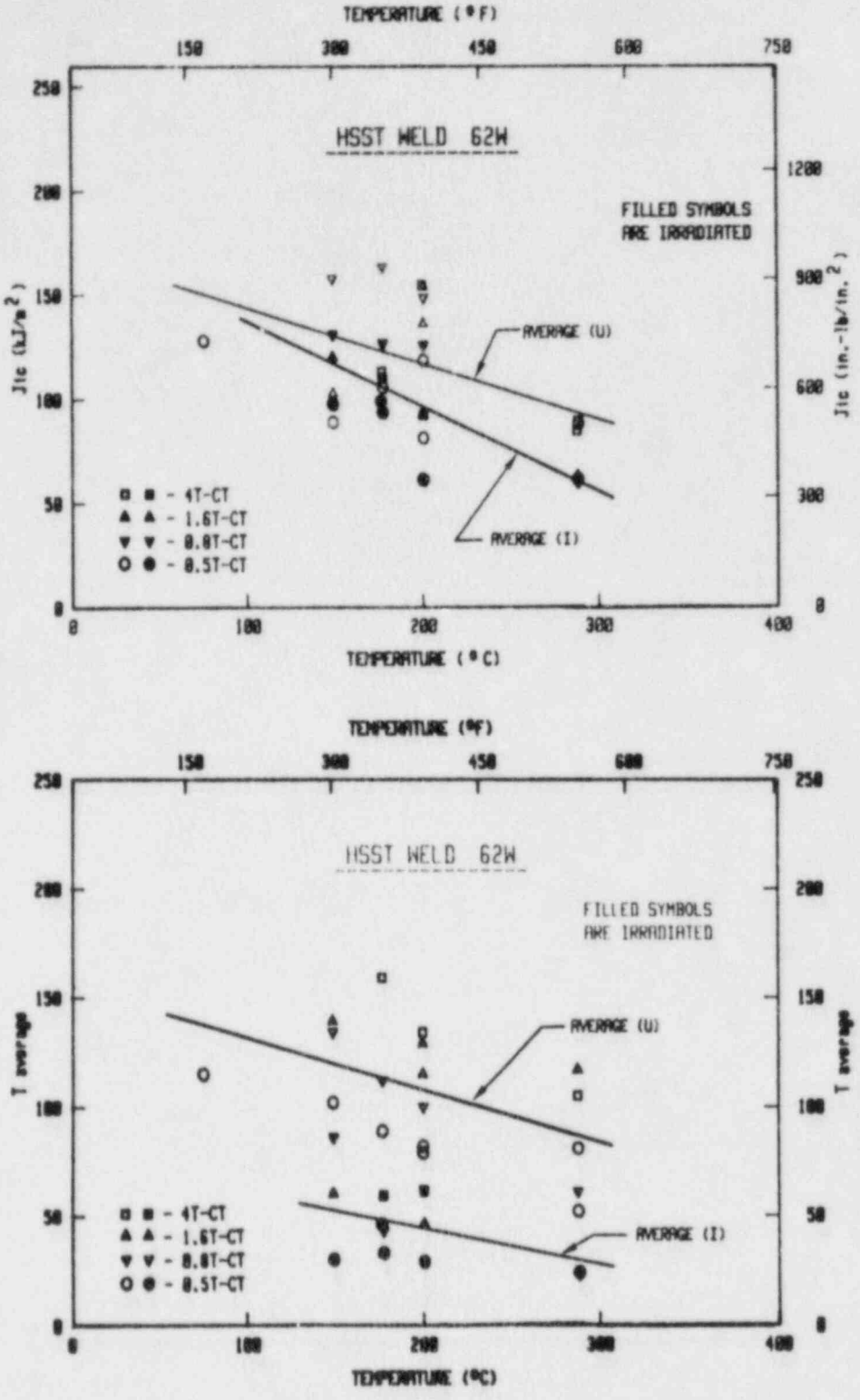

Figure 1.7 Typical variation of J_{Ic} (top) and T_{avg} (bottom) with temperature. Trend lines in each figure are from linear least square regression analysis.

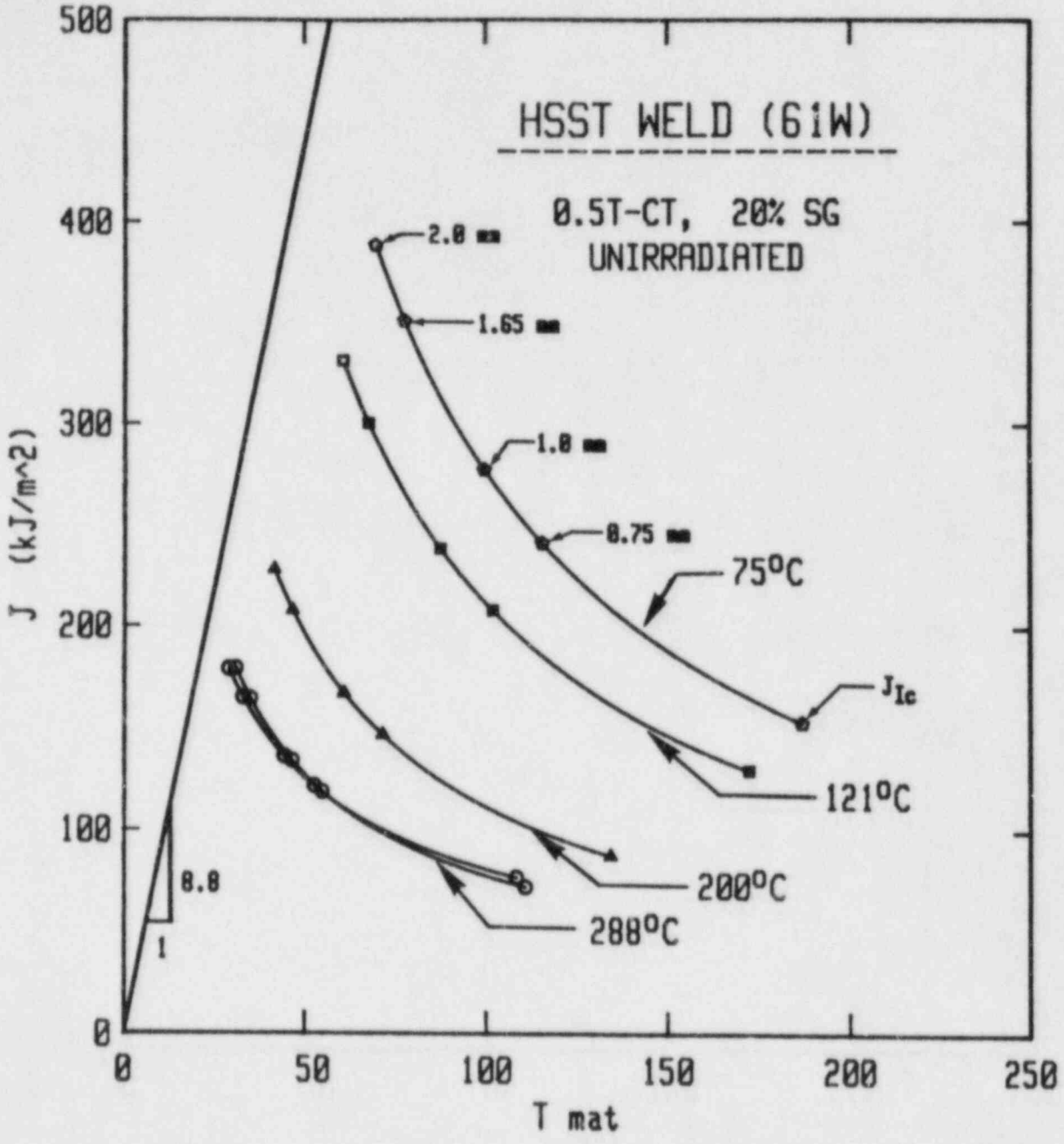

Figure 1.8 Effect of temperature on the J-T curves. These are from the J-R curves depicted in Fig. 1.6 (top).

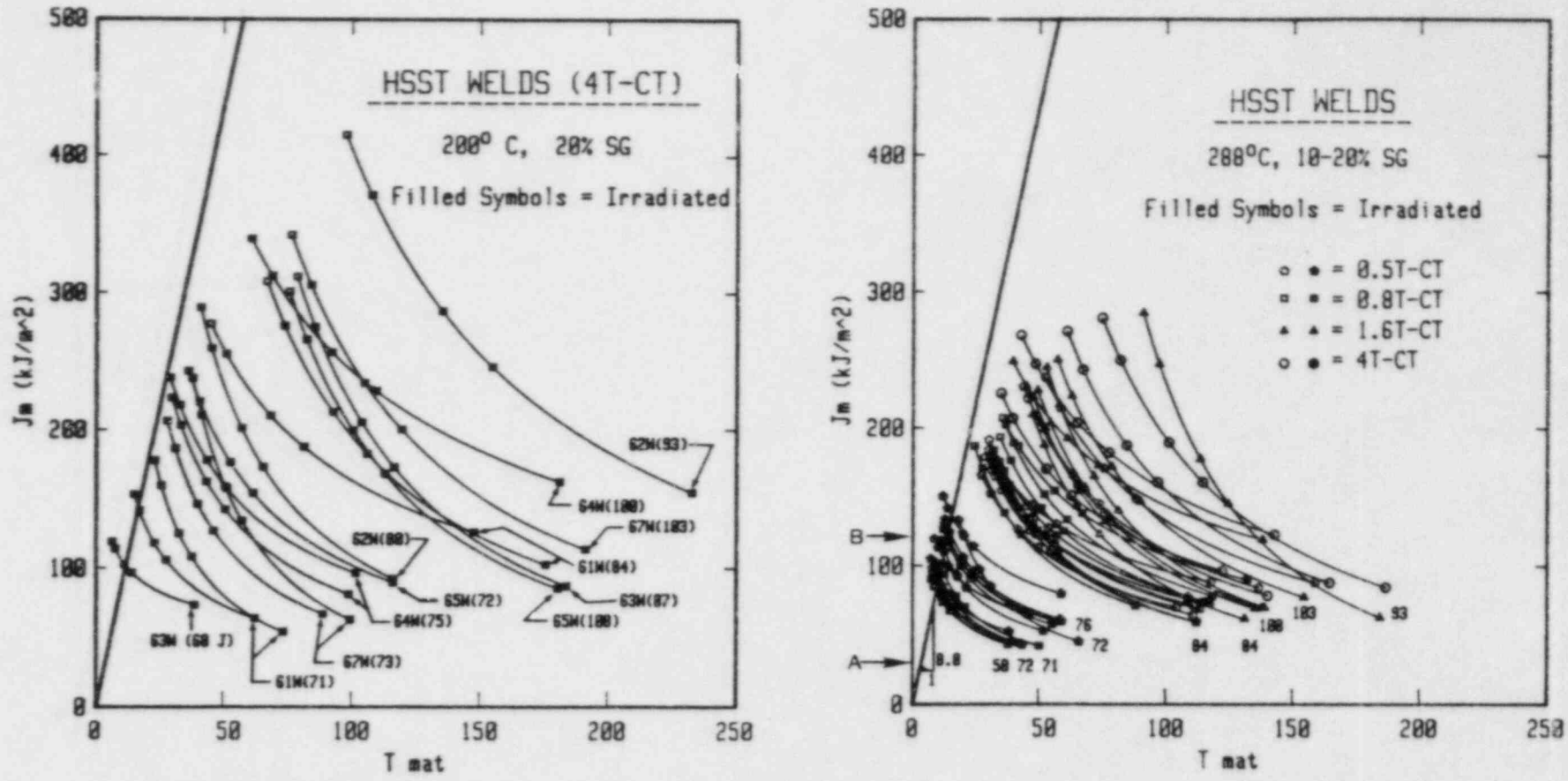

Figure 1.9 The 4T-CT curves at 200°C (left), and all of the curves at 288°C (right). The general trend is increasing J-T curve with increasing C_v energy.

1.1.5 Correlations with Charpy-V Results

Correlations between several J-R curve parameters, namely J_{Ic}, T_{avg} and the J value at $J/T = 8.8\ kJ/m^2$, and Charpy upper shelf energy have been observed by the authors for 1T-CT tests at 200°C in other NRC-sponsored programs as well as in an Electric Power Research Institute (EPRI) program (Ref. 6). These correlations were originally in terms of deformation theory J, but since have been restated in terms of modified J (Ref. 7).

Figure 1.10 (left) depicts the placement of J_{Ic} values from this program in relation to the trend band established in Ref. 7. The agreement of these data with the trend band is quite good, except for several tests which lie slightly above the band. The two highest irradiated points are 10% side grooved, indicating that these values are artificially high. The high unirradiated tests are predominantly from 4T-CT specimens, which confirms the possible size effect noted earlier.

The HSST welds data in terms of T_{avg} are illustrated in Fig. 1.10 (center) with the trend band from the 1T-CT data of Ref. 7. Here, all of the irradiated data lie within the band, while virtually all of the high unirradiated data are from 4T- and 1.6T-CT specimens, again suggesting a modest size effect.

The last correlation, with J at $J/T = 8.8\ kJ/m^2$, is illustrated for the HSST welds in Fig. 1.10 (right). Here, all of the 20% side-grooved, irradiated data lie within the 1T-CT trend band, with all of the points outside of the band from 10% side-grooved specimens. Surprisingly, all of the unirradiated data from weld code 62W lie above the trend band.

From these correlations and the earlier J-R curve comparisons, a size effect appears evident for the unirradiated condition, with larger specimen size (and thickness) associated with higher J-R curves. The hypothesis suggested here is that the larger specimens are proportionally less weld metal than the smaller specimens, which may be composed of all weld metal. With the relatively low strength levels of the unirradiated weld material (in comparison to the irradiated weld metal), deformations more attributable to the base metal may be erroneously included in the J values computed from the global displacements measured in the J-R curve test. Given this hypothesis, the observed size effect is not inconsistent with earlier work by McCabe and others (Ref. 8), wherein J-R curves from 0.5T- and 10T-CT specimens had similar behavior. In that study, the material characterized was a base metal, an A 508 tube plate. The relative homogeneity of these specimens, of course, would not have given any erroneous deformations, yielding "correct" J-R curves for all of the specimen sizes.

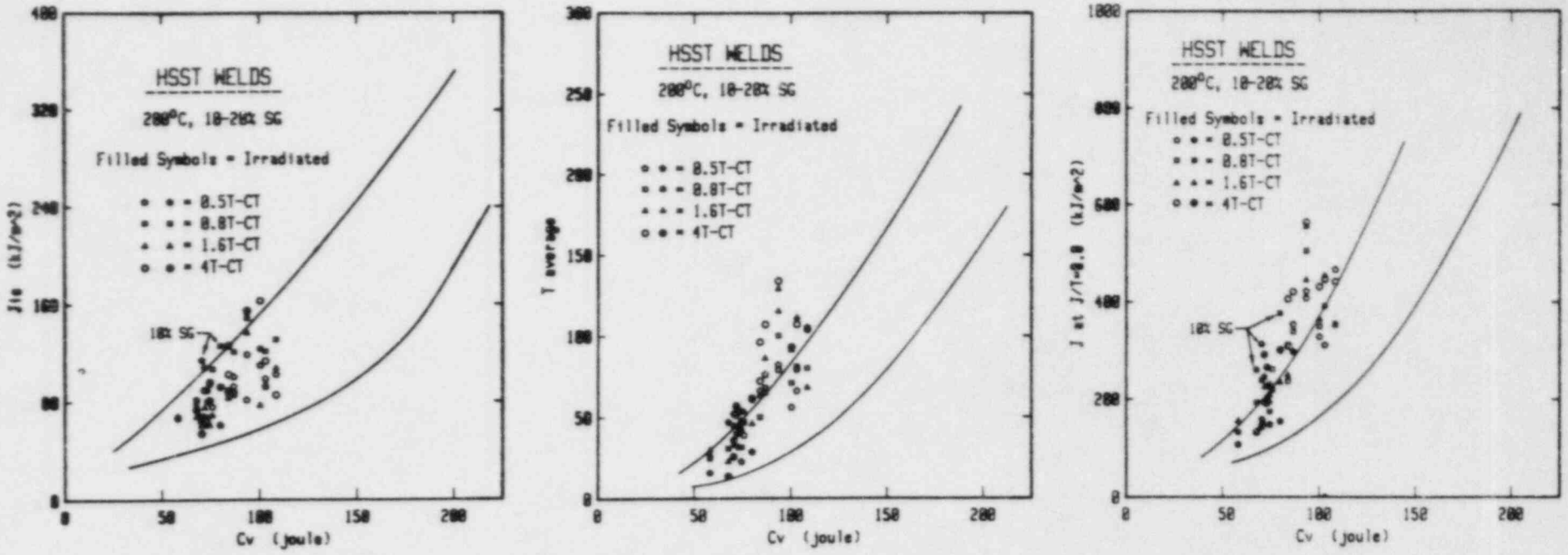

Figure 1.10 Trends of J_{Ic} (left), T_{avg} (center) and J = 8.8T (right) with C_v USE for the HSST welds at 200°C. The trend bands shown are from Ref. 5.

1.1.6 Conclusions

The J-R curves were developed here by the single specimen compliance (SSC) technique. The latter has been shown in this and other investigations by the authors to be an effective method to characterize the J-R curve behavior of irradiated steels. The majority of the specimens were side grooved by 20% to produce a straight crack-front extension. Since side grooving is known to reduce the level and slope of the J-R curve, it is believed that the present results could be used to characterize the behavior of a flaw in the thick wall of a reactor vessel.

In addition, a new procedure, the double clip gage technique (Ref. 5), was developed for the testing of the smaller size specimens in this program. This procedure has indicated that J-R curves can be developed on the basis of deflection measurement points different from that recommended by the ASTM. This finding could be of particular benefit for the testing of surveillance capsules involving CT specimens which were not machined to permit load-line displacement measurement in accordance with ASTM E 813.

Principal conclusions of this study are:

- Irradiation to a fluence of ~ 1×10^{19} n/cm^2 E > 1 MeV decreased the values of J_{Ic} and T_{avg} significantly from the preirradiation values. On average, at 200°C J_{Ic} and T_{avg} decreased by ~ 24% and ~ 53%, respectively. At 288°C, larger decreases in J_{Ic} and T_{avg} were observed, i.e., decreases of ~ 35% and ~ 69%, respectively.

- The data show that T_{avg} is a more discriminating indicator of the degradation in fracture toughness than is J_{Ic}. For example, in some cases very little change in J_{Ic} was observed with irradiation whereas a significant decrease in T_{avg} always occurred.

- A modest size effect associated with larger specimens was indicated for the unirradiated condition; however, no size effect was apparent for the irradiated condition, although T_{avg} showed a slight bias towards higher values with larger specimen size.

- Temperature-dependent correlations between J-R curve parameters (J_{Ic}, T_{avg} and J at J/T = 8.8 kJ/m^2) and C_v upper shelf energy have been suggested. If further verified, these findings could enhance the significance of C_v reactor surveillance data with respect to structural integrity.

- J_{Ic} and T_{avg} have demonstrated an inverse relationship with temperature which is not reflected by Charpy upper shelf energy. Therefore, correlations between Charpy energy and J-R curve properties must be adjusted to reflect the effect of temperature.

1.2 Piping Fracture Mechanics Data Base

A. L. Hiser, Jr., M. E. Mayfield and B. H. Menke

1.2.1 Background

Structural integrity evaluations in LWR piping systems require fracture toughness data from the constituent materials used in the piping. Currently, the tearing instability approach is receiving attention as a suitable analysis technique for evaluating piping systems. This approach requires J-R curve data from the materials of interest. However, these data are generally unavailable for many of the materials. To facilitate application of the tearing instability approach, a comprehensive J-R curve data base from appropriate piping materials is being created by MEA for the NRC. This data base will be formulated in a computer-based system which will be readily accessible by potential users.

1.2.2 Summary of Results

Initial activities under this subtask centered on defining the various piping materials for which J-R curve data are required. This list (Table 1.4) includes carbon steels, cast and wrought stainless steels, and welds from all types.

Data collection efforts thus far have concentrated on identifying potential sources of J-R curve data from all types of piping material, not restricted to the list mentioned previously. Initial collection efforts are being focused on sources of data within the U.S.A. Preliminary discussions with the various sources have revealed that few data are available from the list of essential materials. However, sources of steel pipe have been identified, so that some of these steels can be procured and J-R curve tests can be conducted. Preference here will be given to nuclear-grade piping obtained from actual plant construction. However, sources of material are not plentiful.

J-R curve testing of an A 106 grade C pipe steel has been completed. Additionally, tensile and C_v specimens have been tested for this material. A summary of the orientations in which each specimen-type was tested is given in Table 1.5. Two tensile specimens were tested from each orientation at 20°C and 343°C, with a single determination at 232°C. Both the 0.2% offset yield and the ultimate stress curves are fairly invariant with temperature for both of the orientations tested, although the yield stress does decrease slightly and the ultimate stress does increase slightly with increasing temperature.

Charpy-V specimens from two orientations of the A 106 pipe steel and three thickness locations were tested, with three replicate tests at each temperature. The C_v levels show large differences with orientation. Specifically, at the three test temperatures the L-R data are 76% higher than the C-R data, on average. Large through-thickness variations are seen for each orientation, with the ID yielding higher levels for the L-R orientation, while the OD specimens give higher energy levels for the C-R orientation. As indicated in Table 1.6, all six sets of data show increases in energy level with temperature.

Table 1.4 List of Commonly Used Piping Materials to be Included in the Fracture Toughness Data Base

Material Specification	Nominal Diameter (in.)	Wall Thickness (in.)	Typical Application/Comments
SA-516 Gr. 70	30 to 42	2-1/2 to 4-1/2	Straight Pipe and Elbows in Main Coolant Loop/Plate Material formed into Product
SA-106 Gr. C	30 to 42	2-1/2 to 3	Straight Pipe in Main Coolant Loop/Seamless Pipe
SA-351 Gr. CF8M	30 to 32	2 to 2-1/2	Straight Pipe and Safe-ends in Main Coolant Loop/Cent. Cast 316
SA-351 Gr. CF8M	30 to 32	2-1/2 to 3	Elbows in Main Coolan Loop/Cont. Cast 316
SA-351 Gr. CF8A	30 to 32	2 to 2-1/2	Straight Pipe and Safe-ends in Main Coolant Loop Cont. Cast 304
SA-351 Gr. CF8A	30 to 32	2-1/2 to 3	Elbows in Main Coolant Loop/Cent. Cast 304
SA-351 Gr. CF8M	12	Sch. 160	Surge Line and Branch Pipe Safe-ends/Cent. Cast 316
SA-182 F316	30 to 32	2-1/2 to 3	Safe-end in main coolant loop/Forging 316
SA-182 F316	12	Sch. 160	45° and 90° Branch Nozzle in Main Coolant Loop/Forging 316
SA-182 F316	4 to 6	Sch. 80 to 160	Branch Nozzles in Main Coolant Loop/Forging 316
SA-182 F304	30 to 32	2-1/2 to 3	Safe-end in Main Coolant Loop/Forging 304
SA-182 F304	12	Sch. 160	45° to 90° Branch Nozzle in Main Coolant Loop/Forging 304
SA-182 F304	4 to 6	Sch. 80 to 160	Branch Nozzles in Main Coolant Loop/Forging 304
SA-376 Type 316	12	Sch. 160	Surge Line and Branch Line Safe-ends/Seamless Pipe 316
SA-376 Type 316	4 to 6	Sch. 80 to 160	Auxiliary Piping/Seamless Pipe 316
SA-376 Type 304	4 to 12	Sch. 80 to 120	BWR Piping/Seamless Pipe 304
SA-376 Type 304	20 to 24	Sch. 160	BWR Piping/Seamless Pipe 304
SA-358 Gr. 304 Cl.1	4 to 12	Sch. 80 to 120	BWR Piping/Welded Pipe 304
SA-106 Gr. B	4 to 12	Sch. 80 to 120	BWR Piping/Seamless Pipe-Carbon Steel
SA-105 Gr. 2	4 to 12	Sch. 80 to 160	Branch Pipe Nozzles/Carbon Steel Forging
Weld: SA-516 Gr. 70 to SA-516 Gr. 70	30 to 42	2-1/2 to 4-1/2	Pipe to Pipe or Pipe to Elbow Weld in Main Coolant Loop/Field Weld
Weld: SA-106 Gr. C to SA-516 Gr. 70	30 to 42	2-1/2 to 3	Pipe to Elbow Weld in Main Coolant Loop/Field Weld
Weld: SA-106 Gr. C to SA-351 CF8M	30 to 42	2-1/2 to 3	Pipe to Safe-end Dissimilar Metal Weld/Field Weld
Weld: SA-106 Gr. C to SA-182 F316	30 to 42	2-1/2 to 3	Pipe to Safe-end Dissimilar Metal Weld/Field Weld
Weld: SA-376 Type 316 to SA-182 F316	4 to 12	Sch. 80 to 160	Pipe to Safe-end (Forging) Weld/Field Weld
Weld: SA-376 Type 316 to SA-351 Gr. CF8M	4 to 12	Sch. 80 to 160	Pipe to Safe-end (Cent. Cast Pipe) Weld/Field Weld

Table 1.5 Orientation of A 106 Gr. C Tests

	L-R[a]	C-R[a]	L-C[a]	C-L[a]
J-R Curve	X	X	X	X
C_v	X	X		
Tensile	X[b]	X[c]	X[b]	X[c]

[a] ASTM E 399 designations.
[b] Loading was coincident with the longitudinal orientation.
[c] Loading was coincident with the cirumferential orientation.

Table 1.6 Summary of Charpy-V Results

Orientation/Location		Absorbed Energy[a](J) at 22°C	93°C	288°C
C-R[b]	ID	76	83	85
	1/2T	64	91	98
	OD	81	102	114
	Average	74 ± 8.7[c]	92 ± 9.5	99 ± 14.5
L-R[b]	ID	141	163	206
	1/2T	104	149	169
	OD	138	160	176
	Average	128 ± 20.6	157 ± 7.4	184 ± 19.7

[a] Average of three tests
[b] ASTM E 399 designations
[c] Standard deviation of the nine values

J-R curves were determined for this material at five temperatures from 20°C (ambient) to 343°C. Thus far, only the L-R and C-R orientation results have been finalized. To assess scatter in this material, three replicate 1T-CT specimens, side-grooved by 20% total, were tested at each temperature from each orientation. The one exception is two specimens from the C-R orientation tested at 232°C. All of the J-R curves are plotted together in Figs. 1.11 and 1.12, for the C-R and the L-R orientations, respectively. One point to consider here is that, by the provisions of the ASTM proposed J-R curve test method, J-R curves from this strength of material and this size of specimen are limited to about 2.5 mm of crack extension and 440 kJ/m^2 in J

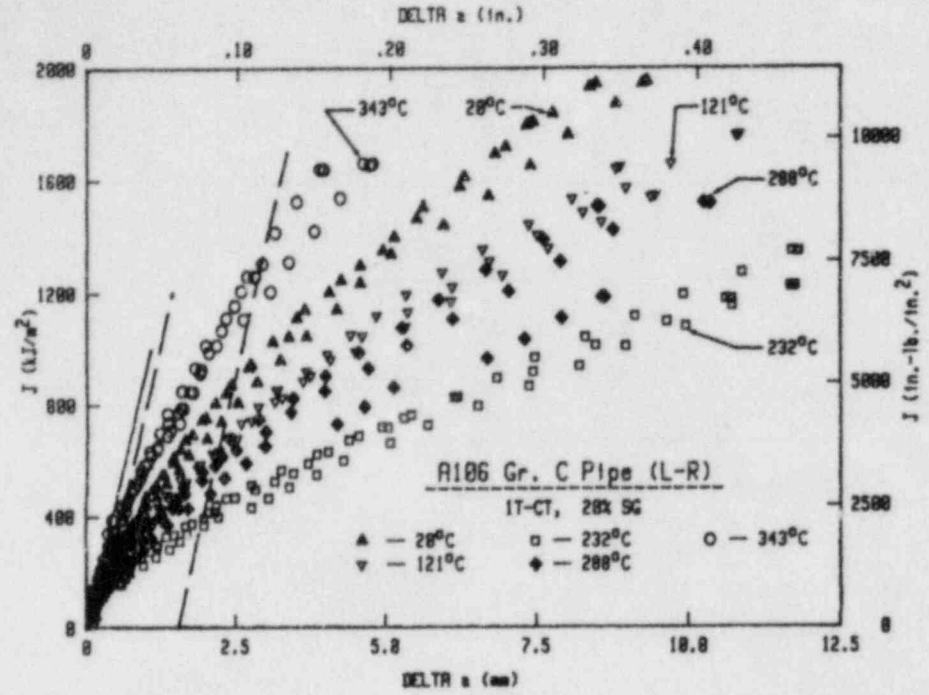

Figure 1.11 The J-R curves for the C-R orientation of an A 106 Gr. C pipe. The J-R curve level decreases with increasing temperature up to 232°C, with increasing level with increasing temperature thereafter.

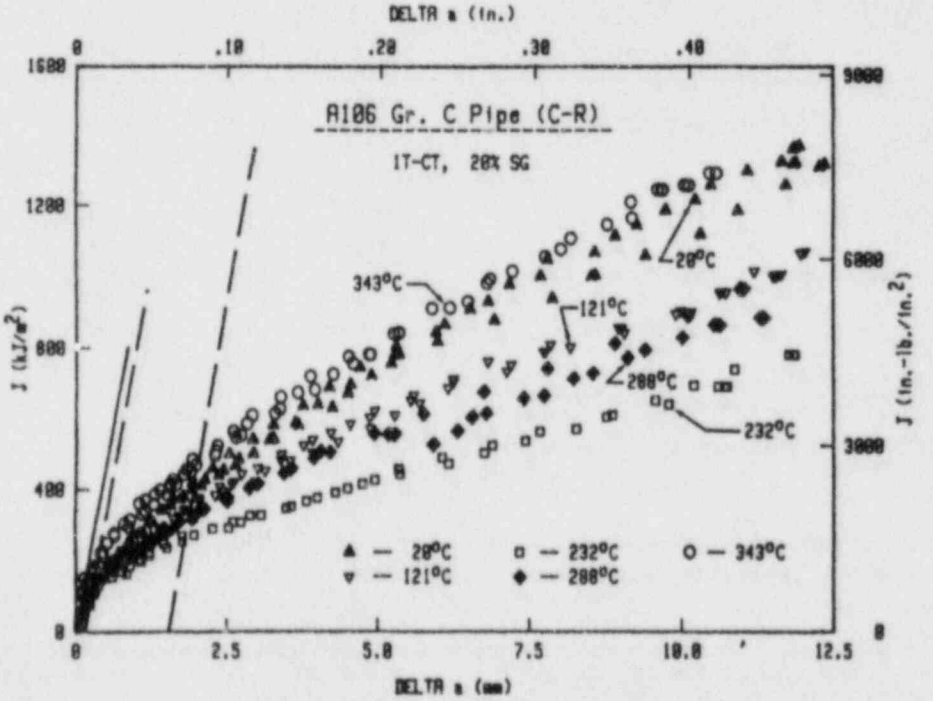

Figure 1.12 The J-R curves for the L-R orientation of an A 106 Gr. C pipe. The J-R curve behavior here is identical to that of the C-R orientation (Fig. 1.11), except that the J-R levels are approximately twice that from the C-R specimens.

level. Regardless of this, relative comparisons of R-curves beyond those limits should be unaffected by the violation of the limits. In virtually all cases, the scatter is not too severe. As well, data from each temperature separate into distinct bands, with little mixing of data. For each orientation, the layering of the R-curves with temperature follows the same pattern from highest J-R curve level to the lowest: 343°C, 20°C, 121°C, 288°C and 232°C. This behavior is unexpected when compared to that exhibited by the HSST low upper shelf welds and in EPRI-sponsored research on materials with higher upper shelf levels, where increasing temperature resulted in progressively lower J-R curve level, at least up to 288°C. The difference in R-curve level between the two orientations is very large, as the lowest R-curves from the L-R orientation (at 232°C) are just slightly lower than the highest R-curves from the C-R orientation (at 343°C).

The effect of temperatures on J-R curve parameters, specifically J_{Ic} and T_{avg}, is illustrated in Figs. 1.13 and 1.14 and is summarized in Table 1.7. For both orientations J_{Ic} and T_{avg} are either invariant with temperature or inversely proportional with temperature, from 20°C to 232°C. Thereafter, both quantities increase sharply with temperature.

Table 1.7 Summary of Fracture Toughness Results

Orient.	20°C	121°C	232°C	288°C	343°C
			$J_{Ic}(kJ/m^2)$		
C-R[a]	112 (± 4.5)	119 (±14.7)	88 (±19.5)	120 (±10.3)	213 (± 9.0)
L-R[a]	201 (±29.9)	177 (±20.5)	118 (± 5.2)	146 (±11.7)	442[b](±31.4)
			T_{avg}		
C-R[a]	160 (± 4.6)	122 (± 9.5)	96 (± 5.7)	107 (± 5.6)	146 (±10.6)
L-R[a]	300 (± 5.1)	253 (±21.0)	158 (±15.1)	224 (±34.0)	355 (±34.5)

[a] ASTM E 399 designations.
[b] Violates ASTM E 813 thickness and initial ligament requirements (B_N, $b_o > 25J_{Ic}/\sigma_f$)

T_{avg} and J_{Ic} in Table 1.7 show identical ordering with temperature as do the J-R levels at large crack extensions, except for J_{Ic} in the C-R orientation. J_{Ic} and T_{avg} for the L-R orientation give much larger deviations from the mean, indicating greater absolute scatter than for the C-R orientation. However, on a percentage basis the scatter is similar to that observed in the C-R orientation. On average (excluding 343°C), J_{Ic} is 44% higher and T_{avg} 92% higher for the L-R orientation as compared to the C-R orientation. This finding is consistent with earlier comparisons of preirradiation vs. postirradiation J-R curve behavior where T_{avg} is a much more sensitive indicator of R-curve difference than is J_{Ic}.

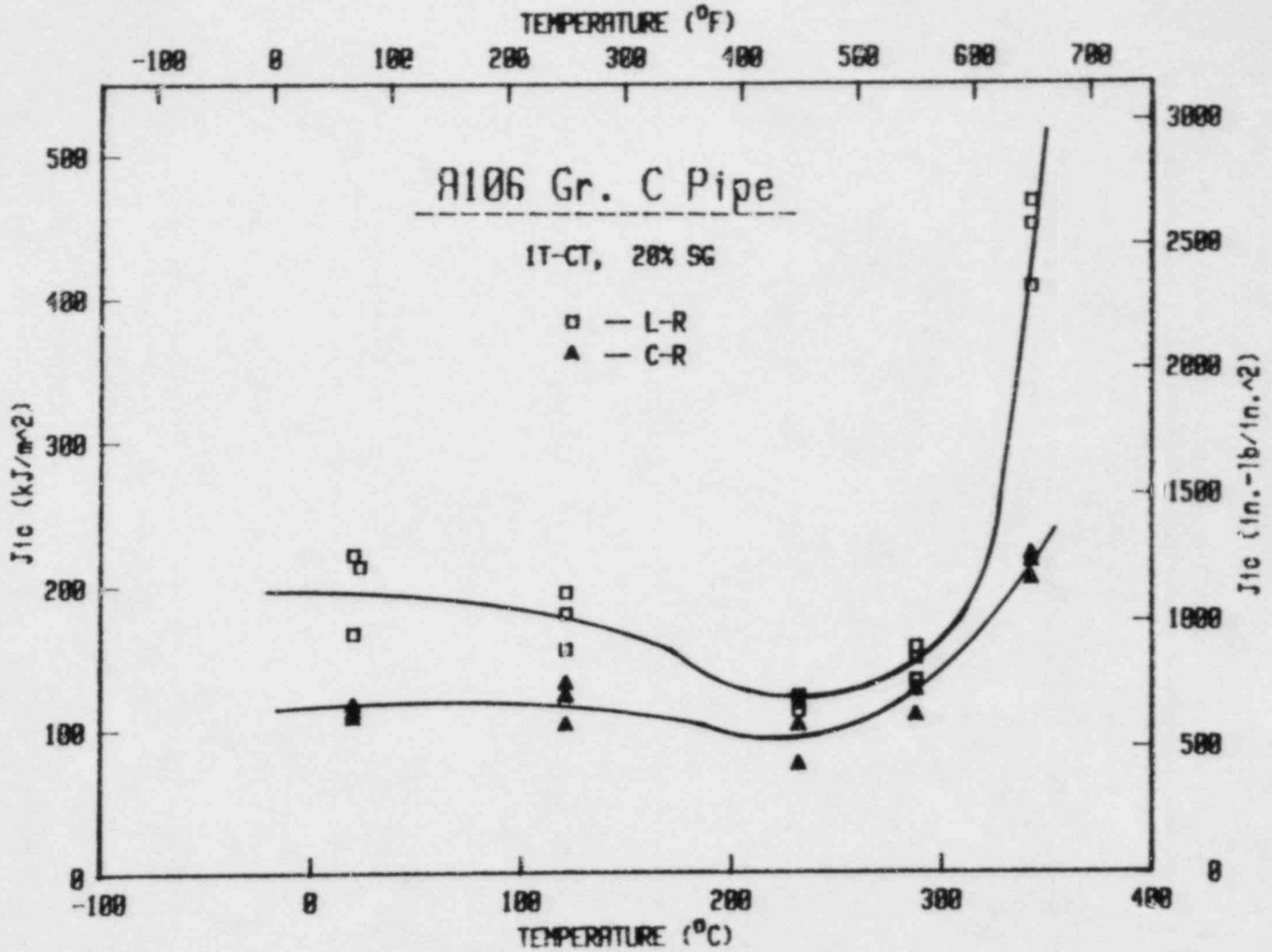

Figure 1.13 Trends of J_{Ic} with temperature for two orientations. Similar behavior is observed for each orientation, with minima at 232°C and sharply increasing levels thereafter. The L-R orientation data lie significantly higher than the C-R orientation data.

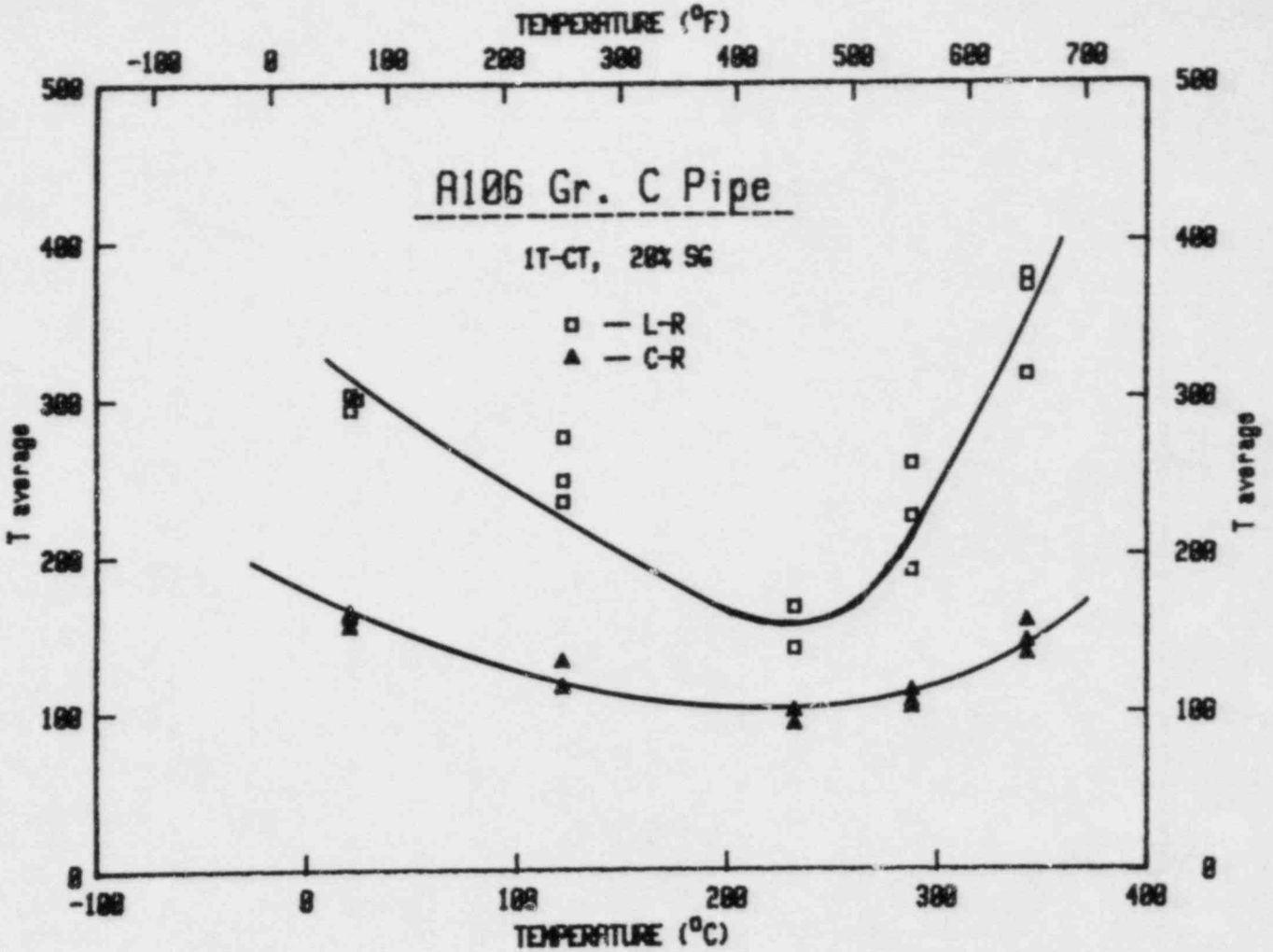

Figure 1.14 Trends of T_{avg} with temperature for two orientations. The behavior here is identical to that observed with J_{Ic}, with only the curve shapes differing.

A cast stainless steel and several other materials are scheduled for testing in 1984. Data collection efforts in 1984 should result in all current data assembled. In the following years, only additional results from the sources would require collection. By the end of 1984, the data base should be implemented, with initial data being placed into the system.

1.3 Elastic-Plastic Fracture Toughness Characterization of HSST Intermediate Vessel Material

B. H. Menke, A. L. Hiser and F. J. Loss

1.3.1 Background

The objective of this study was to develop an elastic-plastic fracture mechanics material property data base for use in a tearing instability analysis of specific Heavy Section Steel Technology (HSST) program pressure vessel tests. The HSST program includes the testing to failure of a number of intermediate-size pressure vessels. These vessels were fabricated from A 533 Grade B Class 1 plate and A 508 Class 2 forging with an outside diameter of 1 m and a wall thickness of 152 mm. Sharp-tipped flaws of known geometry were introduced into the vessel walls prior to testing and the vessels were tested at temperatures both on the upper shelf and in the brittle-to-ductile transition region. However, the elastic-plastic J-R curve characterization described herein applies only to those vessel tests where significant ductile tearing occurred in the vessel wall, i.e., those upper shelf tests where the flaw was contained in the base material as opposed to welds or nozzle projections. Specifically, the information obtained in this study is applicable to three particular vessel tests designated as V1, V7 and V7A. These vessels were tested at 54°C, 91°C and 88°C, respectively, and these temperatures correspond to the onset of upper shelf behavior as determined from Charpy tests.

A small section of test vessel prolongation of each material was provided by ORNL from which test specimens were machined. The number and types of specimens is given in Table 1.8.

Table 1.8 Test Specimen Designation

Specimen Type	Vessel V7 and V7A A 533 Plate (Code V8-PID)		Vessel V1 A 508 Forging (Code FP)	
	C-L*	C-R*	C-L*	C-R*
4T-CT	2	0	2	0
1.6T-CT	2	2	2	2
0.5T-CT	12	6	12	6
Charpy	0	0	18	9
Tensile	0		12 Circumferential	

* ASTM E 399 Designation

J-R curve trends related to vessel crack propagation direction and specimen size effects were addressed with tests of 0.5T-, 1.6T- and 4T-CT specimens having C-L orientations and with 0.5T- and 1.6T-CT specimens of C-R orientation. Through-thickness variation in properties was determined in both orientations with 0.5T-CT specimens and additionally with C_v and tensile specimens for the V1 vessel forging material. All specimens were tested at the vessel test temperature, i.e., A 508 forging specimens were tested at 54°C, the V1 vessel test temperature, and A 533 plate specimens were all tested at 90°C, the average of the V7 and V7A vessel test temperatures.

All compact toughness (CT) specimens were side grooved by 20% (10% each side). Side grooving tends to produce a straight crack front which facilitate crack extension prediction by the single specimen compliance (SSC) procedure. In addition, side grooving helps to produce lower bound toughness data. All compact specimens were tested using the SSC technique. Both the ASTM Standard E 813 for initiation toughness determination and the recommended J_I-R curve procedures were followed where applicable. J-integral values were calculated using the modified version of the J integral, J_M.

1.3.2 Summary of Results

The results of all A 508 forging material tests, C_v, tensile and smaller compact specimens indicate little or no material property gradient through the prolongation wall. Tensile and Charpy data are summarized in Table 1.9 and shown graphically in Fig. 1.15 and 1.16, respectively. In Fig. 1.15, a tendency toward higher tensile strength is indicated by the surface specimen tests, however, the tendency is very slight and may be due to data scatter. The Charpy energy and lateral expansion data depicted in Fig. 1.16 indicate uniform properties in both orientations as well as through the thickness.

A 508 forging material fracture toughness parameters, J_{Ic}, and tearing modulus, T_{avg}, are plotted vs. the specimen-thickness location in Fig. 1.17. Again there is no indication of a through-thickness gradient nor any variation resulting from specimen orientation. The mean value and standard deviation for J_{Ic} and T_{avg} are summarized in Table 1.10 for each orientation. As indicated, the results are very nearly identical for the two orientations.

Table 1.9 A 508 Cl 2 Forging Tensile and Charpy Values (54°C)

	Average Value	± 1 σ
Yield Strenth	477 MPa (68.2 ksi)	35.3 MPa (5.1 ksi)
Ultimate Strenth	606 MPa (95.7 ksi)	16.0 MPa (2.3 ksi)
Percent Elongation	24.5%	1.2%
Reduction In Area	61.0%	2.2%
Charpy Level C-L	110 J (81 ft-lb)	9.5 J (7 ft-lb)
Charpy Level C-R	112.5 J (83 ft-lb)	7.1 J (5 ft-lb)

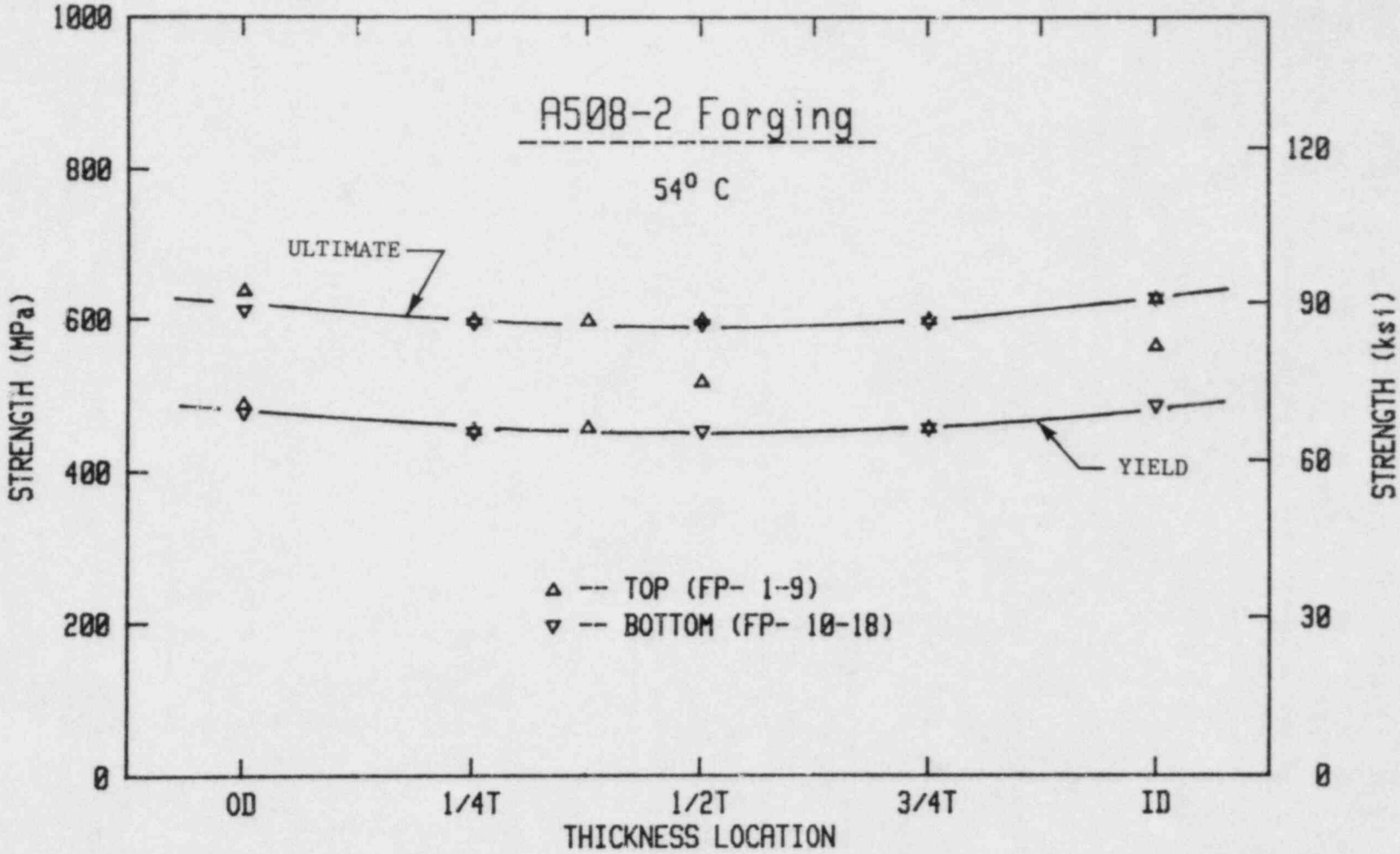

Figure 1.15 Variations of yield and ultimate tensile strength as a function of through-thickness specimen location. Tensile specimens were taken from the extreme top and bottom of the vessel prolongation to facilitate an overall material characterization. A slightly higher ultimate strength at the surface is indicated.

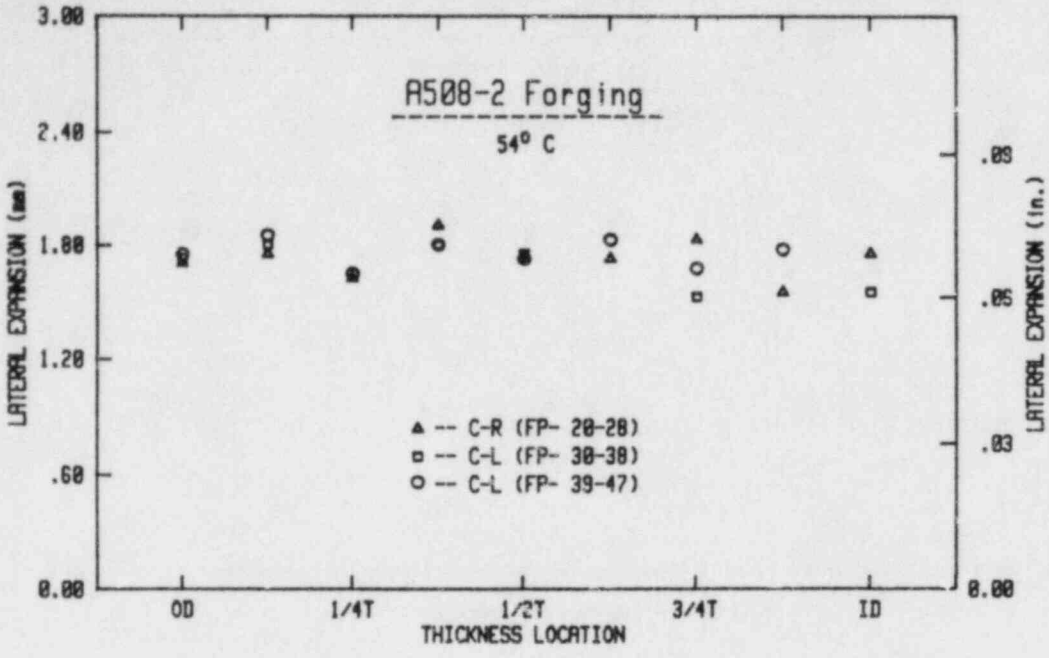

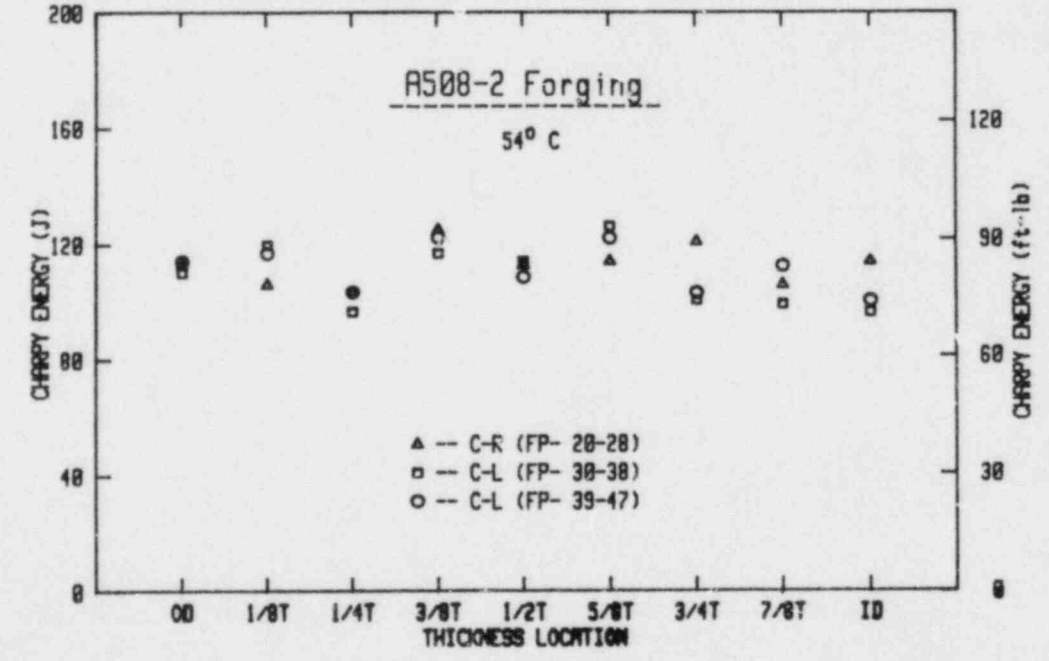

Figure 1.16 Variation of Charpy energy (lower) and lateral expansion (upper) with through-thickness specimen location. No significant variation with thickness location or specimen orientation is indicated.

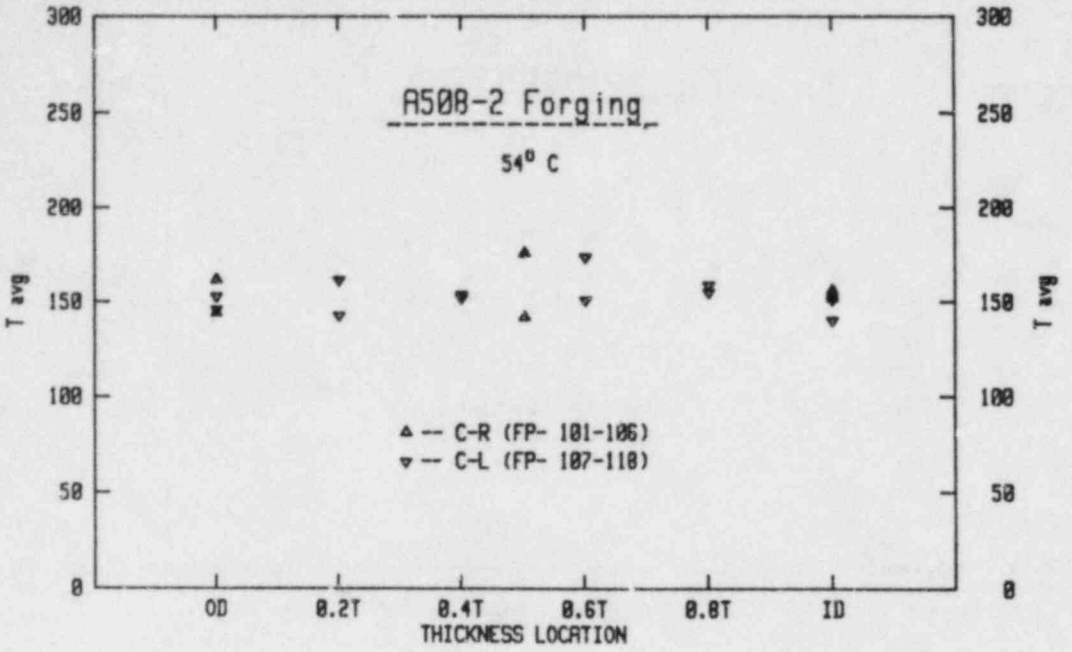

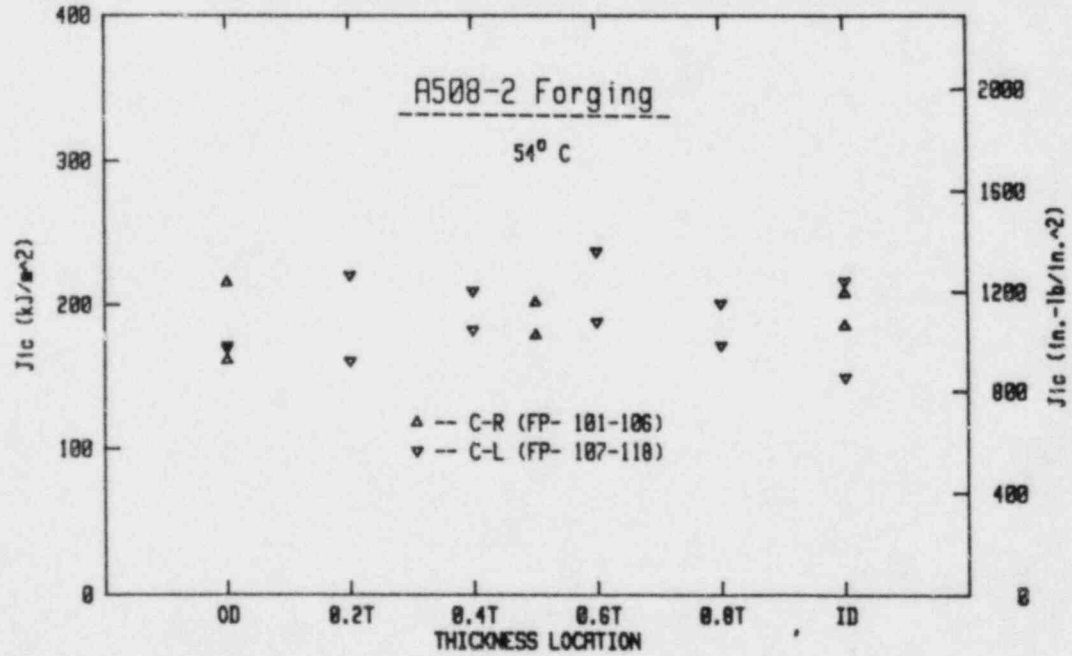

Figure 1.17 Variation of initiation fracture toughness (J_{Ic}) and average tearing modulus (T_{avg}) with through-thickness specimen location. No significant variation is apparent. Data were obtained from 0.5T-CT specimen tests.

A 533 plate material fracture toughness parameters, J_{Ic}, and tearing modulus, T_{avg}, are plotted vs. the specimen-thickness location in Fig. 1.18. In this case, there is a slight gradient which produces higher values near the inside diameter surface. This seemingly small trend might otherwise be attributed to data scatter except that the larger 1.6T and 4T-CT tests also indicated higher toughness near the inside surface. The mean value and standard deviation for all J_{Ic} and T_{avg} data are listed in Table 1.10 for each orientation. These data indicate relatively uniform properties in both directions of crack propagation characterized.

Table 1.10 Summary of J-R Curve Results

	J_{Ic} (kJ/m^2)		T_{avg}	
	Avg.	± 1 σ	Avg.	± 1 σ
A 508-2 Forging				
C-L	189.7	27.2	153.3	9.0
C-R	191.6	20.5	155.3	12.6
A 533-B1 Plate				
C-L	253.3	28.8	209.3	19.5
C-R	259.5	36.6	214.7	20.4

J-R curves obtained with the larger 1.6T and 4T-CT specimens are shown in Figs. 1.19 and 1.20 along with the trend bands developed with the 0.5T-CT specimens for the A 508 forging and the A 533 plate materials, respectively. In general, the larger specimen data are within the 0.5T-CT trend bands. However, there is a slight bias in the region of crack extension initiation toward the upper boundary of the small specimen data scatter band.

In Fig. 1.21, all J-R curve data are summarized in terms of a J vs. T material plot. It is evident in this figure that the A 533 material has the higher toughness of the two. Therefore, the vessels V7 and V7A would have required a greater energy input to cause failure than that required to cause the failure of vessel V1.

To summarize the characterization results: the mean and standard deviation for initiation fracture toughness (J_{Ic}) and average tearing modulus (T_{avg}), based on all J-R curve data obtained, is 198 ± 30 kJ/m^2 and 150 ± 11 for the A 508 forging and 265 ± 40 kJ/m^2 and 210 ± 21 for the A 533 plate. There did not appear to be any significant variation in toughness with regard to either specimen location or orientation for both materials investigated.

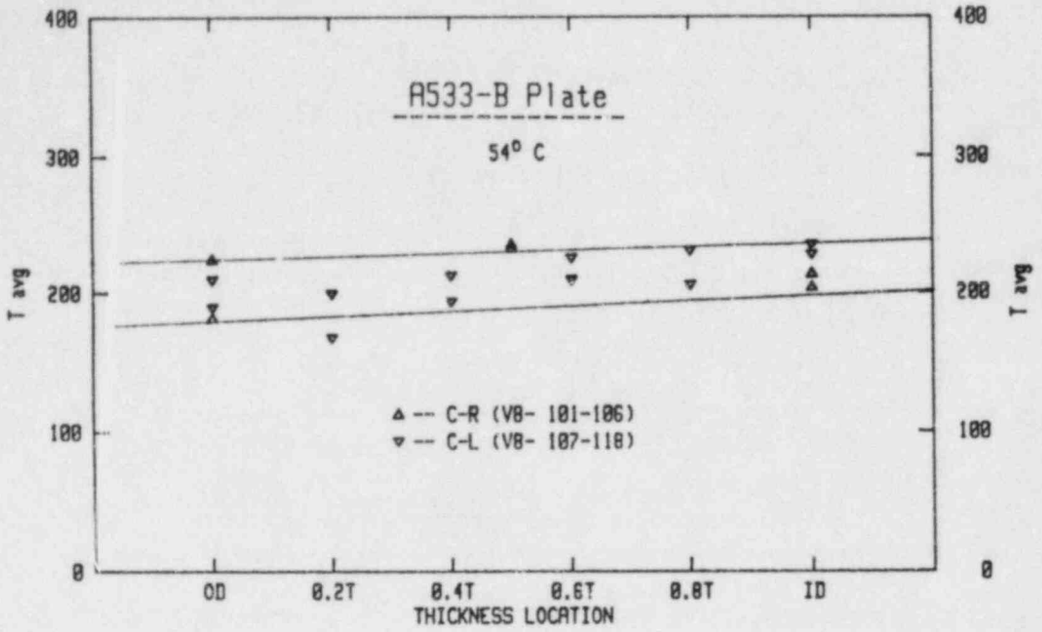

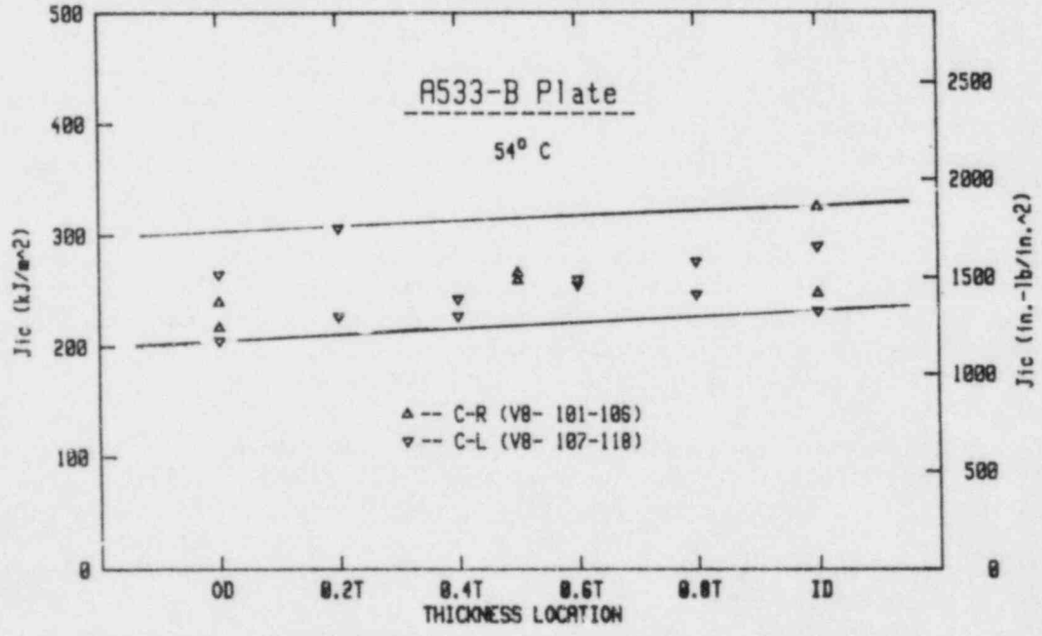

Figure 1.18 Variation of initiation fracture toughness (J_{Ic}) and average tearing modulus (T_{avg}) with through-thickness specimen location. A trend of slightly increased toughness and tearing modulus toward the inside surface is indicated.

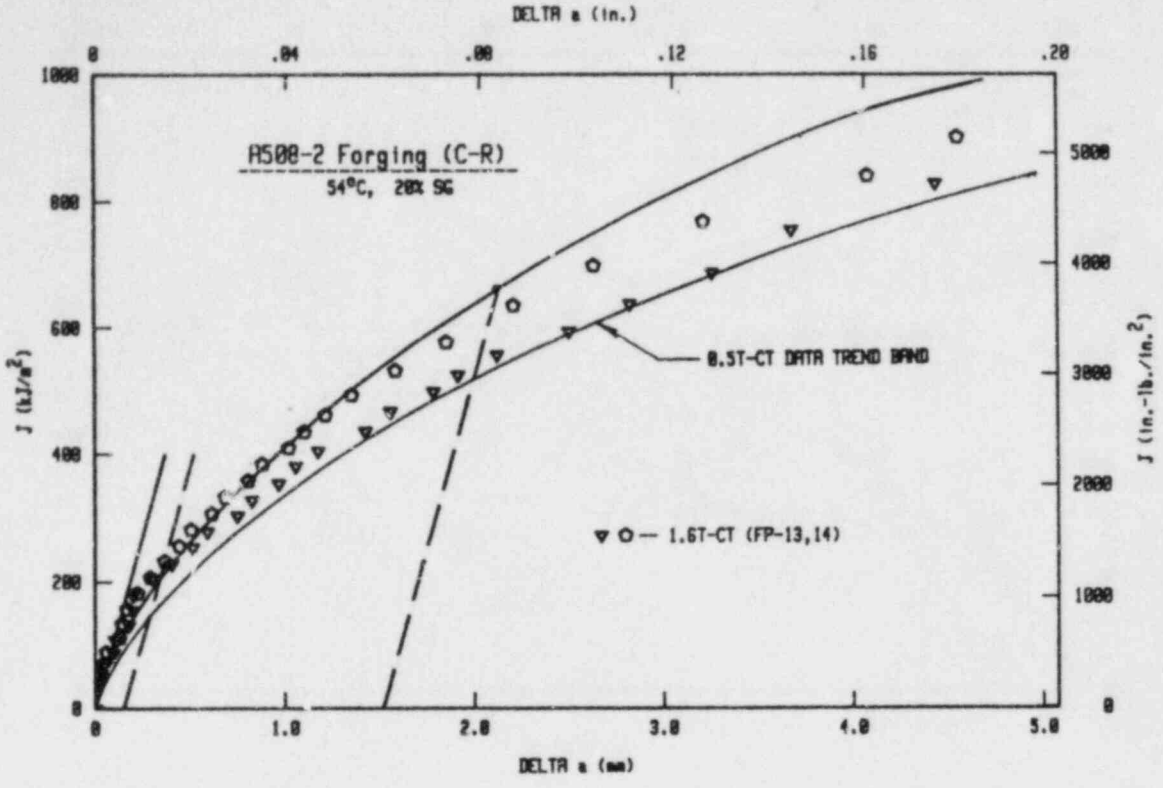

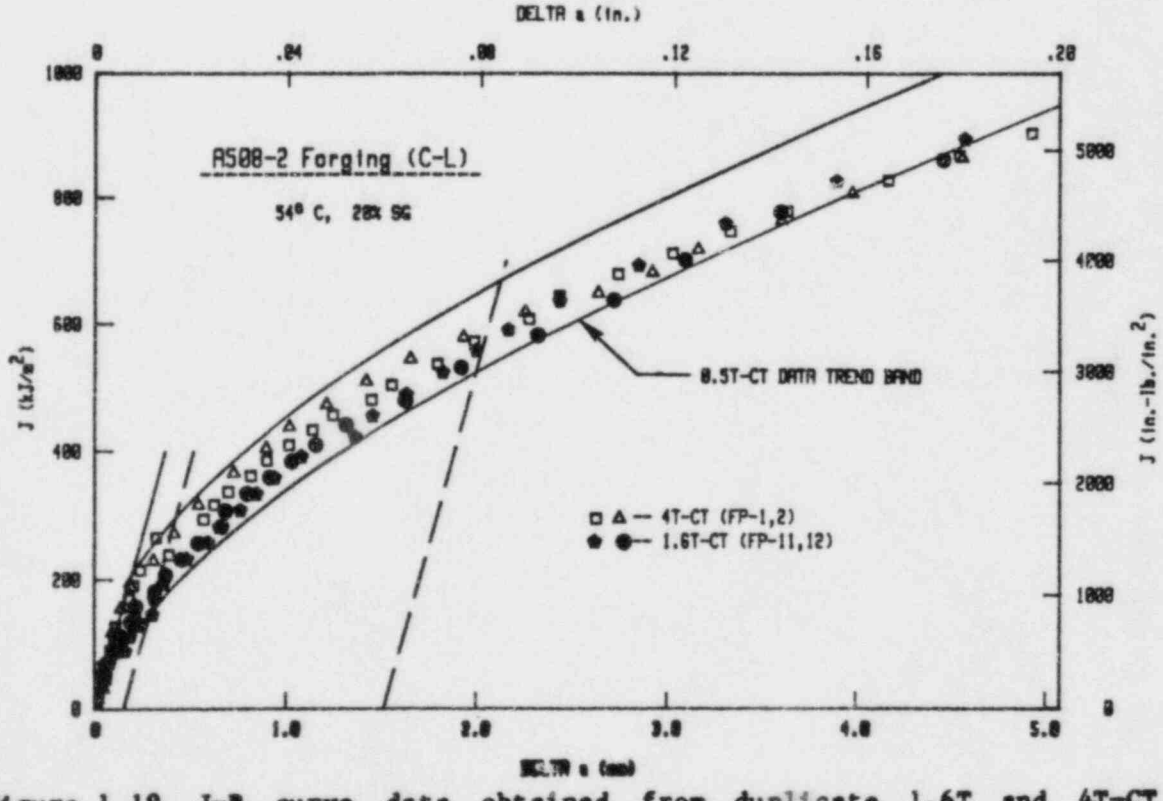

Figure 1.19 J-R curve data obtained from duplicate 1.6T and 4T-CT specimen tests in the C-L orientation (lower plot) and the C-R orientation (upper plot). The scatter band obtained with 0.5T-CT specimens essentially bounds the larger specimen data.

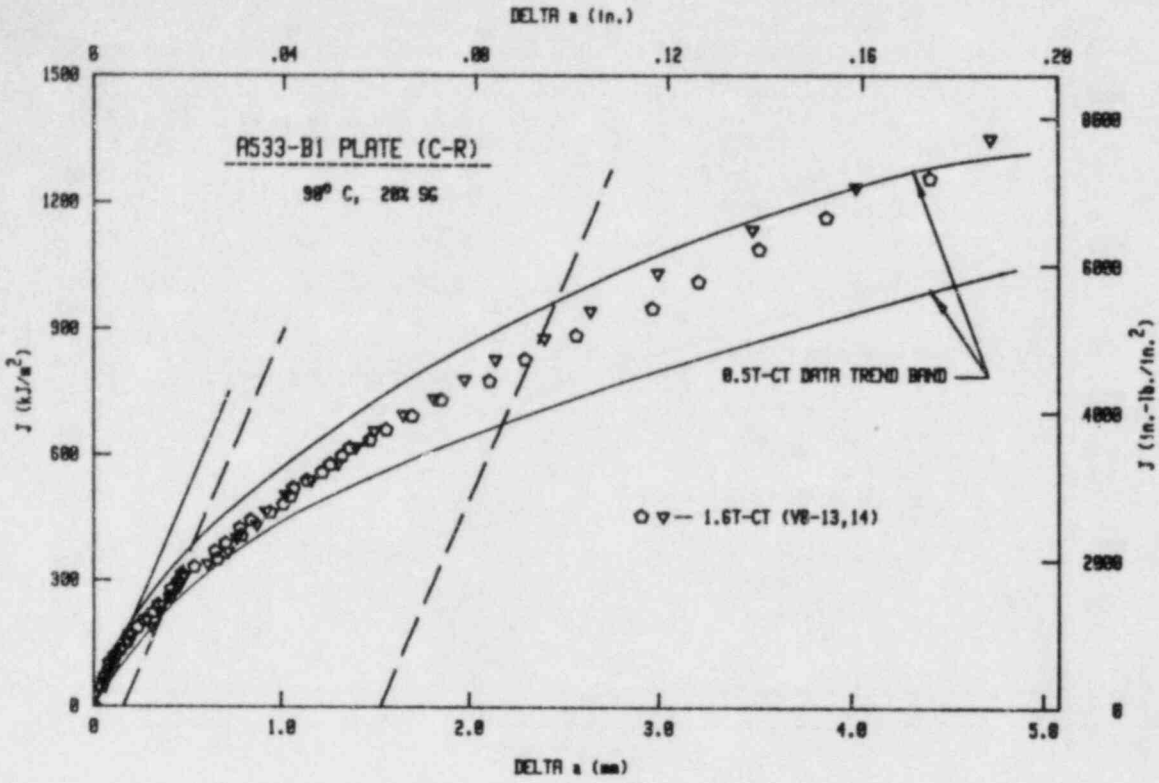

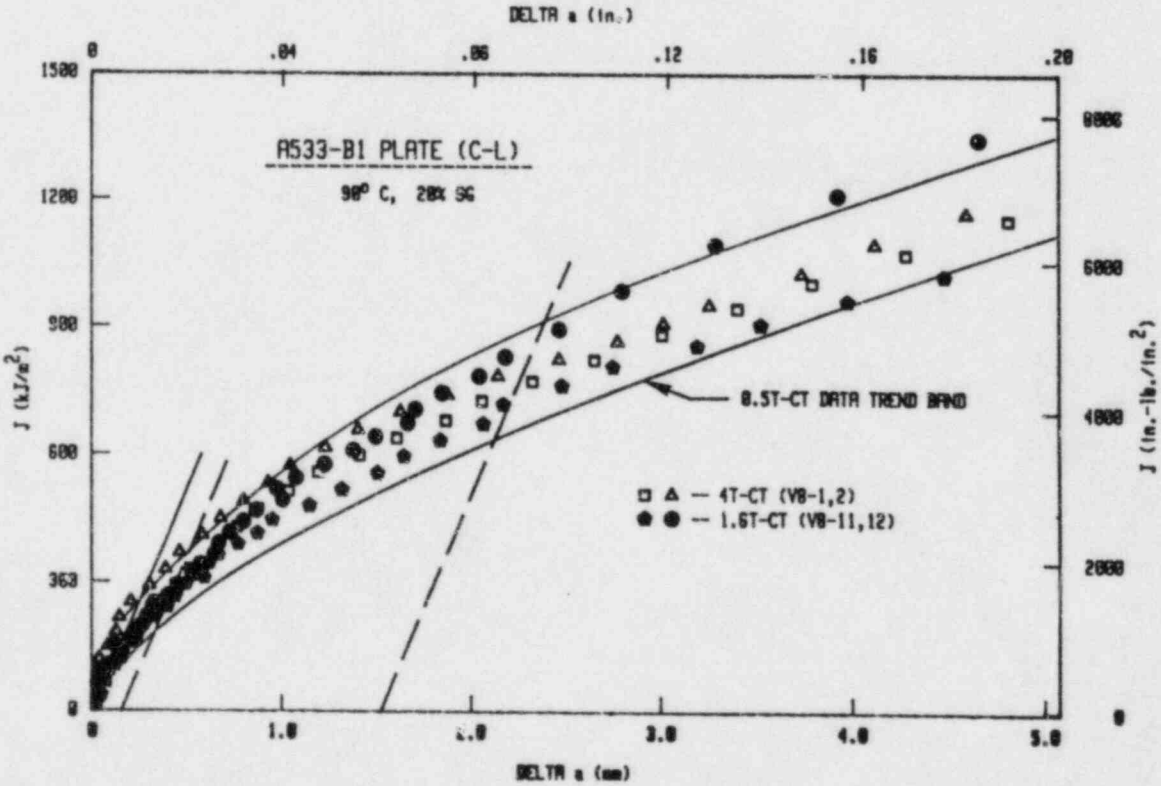

Figure 1.20 J-R curve data obtained from duplicate 1.6T and 4T-CT specimen tests in the C-L orientation (lower plot) and the C-R orientation (upper plot). The scatter band obtained with 0.5T-CT specimens essentially bounds the larger specimen data.

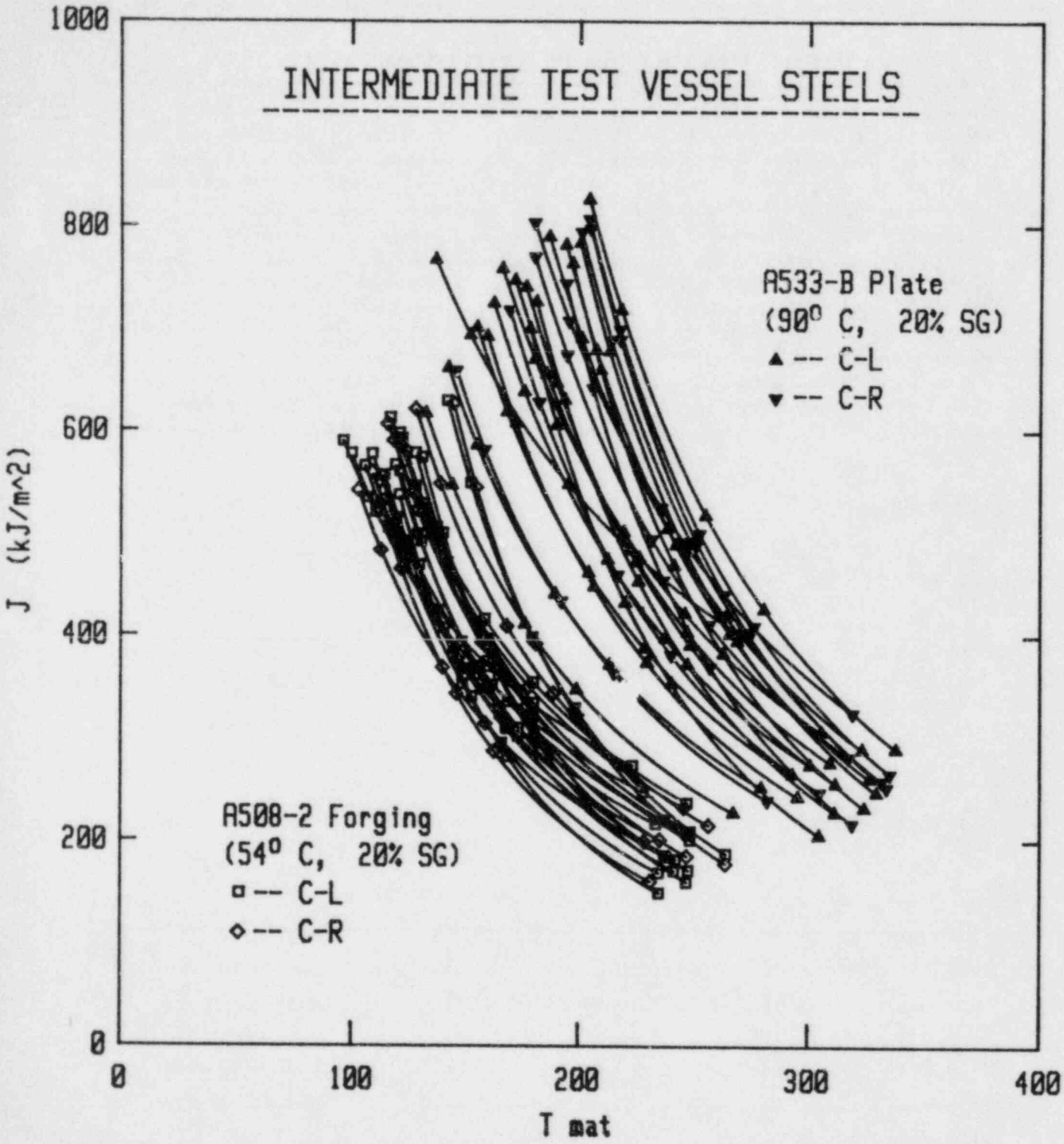

Figure 1.21 All J-R curves obtained in this study.

1.4 Heavy Section Steel Technology (HSST) 4th Irradiation Program

B. H. Menke, A. L. Hiser and F. J. Loss

1.4.1 Background

It has been well documented that neutron irradiation of some steels can produce substantial temperature elevation of the brittle-to-ductile transition region and a reduction in upper shelf toughness. In many instances, the weld material shows the greatest change in properties, particularly when relatively high levels of copper and/or nickel are present. The primary objective of the HSST 4th irradiation is to statistically characterize the irradiation degradation of several materials representative of current steel production practice. Specifically, four submerged-arc weld deposits and the HSST reference plate 02G material were included. These materials are nominally of A 533 Grade B Class 1 chemical compositions with varying copper and nickel contents, and were irradiated to a target fluence of 1.5×10^{19} n/cm^2, E > 1 MeV. Sufficient specimens were machined to obtain the statistical analysis of property changes with irradiation. A second objective of the program is to test the level of correspondence between two independent laboratories in making such determinations. Thus, the specimens are being tested by MEA and ORNL with each laboratory testing approximately half of the specimens. However, tensile property determination was performed exclusively by ORNL.

1.4.2 Summary of Fracture Toughness Results

For ease of identification, the four weld materials were each given the code numbers 68W, 69W, 70W and 71W; the plate was identified as 02G. Nominal fabrication and irradiation parameters for the five materials are given in Table 1.11. Note that weld 68W has the lowest combined Cu and Ni content. The average neutron fluence in the table has a standard deviation of ~ 26% for every material. A detailed dosimetry analysis is given in References 9 and 10.

Table 1.11 Material Parameters

Material Code	Welding Flux	Cu (wt %)	Ni (wt %)	Average Fluence (n/cm^2 x 10^{18} E > 1 MeV)	Weld Groove Geometry
Weld 68W	Linde 91	0.04	0.13	13.5	St. Wall Groove
Weld 69W	Linde 91	0.12	0.10	13.1	Dbl. U Groove, Cyl. Constant
Weld 70W	Linde 124	0.056	0.63	19.7	Dbl. V Groove
Weld 71W	Linde 80	0.046	0.63	20.0	Dbl. V Groove
Plate 02G	—	0.14	0.67	19.9	—

Specimens of three types were machined from each of the five materials: standard type A Charpy (C_v), tensiles (5.5-cm long x 0.452-cm diameter) and 2.54 cm-thick compact toughness (1T-CT) specimens. The 1T-CT specimens were modified to allow measurement of load-line deflection for J-integral testing. Specimens machined from weld material were oriented such that the failure plane was parallel to the weld axis and perpendicular to the weld crown. Plate specimens were machined in the T-L orientation. Compact specimens tested on the upper shelf were side grooved by 10% of the thickness on each side for a total reduction in thickness of 20%. Specimens tested in the transition temperature region were not side grooved.

Testing of all compact specimens was performed using the single specimen compliance (SSC) technique (Refs. 11 and 12). For transition temperature region tests, the procedure was modified by excluding crack length determination unloadings during the initial elastic portion of specimen loading. Values of the J integral were calculated using the modified version known as J_M as proposed by Ernst (Ref. 8). Initiation toughness (J_{Ic} and K_{Jc}) and tearing modulus (T) values determined using the power-law procedure of Loss, et al. (Refs. 11 and 12).

Results from Charpy V-notch (C_v) tests performed jointly by MEA and ORNL in both the irradiated and unirradiated conditions are summarized in Table 1.12. Note that results for Plate 02 show the greatest change due to irradiation in both the upper shelf level and the brittle-to-ductile transition temperature shift. Results for weld 68W

Table 1.12 Irradiation-Induced Charpy Property Degradation

Material	Observed transition[a] temperature shift	Observed upper shelf energy change
Plate HSST-02	68	-16
Weld 68W	6	9
Weld 69W	34	-3
Weld 70W	31	-10
Weld 71W	26	8

[a] Indexed at the 41 J level

show the smallest change in properties. Thus, the irradiation sensitivity, as evidenced by C_v results, directly corresponds with the copper and nickel content in the material. The greatest sensitivity occurs in the materials with higher copper and/or nickel content, i.e., Plate 02 and weld 69W. When both elements are reduced, very little change is observed (weld 68W). Historically, both phosphorus

and sulfur have been shown to induce radiation sensitivity. However, in all the subject materials both elements were low, i.e., less than 0.014 wt.%. Charpy results are discussed in greater detail in Ref. 13.

Tensile testing was performed by ORNL and the results are summarized in Table 1.13. The same direct correspondence between copper and nickel content and radiation effect observed in Charpy results is also indicated by ultimate strength results. However, this trend is not evidenced by the yield strength data. In general, the yield strength was affected more than the ultimate strength by irradiation and Plate 02 material showed the greatest change in properties.

Table 1.13 Average Tensile Strength[a]

Material	$\sigma_{Y,U}$ (MPa)	$\sigma_{Y,I}$ (MPa)	$\frac{\sigma_{Y,I} - \sigma_{Y,U}}{\sigma_{Y,U}}$ (%)	$\sigma_{U,U}$ (MPa)	$\sigma_{U,I}$ (MPa)	$\frac{\sigma_{U,I} - \sigma_{U,U}}{\sigma_{U,U}}$ (%)
Plate 02	432	564	31	590	707	20
Weld 68W	496	590	19	604	620	3
Weld 69W	584	672	15	692	752	9
Weld 70W	440	493	12	562	608	8
Weld 71W	430	489	14	563	602	7

[a] where

$\sigma_{Y,U}$ = average unirradiated yield strength from 22°C to 288°C

$\sigma_{Y,I}$ = average irradiated yield strength from 22°C to 288°C

$\sigma_{U,U}$ = average unirradiated ultimate strength from 22°C to 288°C

$\sigma_{Y,U}$ = average irradiated ultimate strenth from 22°C to 288°C

J-R curves obtained from upper shelf tests at 121°C, 200°C and 288°C are illustrated in Figs. 1.22, 1.23 and 1.24 in a tearing instability format showing the variation of J_M with the material tearing modulus, T_{Mat}. The R curves result from the plotting the power law curve fit of the J_M and crack extension data in terms of J_M and T_{Mat}. Data symbols indicate crack extension at J_{Ic} (lower right), 0.5 mm, 1 mm, 1.5 mm and 2.0 mm, respectively.

It is clear in these figures that the R curve levels are generally reduced with both irradiation and with increased test temperature. Note that both the J level, and to a greater extent the tearing

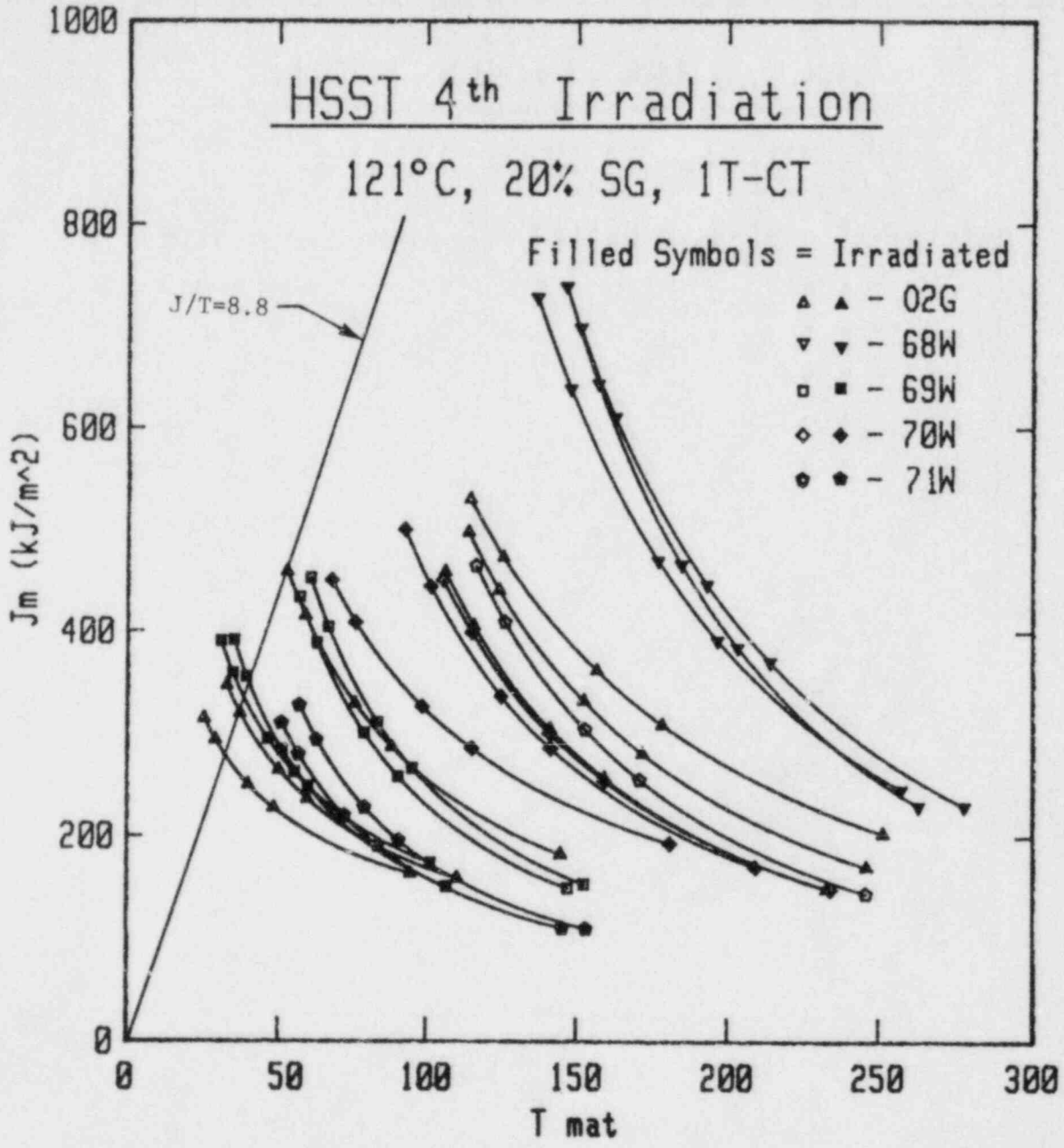

Figure 1.22 Instability diagram illustrating the effect of irradiation and copper-nickel content on J-R curves obtained at 121°C.

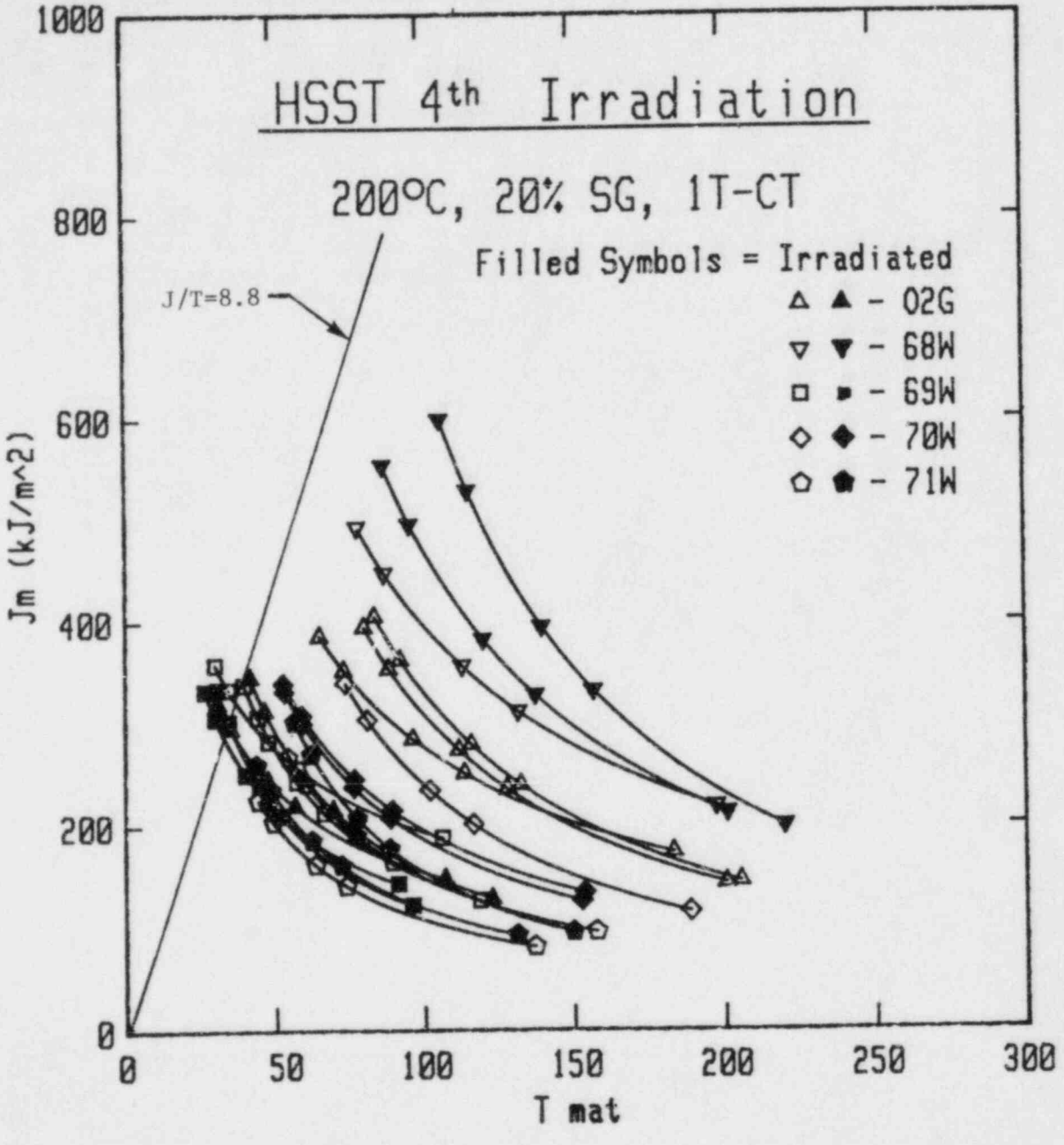

Figure 1.23 Instability diagram illustrating the effect of irradiation and copper-nickel content on J-R curves obtained at 200°C.

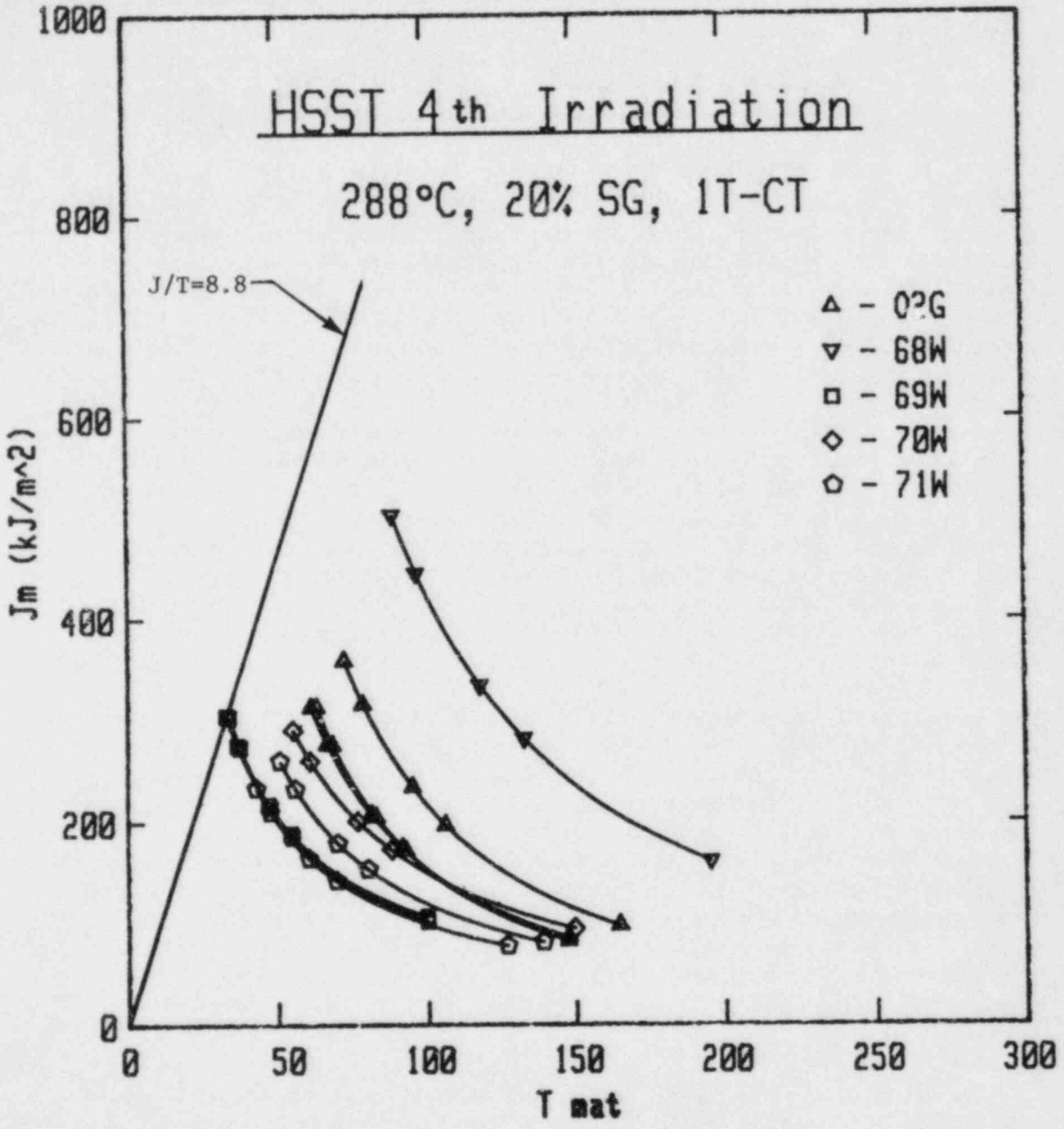

Figure 1.24 Instability diagram showing J-R curves for unirradiated material obtained at 288°C. Note the substantial drop in toughness level from that of the R curves obtained at lower temperature (Figs. 1.22 and 1.23).

modulus, is reduced. In addition, there is a direct correspondence between the R curve response to irradiation and the copper and nickel content. As with the Charpy and tensile results, the greatest effect of irradiation occurs with the R curves from those materials with the highest copper and nickel content.

The fracture behavior, in terms of the quasi-elastic parameter K_{Jc}, is illustrated in Figs. 1.25 through 1.29. In these figures, the solid trend lines are the resulting regression curves fit to all data points. A linear regression was used for upper shelf data and an exponential regression was used to fit transition region data. Shifts in transition temperature were calculated using the exponential curve fit equations.

Transition region data for Plate 02 material (Fig. 1.25) indicate the greatest shift in the transition to higher temperature. Moreover, the data indicate a substantial change in the shape of the irradiated transition curve from that of the unirradiated. The material with the second highest copper content but low nickel (weld 69W) indicates the second greatest shift in transition temperature (Fig. 1.26) Here, however, there is less of a change in the transition curve shape. Welds 70W and 71W (Figs. 1.27 and 1.28) have low copper but high nickel contents. The observed transition shift with these welds is relatively small compared with that for Plate 02 and weld 69W, thus indicating that nickel does not affect as large a change as does copper. The material with the lowest combined copper-nickel content (weld 68W) also showed the least radiation effects. The shift in transition temperature (Fig. 1.29) of 8°C is almost insignificant when compared with that for Plate 02 and weld 69W. In addition, this material has the highest upper shelf toughness of the five materials investigated.

The transition temperature shift for all five materials is summarized in Fig. 1.30. In this figure, the shifts indicated by the Charpy results (Ref. 13) are directly compared with those based upon K_{Jc} and $K_{\beta c}$. The $K_{\beta c}$ parameter results from correcting K_{Jc} values using the Irwin-Merkle β_{Ic} correction (Refs. 14 and 15). This correction accounts for the lack of constraint in test specimens from that required by linear elastic fracture mechanics criteria. The transition temperature shifts of Fig. 1.30 are indexed at the 41 J, 125 MPa$\sqrt{m}$ and 90 MPa$\sqrt{m}$ levels for Charpy, K_{Jc} and $K_{\beta c}$, respectively. The $K_{\beta c}$ index roughly corresponds to the 125 MPa$\sqrt{m}$ K_{Jc} index, i.e., for these five materials β_{Ic} correction at the 125 MPa$\sqrt{m}$ results in a $K_{\beta c}$ level of 90 ± 5 MPa$\sqrt{m}$.

It is clear in Fig. 1.30 that the transition temperature shift is reduced by decreasing both the copper and the nickel content. Reducing either one separately does not produce as substantial a change in the shift as reducing both. Although the magnitude of the transition temperature increase varies somewhat between the three parameters, all three suport this observation.

In terms of initiation fracture toughness, J_{Ic} and K_{Jc}, the upper shelf level was essentially insensitive to all variables, i.e.,

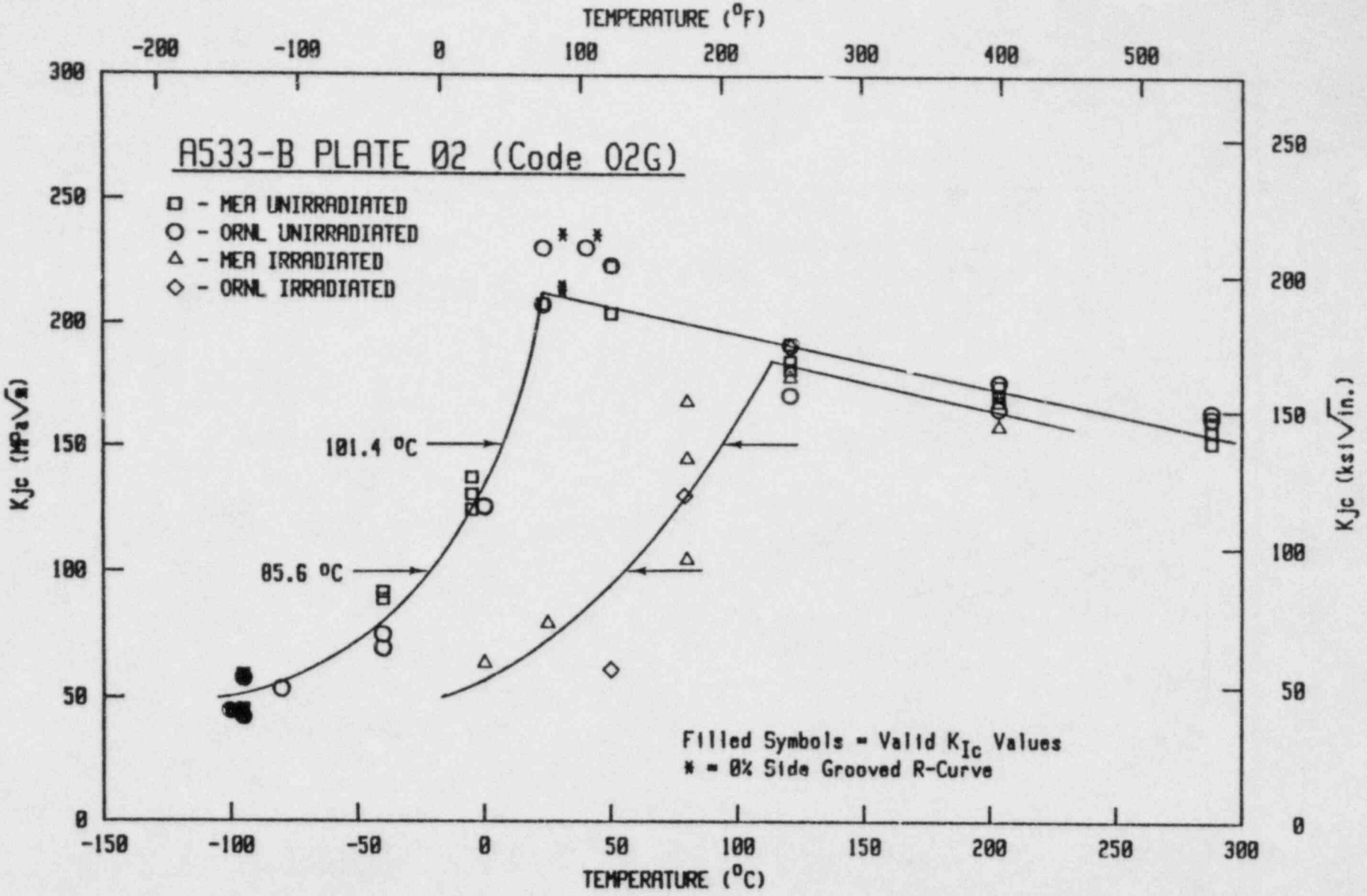

Figure 1.25 Variation of initiation fracture toughness, K_{Jc}, with temperature for Plate 02 material. Note the apparent change in shape of the transition curve with irradiation.

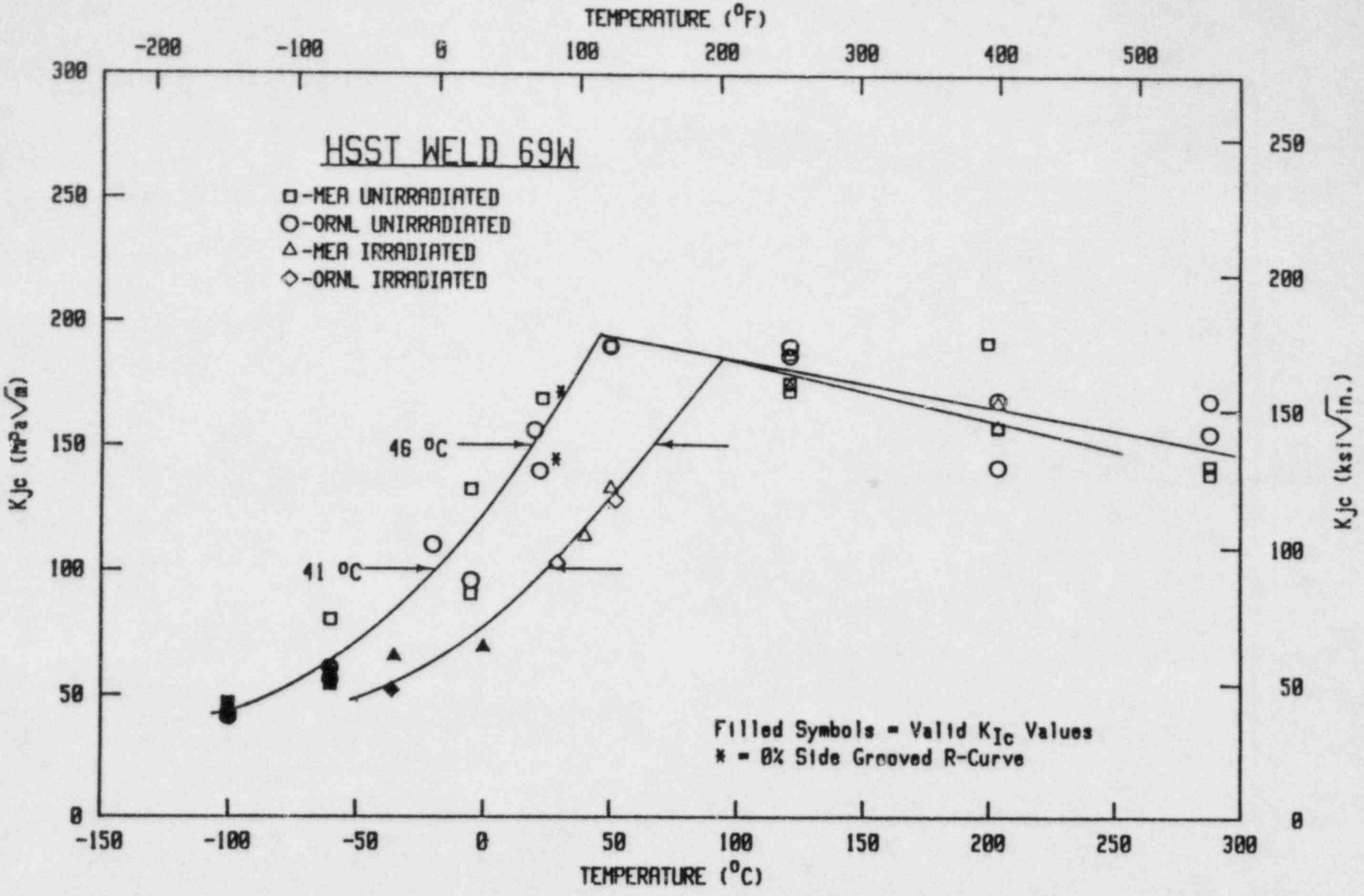

Figure 1.26 Variation of initiation fracture toughness, K_{Jc}, with temperature for Weld 69W. Note the small change in shape of the transition curve with irradiation.

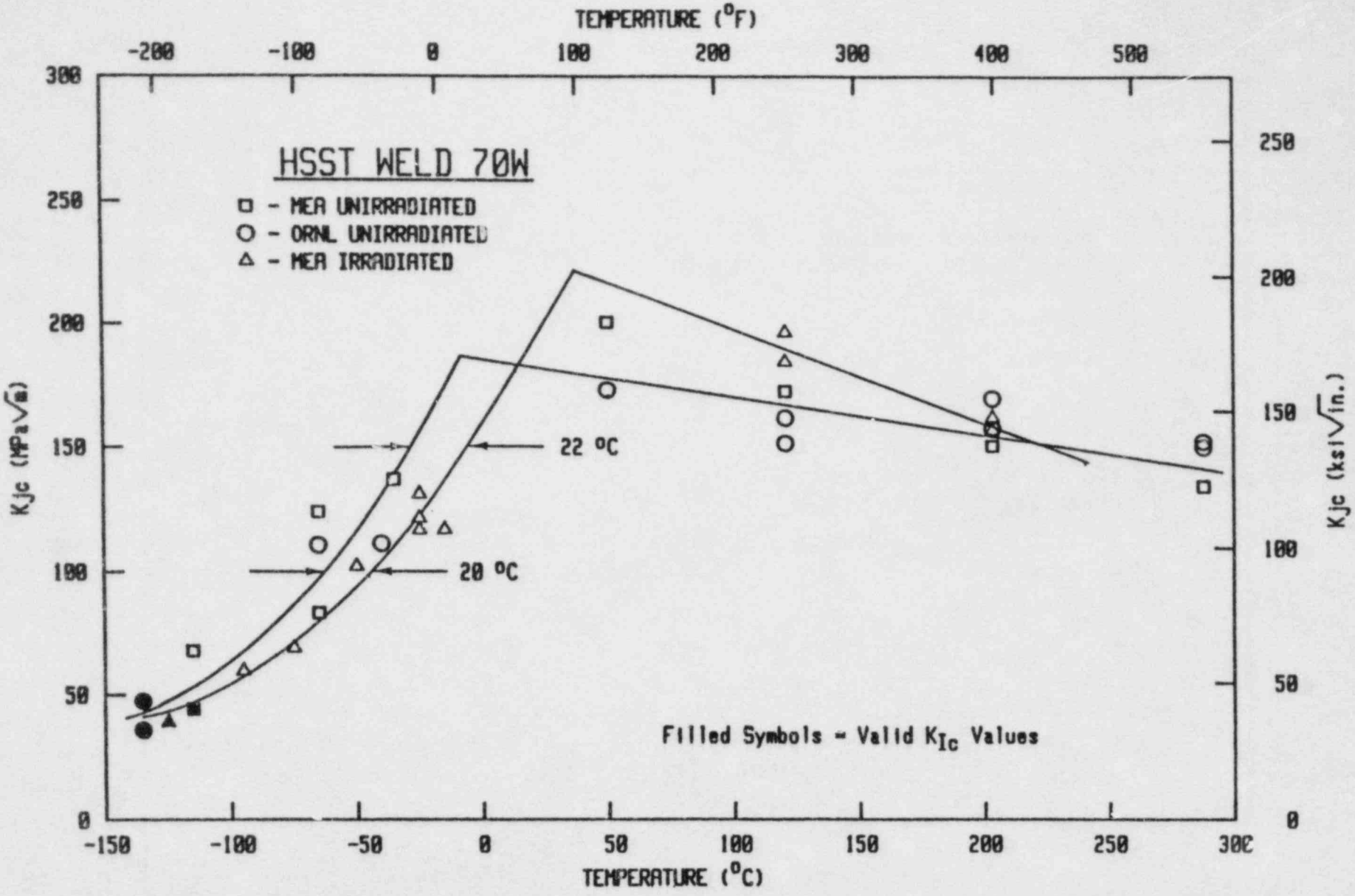

Figure 1.27 Variation of initiation fracture toughness, K_{Jc}, with temperature for Weld 70W.

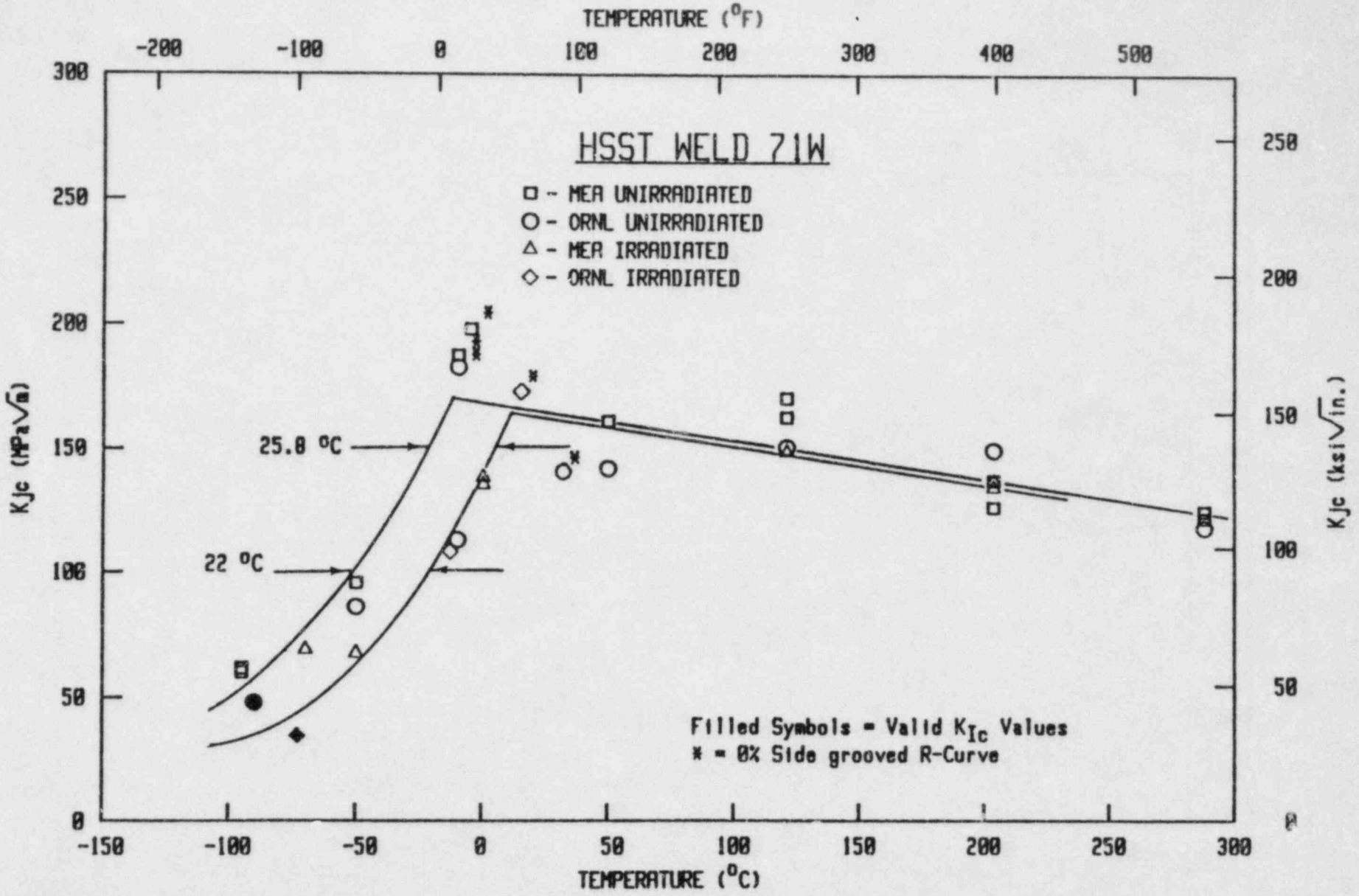

Figure 1.28 Variation of initiation fracture toughness, K_{Jc}, with temperature for Weld 71W.

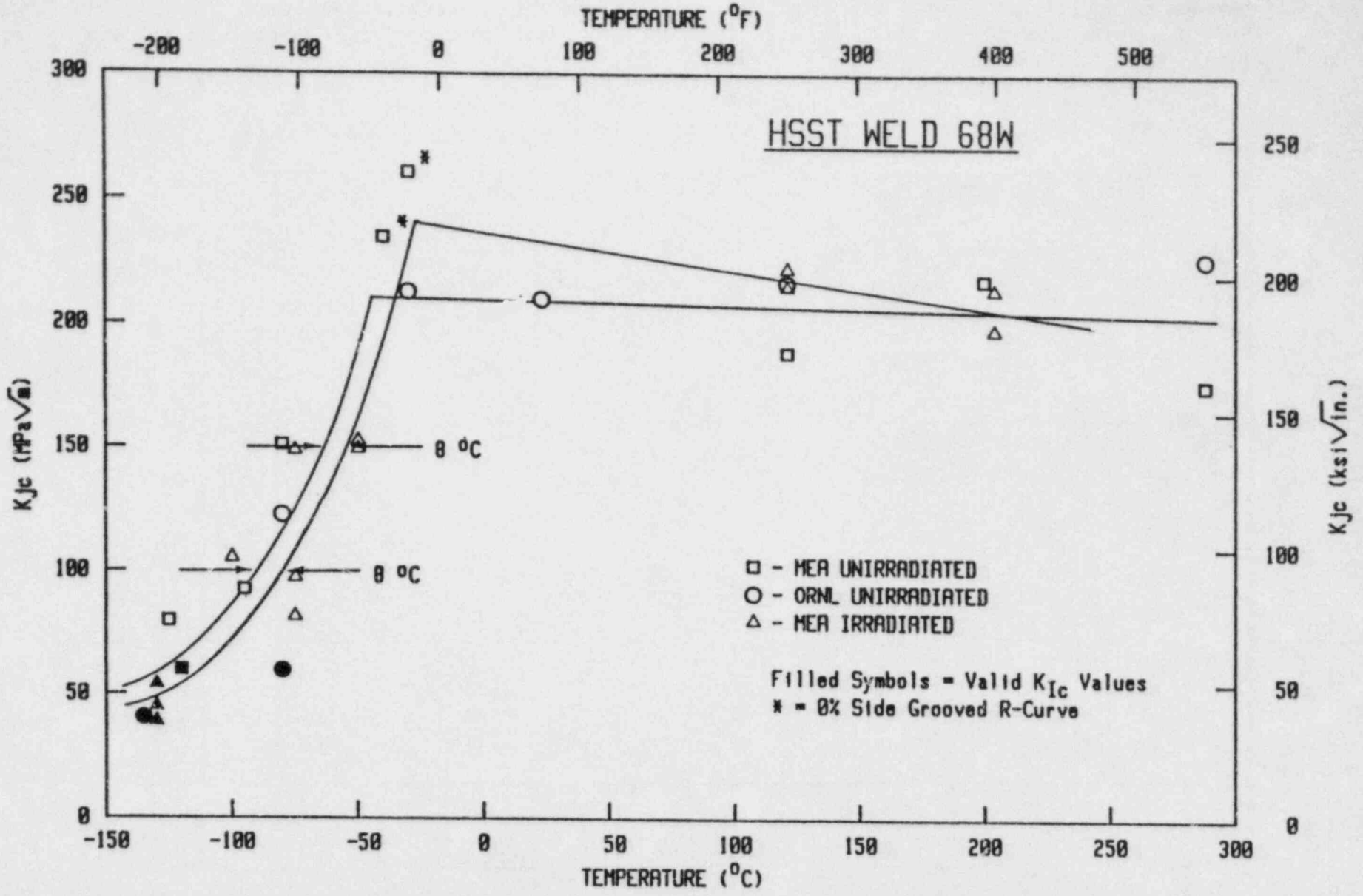

Figure 1.29 Variation of initiation fracture toughness, K_{Jc}, with temperature for Weld 68W. This material had the lowest copper-nickel content and exhibits the least radiation effects.

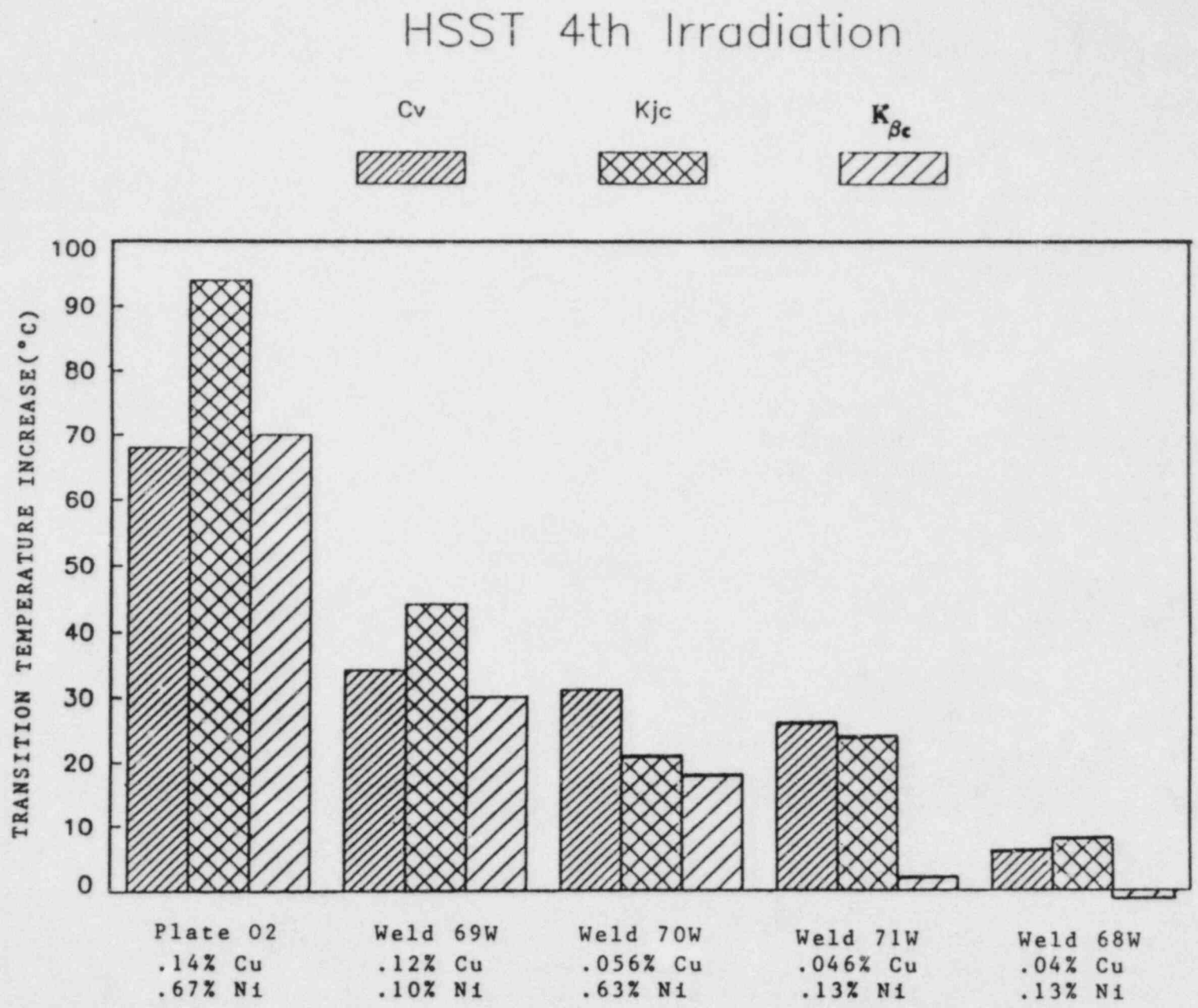

Figure 1.30 Summary illustration comparing the shift in the brittle-to-ductile transition as indicated by Charpy, K_{Jc} and $K_{\beta c}$ results. Note the direct correspondence between copper-nickel content and the magnitude of the transition temperature shift.

radiation, copper content and nickel content appeared to have little effect. However, the effect on the overall J-R curves was directly related to the copper-nickel content as discussed earlier.

Regarding the shape of the brittle-to-ductile transition curve before and after irradiation, the data indicate that for small shifts, the shape does not change. However, as the shift to higher temperature increases the irradiated curve appears to rise less sharply. This observation may be significant, particularly for high copper-nickel materials used in some older reactor vessel construction. Currently structural integrity assessments, in part, are based on the assumption the K_{Ic} curve does not change shape with shifts to higher temperature. Additional research in this area is required and will be specifically addressed by the HSST subtask on the K_{Ic} curve shift being conducted at ORNL and MEA under NRC sponsorship.

2.0. ENVIRONMENTALLY-ASSISTED CRACK GROWTH IN LWR MATERIALS

W. H. Cullen

Research on fatigue crack growth rates of pressure vessel and piping steels in LWR environments has demonstrated that there are a number of critical variables which influence these results. Chief among these are test frequency, load ratio, material chemistry, dissolved oxygen content, and waveform. The magnitude of influence of each of these has been reasonably well determined, although synergistic interactions of these (load ratio + cyclic frequency + material chemistry) have not been carefully defined, and in fact, are just being recognized for the effects which they manifest.

Tests are conducted using compact specimens of various piping and pressure vessel steels. Usually a test matrix is designed to encompass a specific variable, such as temperature or crack plane orientation, while keeping other variables fixed, in order to better ascertain the influence of the variable of interest. Tests are carried out in typical PWR-grade water (Table 2.1) using a testing methodology which has been developed specifically for this type of fatigue crack growth rate evaluation. The testing and data processing methods, including post-test correction procedures have been described in a recent report (Ref. 16).

Table 2.1. Water Chemistry Specifications

Boron (as boric acid)	1000 ppm
Lithium (as lithium hydroxide)	1 ppm
Chloride ions	< 0.15 ppm
Fluoride ions	< 0.10 ppm
Dissolved oxygen	~ 1 ppb
Dissolved hydrogen (saturation)	30 to 50 cm^3/kg water

All other metallic or ionic species should be at about trace levels. Some iron, both in solid and soluble form is the inevitable result of a corroding specimen.

While the primary interest is the fatigue crack growth rate data itself, the interpretation of these data is also of importance. The degree of influence of each of the critical variables is taken into account, and fractographic interpretation of the fatigue fracture surfaces often suggests some characteristic of the micromechanism of the environmentally-enhanced crack advancement. Several of the studies in this task are supported by fractographic studies, and some of these results are included in this review.

2.1. Temperature Dependence of Fatigue Crack Growth in Irradiated A 508 Steel

Recently, a NUREG report was published which described the effect of temperature on the fatigue crack growth rates of A 508-2 steel over a range from 93°C to 288°C (Ref. 17). For these tests conducted in the low dissolved oxygen environment, it was found that there was a minimum in the crack growth rates at a temperature of about 200°C. Examination of the fractography showed that brittle appearing features covered the fatigue fracture surfaces of the specimens tested at all the temperatures, but that the percentage of fan-shaped features seemed to increase with temperature. An X-ray diffraction chracterization of the oxides on the fatigue fracture surface showed that magnetite formed at all temperatures.

As a logical follow-on to this investigation, three 1T-CT specimens of the same heat of steel (material chemistries and mechanical properties are shown in Table 2.2) were irradiated to a typical end-of-life fluence, and were tested at three temperatures spanning a range from 200°C to 288°C. The testing methodology followed that described in an earlier report on crack growth in irradiated pressure vessel steels. The test parameters on each of the three specimens were identical: R = 0.2, 17 mHz sinusoidal waveform, and PWR conditions.

Table 2.2. Chemical Composition of A 508-2 Steel Used in Irradiated Tests

Element	C	S	Si	Mo	Ni	Mn	Cr	V	P
A 508-2 Code Q-71	0.19	0.009	0.31	0.62	0.82	0.69	0.38	0.13	0.007

Yield Strength, 0.2% Offset -- 546 MPa (79.2 ksi)
Ultimate Tensile Strength -- 686 MPa (99.5 ksi)
(Each value is average of two tests at room temperature)

When differentiated, the three data sets appear as shown in Fig. 2.1. For comparison, the results for unirradiated steels at two of the same temperatures are shown in Fig. 2.2. It can be seen that the results are essentially independent of the irradiation. A direct comparison of the results is shown in Fig. 2.3 in which crack growth rates at specific values of ΔK are shown for the entire temperature range. There is almost perfect agreement between the irradiated and unirradiated cases. This fact provides additional confirmation that irradiation does not aggravate the environmentally-enhanced fatigue crack growth rates to any degree beyond that of the environment alone.

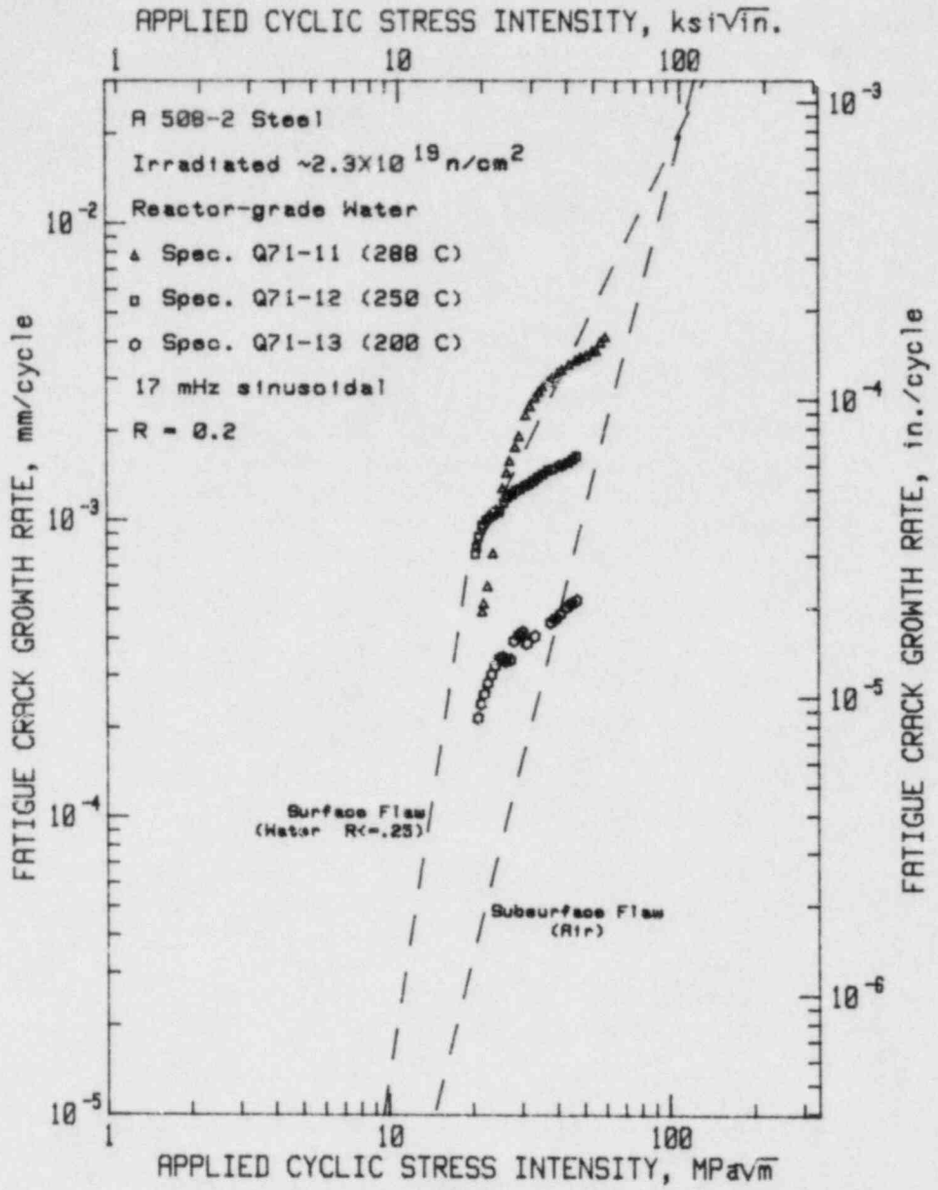

Figure 2.1 Fatigue crack growth rates vs. applied cyclic stress intensity factor for irradiated A 508-2 steel at different temperatures.

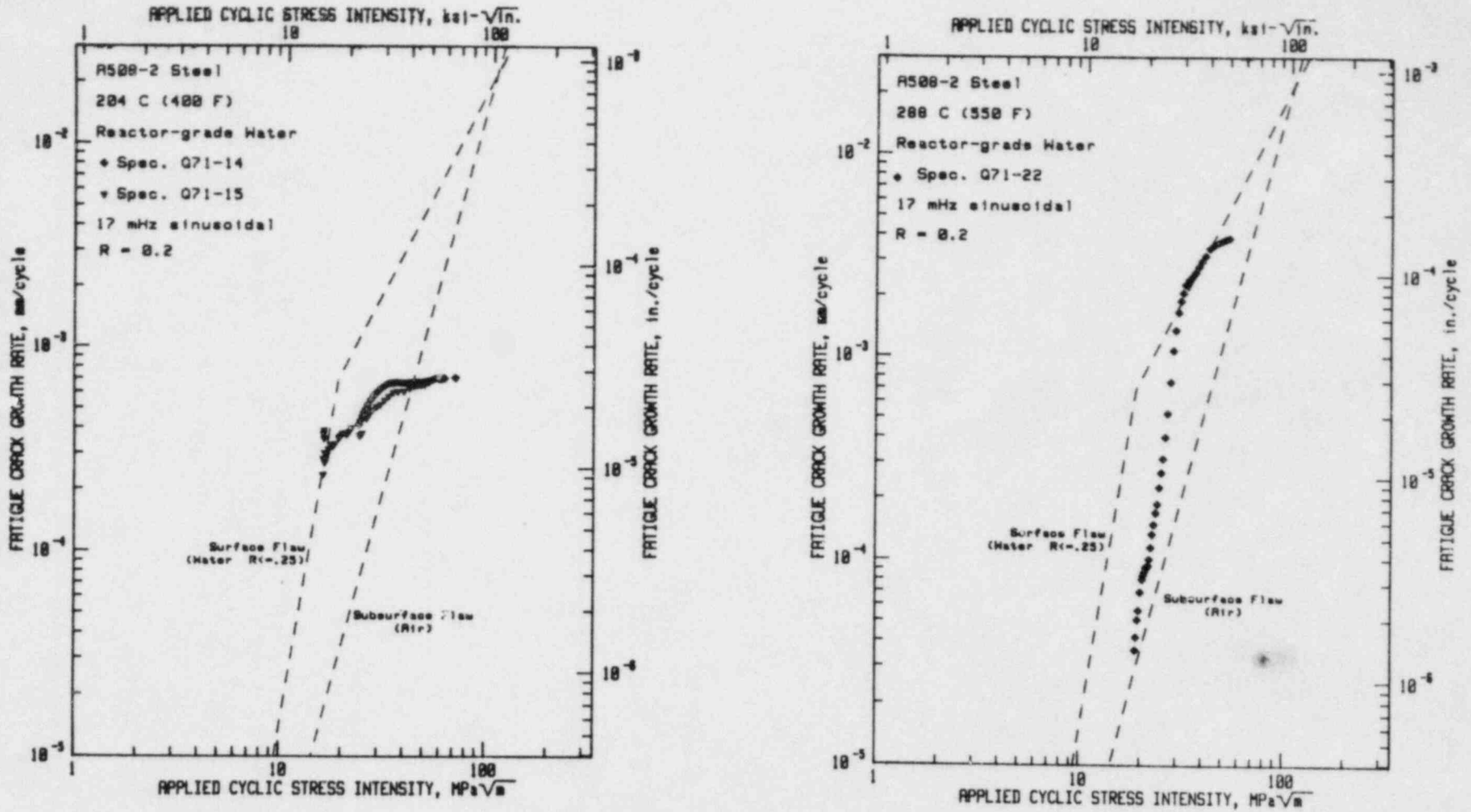

Figure 2.2 Fatigue crack growth rates vs. applied cyclic stress intensity factor for unirradiated A 508-2 steel at different temperatures: 204°C on the left, and 288°C on the right.

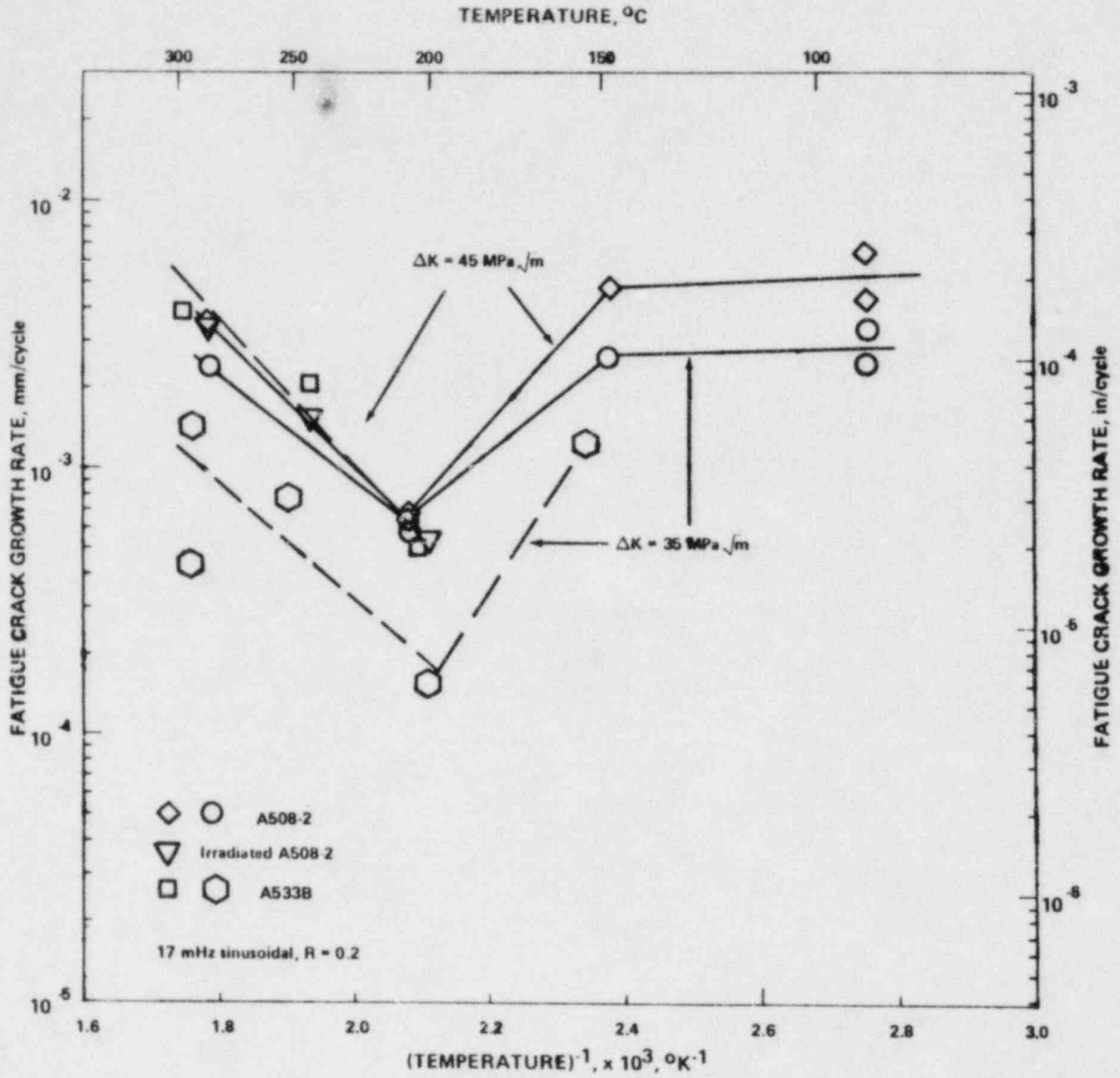

Figure 2.3 Fatigue crack growth rates at specific ΔK values vs. reciprocal temperature for irradiated and unirradiated A 508-2 steel. Data from Atkinson (Ref. 18), on A 533-B steel is for comparison.

2.2. Influence of Sulfur Content on Fatigue Crack Growth

In order to determine directly the influence of sulfur chemistry, and to provide an intralaboratory comparison using the same heats of steel tested at other research facilities, MEA has undertaken a task to perform two multispecimen tests. Each of these multispecimen assemblies contains specimens from three heats of A 533-B; the heat codes and sulfur contents are W7 - 0.004%, 1HT - 0.013%, and CQ2 - 0.025%. The first of these tests, conducted in water with a very low flow rate (~ 50 liters/hr.), has been completed. The second test, at a much higher flow rate (~ 3600 liters/ hr.) will begin in early 1984. The chemical compositions for these steels are given in Table 2.3.

Table 2.3 Chemical Composition of the Heats of A 533-B Used in the Sulfur Effects Study

Element	C	S	Si	Mo	Ni	Mn	P	Cu
W7 Code	0.23	0.004	0.25	0.57	0.70	1.40	0.005	----
1HT Code	0.21	0.013	0.31	----	0.63	1.35	0.017	----
CQ2 Code	0.21	0.025	0.24	0.53	0.56	1.28	0.006	0.12

When using indirect methods (compliance, electric potential drop, etc.) to monitor fatigue crack extension, it is extremely important to assure that the final crack length can be measured exactly in order to provide confirmation that the indirect method was accurate. This means that no specimen can be allowed to break unexpectedly, thus obliterating any clear beachmark which would serve as a reference point for the final crack length. However, when conducting multispecimen tests, the normal occurence is that one or more specimens will propagate to the predetermined final crack length ahead of the others in the daisy chain. At this point, the test is interrupted, the test frequency is increased to 1 Hz, and the loads are dropped to 50% of their test values. Under this combination, the specimens with the longest crack lengths will continue their crack advance, leaving behind a clear beachmark, while the specimens with shorter crack lengths, and hence lower ΔK values, will show little, if any, crack extension. When the specimens with the longer cracks actually fail, the test is again interrupted, the test parameters are restored to their original load amplitude and frequency values, and the test is continued. At some other time, another specimen will reach its final crack length and the procedure is repeated, until all four specimens in the daisy chain have completed the test objectives.

For the sulfur level test series described above, the a vs. N plot which results from the multispecimen test is shown in Fig. 2.4. This shows that the two specimens with the highest sulfur content (CQ2 and 1HT), exhibited high crack growth rates and achieved their final (CQ2) or nearly final (1HT) crack lengths at the same time. When the loads were reduced, both of these specimens broke, as anticipated. The loads and test frequency were restored to the desired values and the

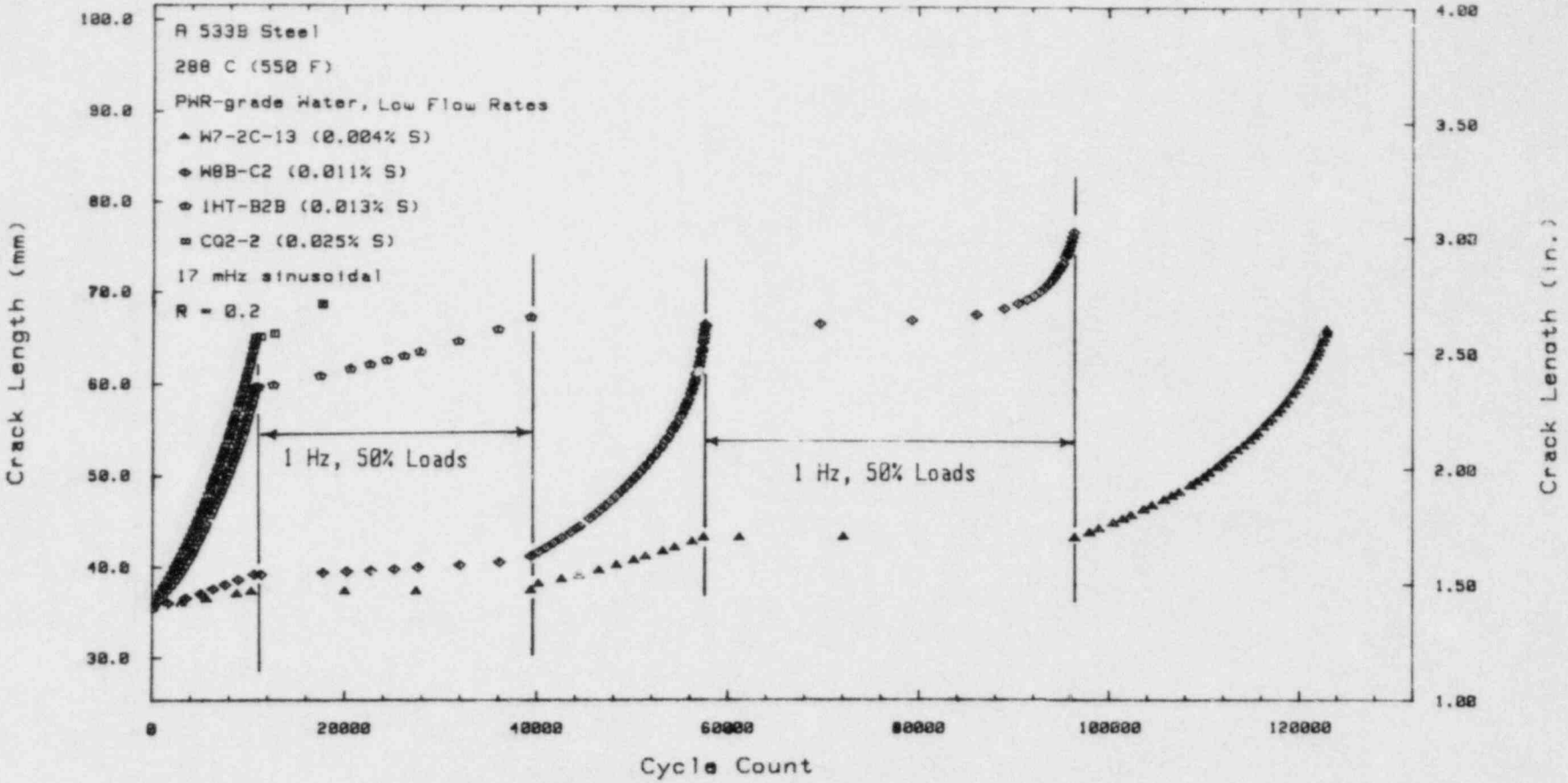

Figure 2.4 Crack length vs. cycles for a multispecimen test of steels of differing sulfur contents. This graph shows the relative crack extensions of specimens of differing crack lengths during the periods of cycling at either 1 Hz, or 17 mHz.

test was continued on the two remaining specimens. Eventually, specimen W8B-C2 achieved its target crack length and the loads were again reduced and the test frequency was increased. After specimen W8B-C2 broke, the test was resumed on specimen W7-2C-13 until it achieved its final crack length, at which point the test was terminated.

After final measurements and post-test corrections, the data can be plotted in final form, shown in Fig. 2.5. This figure clearly shows that the steels with the highest sulfur content exhibit the highest fatigue crack growth rates. Fortunately, even the highest of the growth rates do not exceed significantly the ASME reference lines.

2.3. Fatigue Crack Growth in A 351-CF8A Cast Stainless Steel

Because the low-alloy steels exhibited a strong dependence on temperature, a series of tests of this cast stainless steel were carried out over a temperature range from 93°C to 338°C. Specimens were cut from a section of a decommissioned research pressure vessel which was 0.8-m diameter, 57-mm wall thickness (32-in. diameter, 2.25-in. wall thickness). The chemical composition and mechanical properties of this steel are given in Table 2.4. The results of this investigation, for the three highest test temperatures, are shown in Figs. 2.6 through 2.8. In each case, two crack plane orientations were chosen, but the results indicate no measurable difference in crack growth rates between the two. In general, the fatigue crack growth rates increase slightly with temperature, over the range shown in the figures.

Table 2.4. Chemical Composition and Mechanical Properties of SA 351-CF8A Steel

Element	C	Mn	Si	Cr	Ni	Co	P	S
A9 Code	0.06	0.68	1.17	20.42	8.58	0.07	0.020	0.018

At Room Temperature:
- Yield Strength, 0.2% Offset — 303 MPa (44.0 ksi)
- Ultimate Tensile Strength — 560 MPa (81.2 ksi)
- Elongation in 51 mm (2 in.) — 48%

At 343°C (650°F)
- Yield Strength, 0.2% Offset — 159 MPa (23.1 ksi)

A fractographic examination of the specimens showed that the main characteristic of the fatigue fracture surface was the brittle appearance. This behavior is similar to that of the low-alloy steels, but even more similar to the morphology found on stress-corrosion cracking surfaces of stainless steel specimens which have been sensitized, or specimens which have been tested in very aggressive environments. Many of these characteristics are illustrated in Figs. 2.9 through 2.11. In Fig. 2.9, examples of this brittle-appearing morphology are shown for specimen A9-70, tested at 288°C. The reader should note the

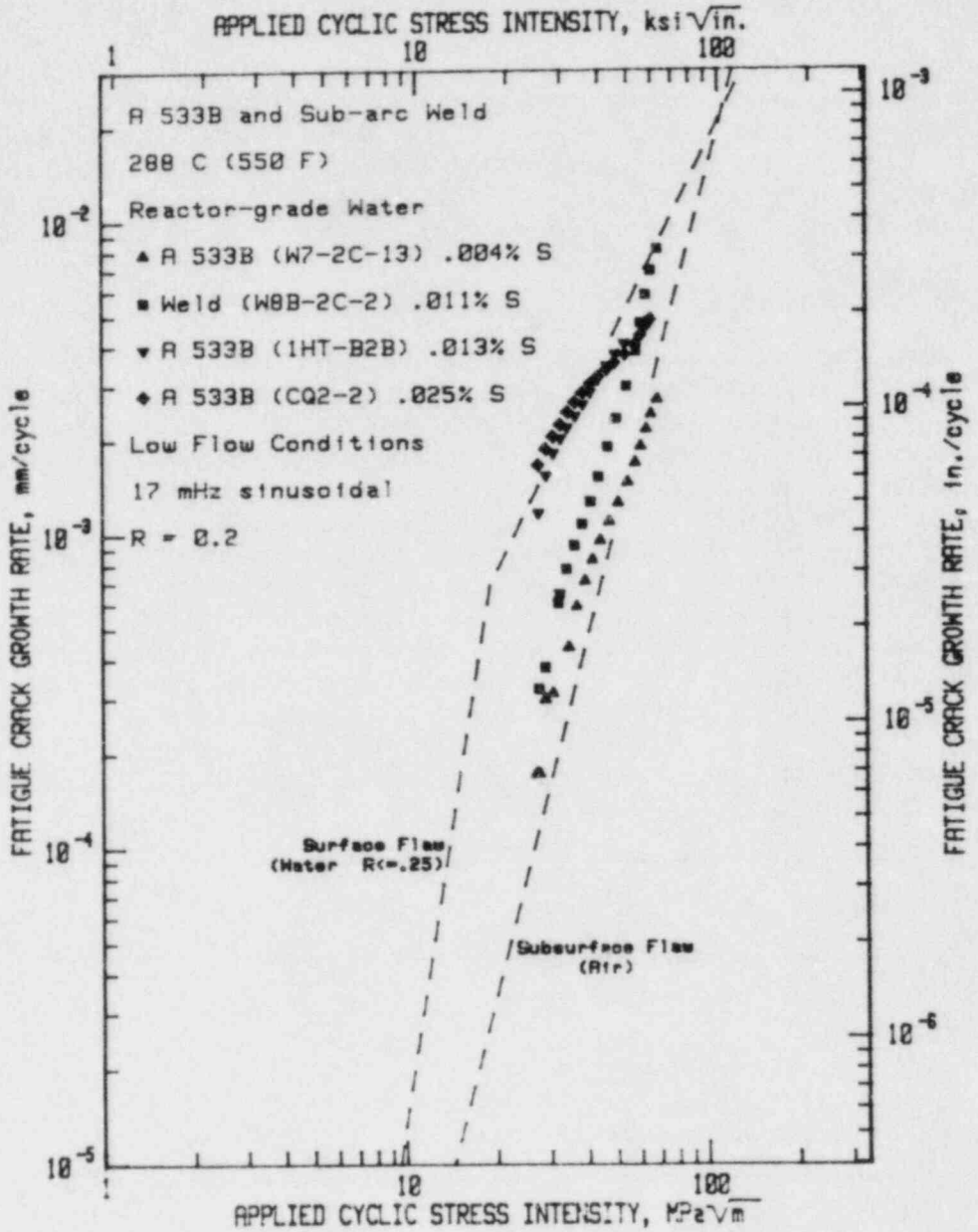

Figure 2.5 Fatigue crack growth rates vs. applied cyclic stress intensity factor for the tests of steels with differing sulfur contents. These tests were conducted at a low recirculation rate of about 50 liters per hour in a 150 liter autoclave.

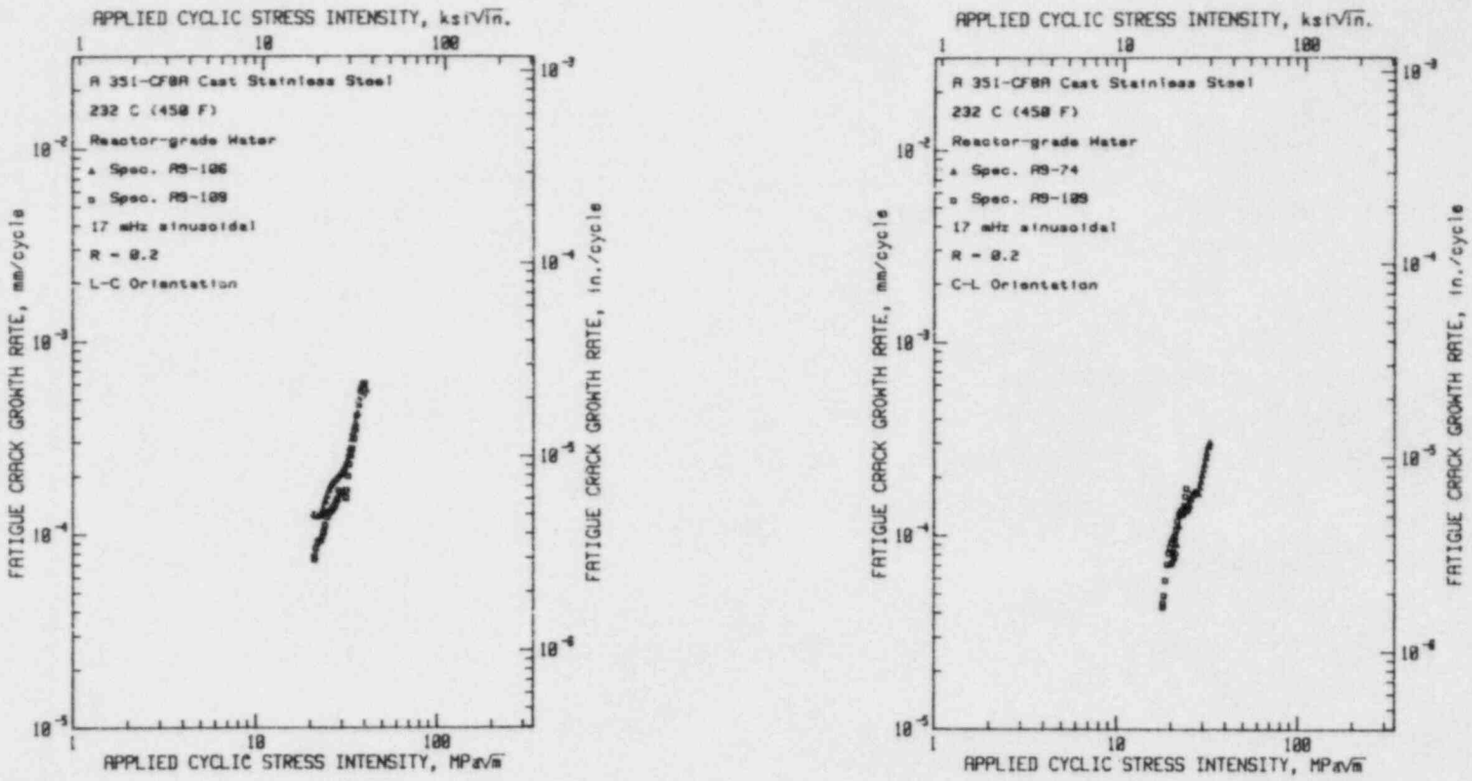

Figure 2.6 Fatigue crack growth rates vs. applied cyclic stress intensity factor for tests of SA 351-CF8A cast stainless steel in pressurized, high-temperature water at 232°C (450°F).

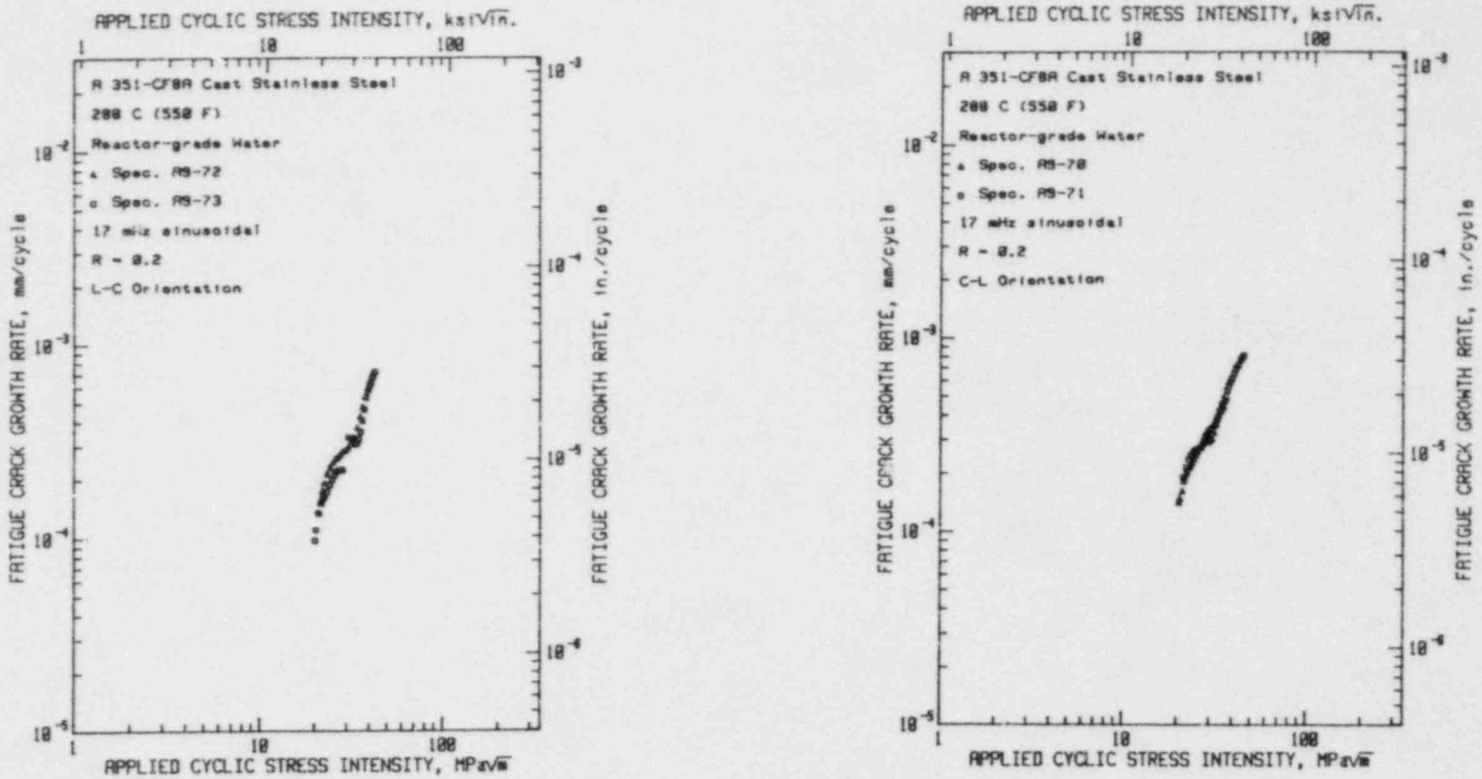

Figure 2.7 Fatigue crack growth rates vs. applied cyclic stress intensity factor for tests of SA 351-CF8A cast stainless steel in pressurized, high-temperature water at 288°C (550°F).

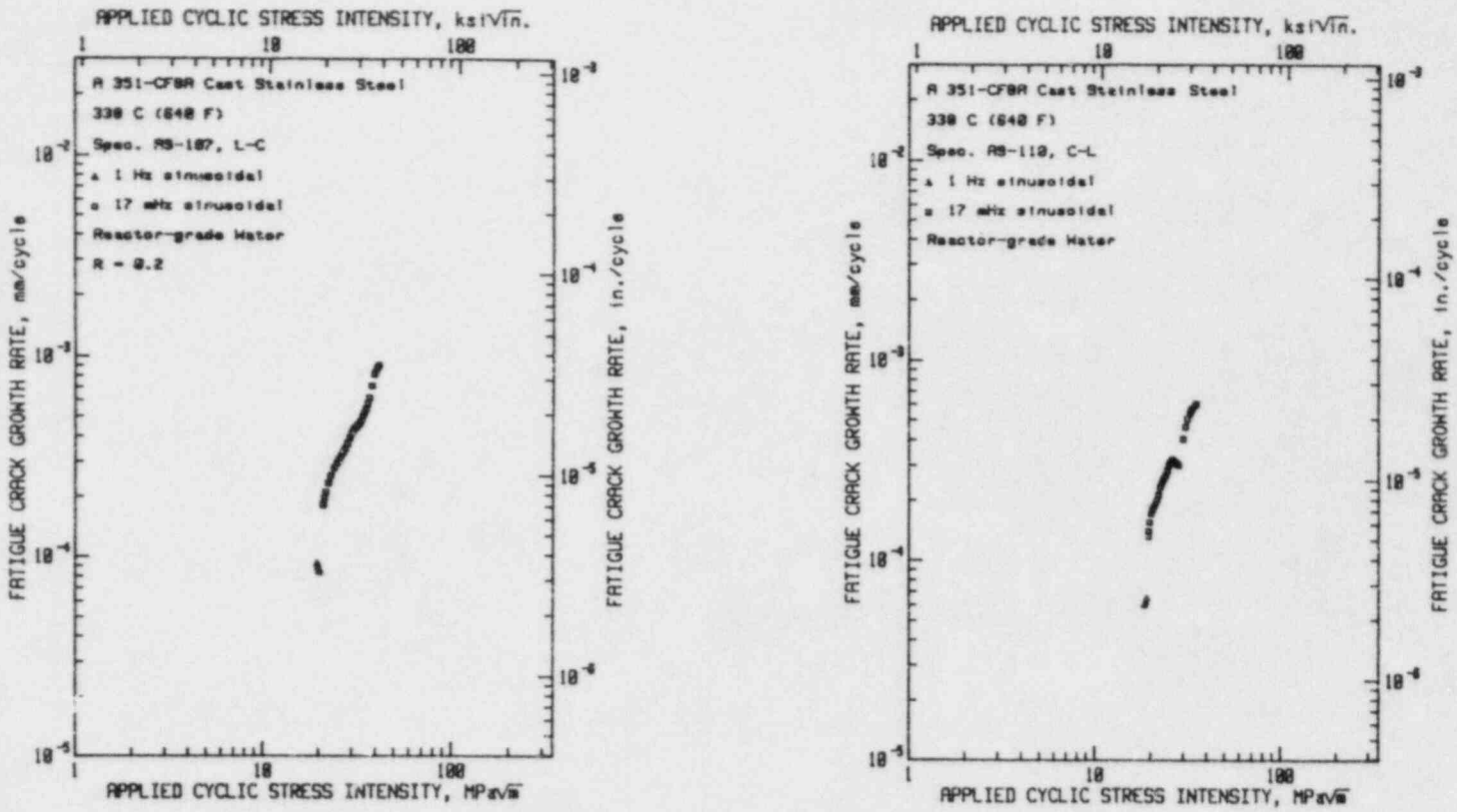

Figure 2.8 Fatigue crack growth rates vs. applied cyclic stress intensity factor for tests of SA 351-CF8A cast stainless steel in pressurized, high-temperature water at 338°C (640°F).

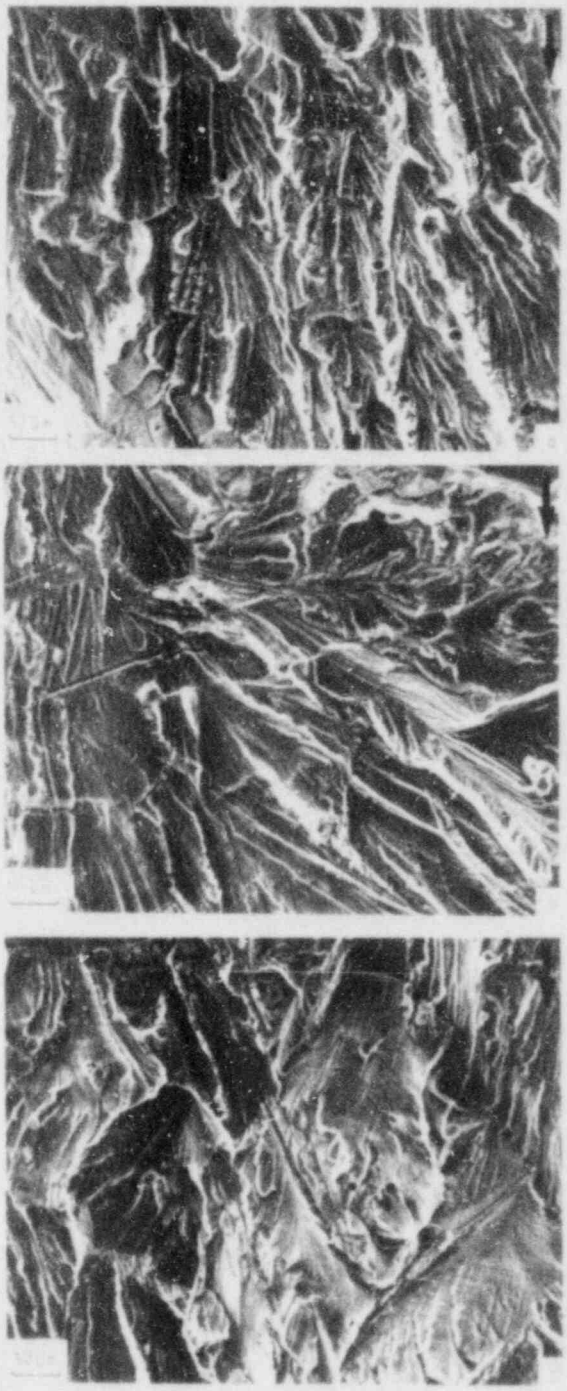

Figure 2.9 Fractographic features of environmentally-assisted fatigue crack growth in SA 351-CF8A cast stainless steel. $\Delta K \sim 25$ MPa$\sqrt{m}$ in (a) and (b); $\Delta K \sim 20$ MPa$\sqrt{m}$ in (c). Test temperature was 288°C. Note the fan-shaped features and overall brittle appearance.

Figure 2.10 Fractographic features of environmentally-assisted fatigue crack growth in SA 351-CF8A cast stainless steel. $\Delta K \sim 30$ MPa$\sqrt{m}$. Test temperature was 288°C. Brittle striations are shown in (a); ductile striations on a fan-shaped feature in (b) and fully ductile striations in (c).

Figure 2.11 Fractographic features of environmentally-assisted fatigue crack growth in SA 351-CF8A cast stainless steel. $\Delta K \sim 20$ MPa$\sqrt{m}$. Test temperature was 288°C. The linear features are slip steps which have been "decorated" with oxide.

fan-shaped features which cover the fracture surface. Many of these fan-shaped features have other markings, such as striations and slip lines. An extensive investigation showed that there were three basic combinations of features in which striations could be found. These are shown in Fig. 2.10. The top panel in this figure shows a high magnification view of "brittle-like" striations found on one of the fan-shaped features. The middle panel shows ductile striations found on a fan-shaped feature, and the bottom panel shows fully ductile striations found on transgranular fatigue fracture surfaces. Another unique feature found within the brittle-appearing regions is the presence of slip lines which have intersected the surface. These are especially visible in the scanning electron microscope because they appear to be "decorated" with oxide. Examples of these characteristics are shown in Fig. 2.11. A more complete description of these observations is contained in References 16 and 19.

2.4. Fatigue Crack Growth in Low-Carbon Piping Steels

Investigations are being carried out on two commonly used, low-carbon piping steels: A 516 Gr. 70, and A 106 Gr. C. In the case of A 516, the emphasis has been on the determination of orientation effects of the crack plane on fatigue crack growth. With A 106, the emphasis has been on load ratio and temperature effects. The chemical composition of these piping steels is given in Table 2.5. Two heats of A 106 were used in this study. Specimens coded FOP-37 through FOP-62 (inclusive) are designated as the "old" heat. Specimen codes FOP-63 through FOP-94 (inclusive) are designated the "new" heat.

Table 2.5. Chemical Composition of the Low-Carbon Piping Steels Examined in this Study.

Element	C	S	Si	Mo	Ni	Mn	Cr	V	P
A 106 Gr. C FOP (Old)	0.25	0.017	0.22	0.033	0.25	0.88	0.10	0.003	0.016
A 106 Gr. C FOP (New)	0.25	0.016	0.18	0.049	0.26	0.92	0.22	0.003	0.018
A 516 Gr. 70 FOK	0.25	0.017	0.23	0.065	0.27	1.05	0.10	0.002	0.018

Fatigue crack growth rate tests have been conducted on A 106 Gr. C at three test temperatures: 93°C, 288°C and 338°C (200°F, 550°F and 640°F). The specimens were fabricated from 83 mm (3-1/4 in.) wall, 0.81 m (32 in.) outside diameter pipe. The results for two orientations, LC and LR, and a test temperature of 93°C, are shown in Figs. 2.12 and 2.13. These are results from 1T specimens. 2T-CT specimens were used in tests at 288°C and 338°C. These results, for

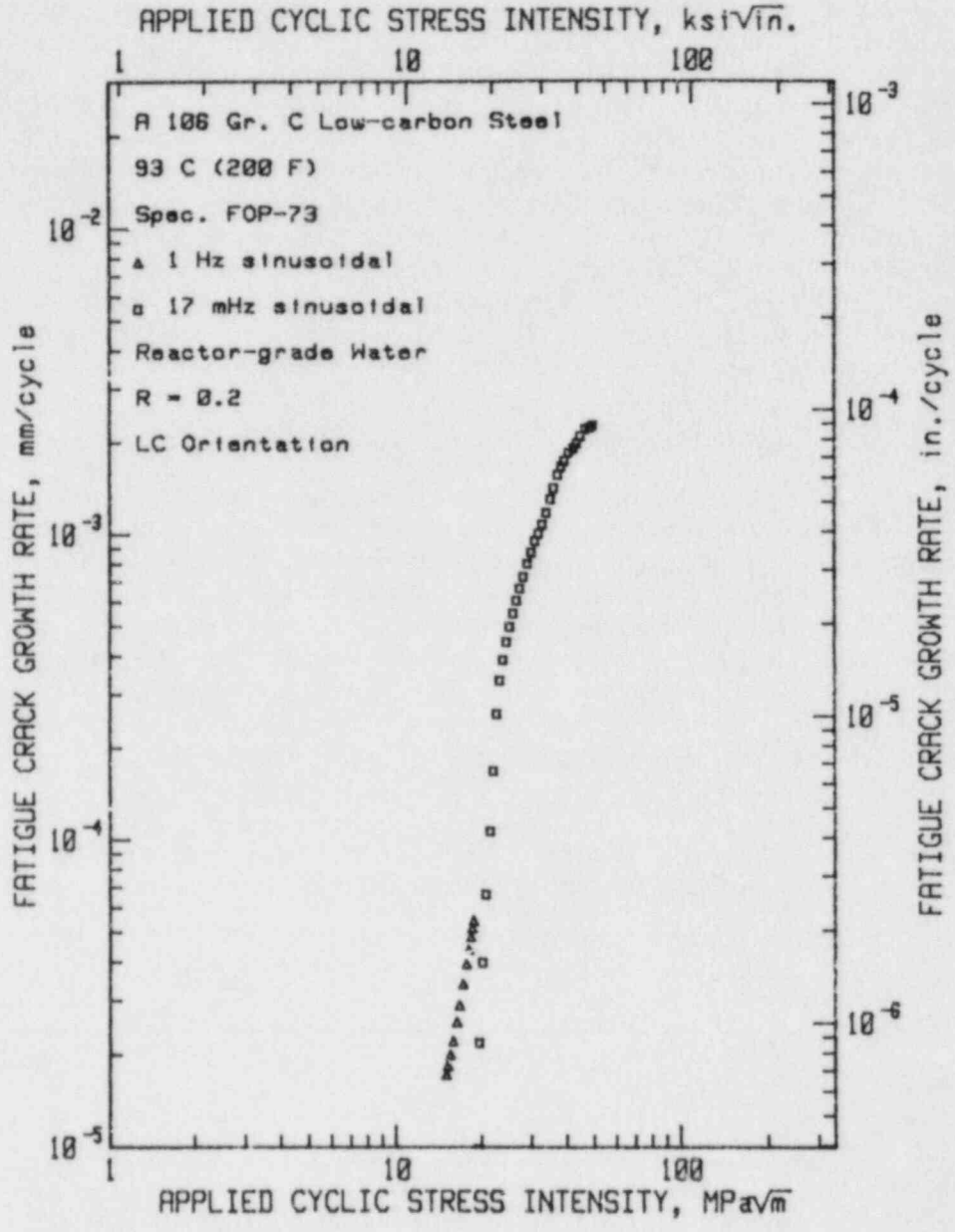

Figure 2.12 Fatigue crack growth rates vs. applied cyclic stress intensity factor for A 106 Gr. C piping steel. Test temperature was 93°C (200°F). Two orientations were tested (compare with Fig. 2.14) with little difference in the growth rates between the two. This data set is for the LC orientation.

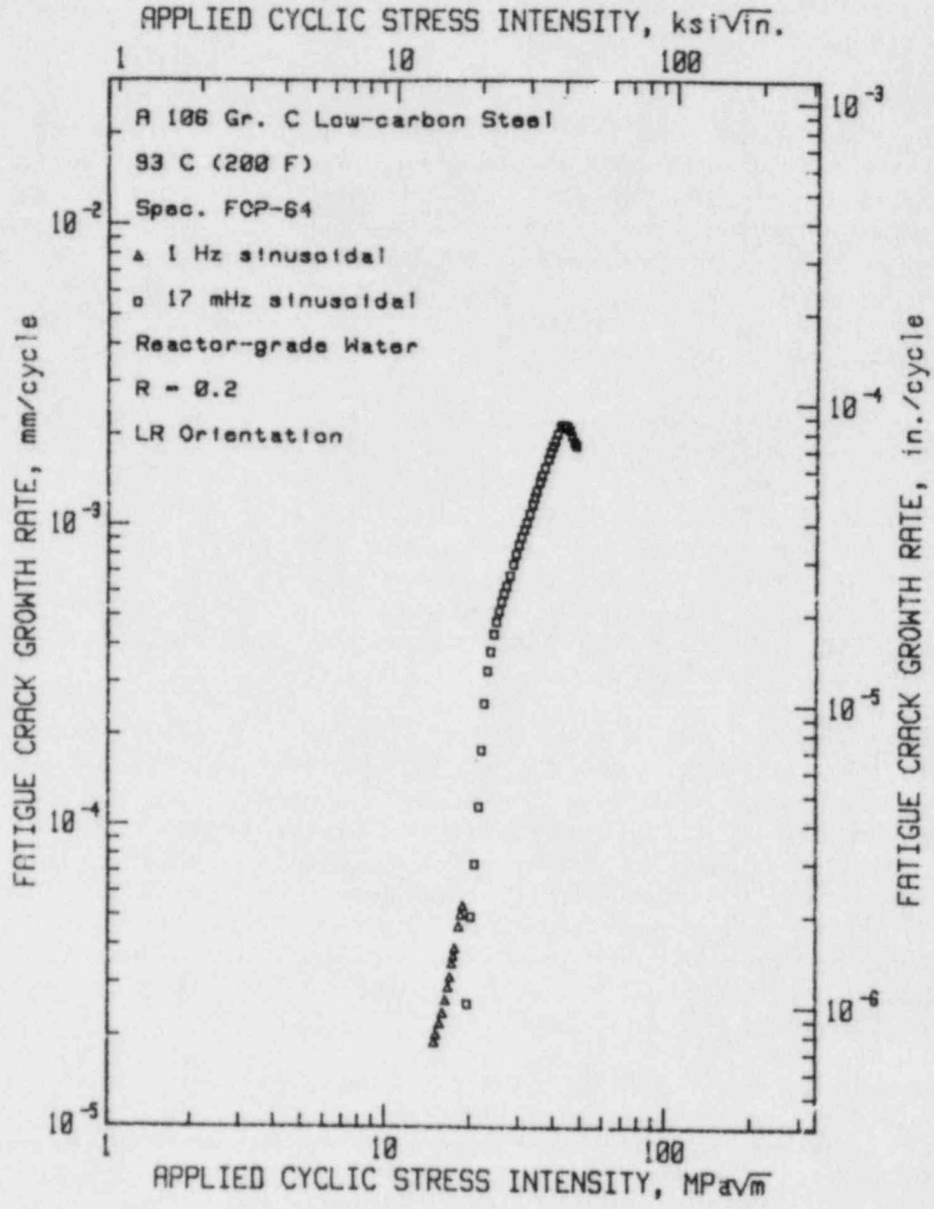

Figure 2.13 Fatigue crack growth rates vs. applied cyclic stress intensity factor for A 106 Gr. C piping steel. Test temperature was 93°C (200°F). This data set is for the LR orientation.

CL and LC orientations, are shown in Figs. 2.14 and 2.15. There is a clear decrease in growth rates for the highest test temperature. Orientation is not a factor at any temperature.

Tests at two load ratios were conducted on A 516 Gr. 70 piping steel. These data sets are shown in Fig. 2.16. These results exhibit the customary higher growth rates at higher load ratios. The wide discrepancy between the FOK-11 and FOK-13 results may be due to material inhomogeneity since other possible variables were carefully controlled. It is somewhat notable that a test at 1 Hz, and the tests at 17 mHz, for R = 0.7, yielded data in the same crack growth rate range. This insensitivity to test frequency, at the higher load range, has been noted for the A 106 steel as well (Ref. 20).

Fatigue crack growth rate data for A 516 in a variety of specimen orientations was presented previously (Ref. 21). Following finalization of those test results, the specimens were examined fractographically to determine the microstructural influences on crack growth rate. The presumption is that the manganese sulfide stringers have a strong influence on the progress of the crack front, both through their influence on the local stress intensity factor (Ref. 22) and because of their participation (through dissolution) in the hydrolysis reaction at the crack tip (Ref. 23).

Figure 2.17 shows a view for a specimen with the fatigue crack in the S-T orientation, for which the sulfide stringers will be met broadside by the crack. In most cases, as the crack approaches the vicinity of a manganese sulfide stringer, the crack front "terraces" or changes planes in order to intercept the stringer, which offers very little mechanical resistance to crack advance. Although not shown explicitly by this data, very high crack growth rates could result from the intersection of such a large number of sulfide inclusions, since dissolved sulfide ions will enchance crack tip hydrolysis by helping to break down oxide films.

These manganese sulfide inclusions also act as sites for the localized tunneling or fingering of the fatigue crack. The exact mechanism for this is speculative, but Fig. 2.18 shows an example taken from the location of the final crack front in a specimen in the S-T orientation. This picture shows a finger developing laterally to the macroscopic direction of crack extension, as shown in the schematic, Fig. 2.19. The brittle-appearing fatigue crack emanates from the inclusion site. The remains of the partially dissolved stringer are visible at the right of the picture. This particular finger extends almost one millimeter ahead of the main crack front, although only the tip end of the finger is shown in the photo.

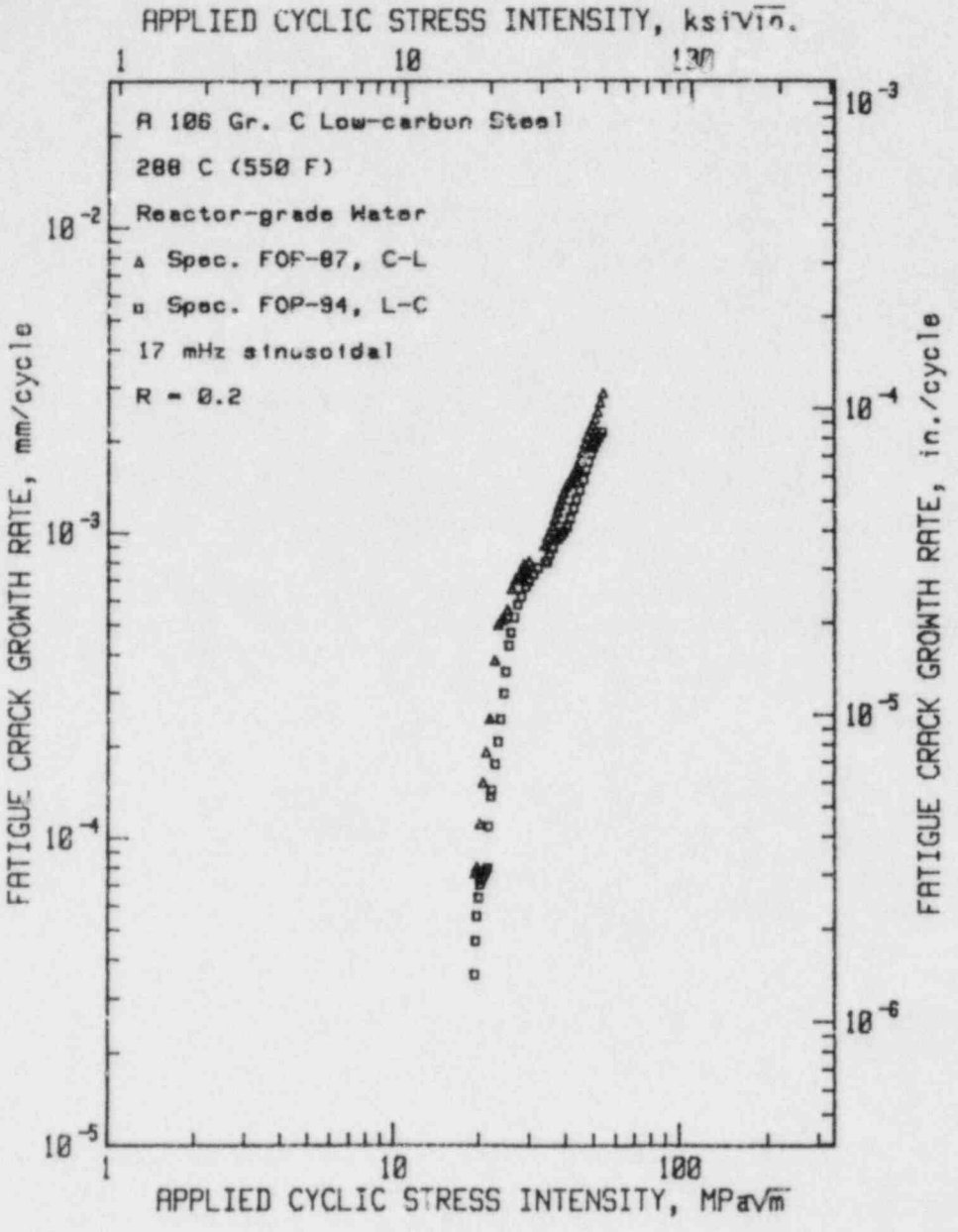

Figure 2.14 Fatigue crack growth rates vs. applied cyclic stress intensity factor for A 106 Gr. C piping steel. Test temperature was 288°C (550°F). Two orientations were tested, with little difference in the growth rates between the two.

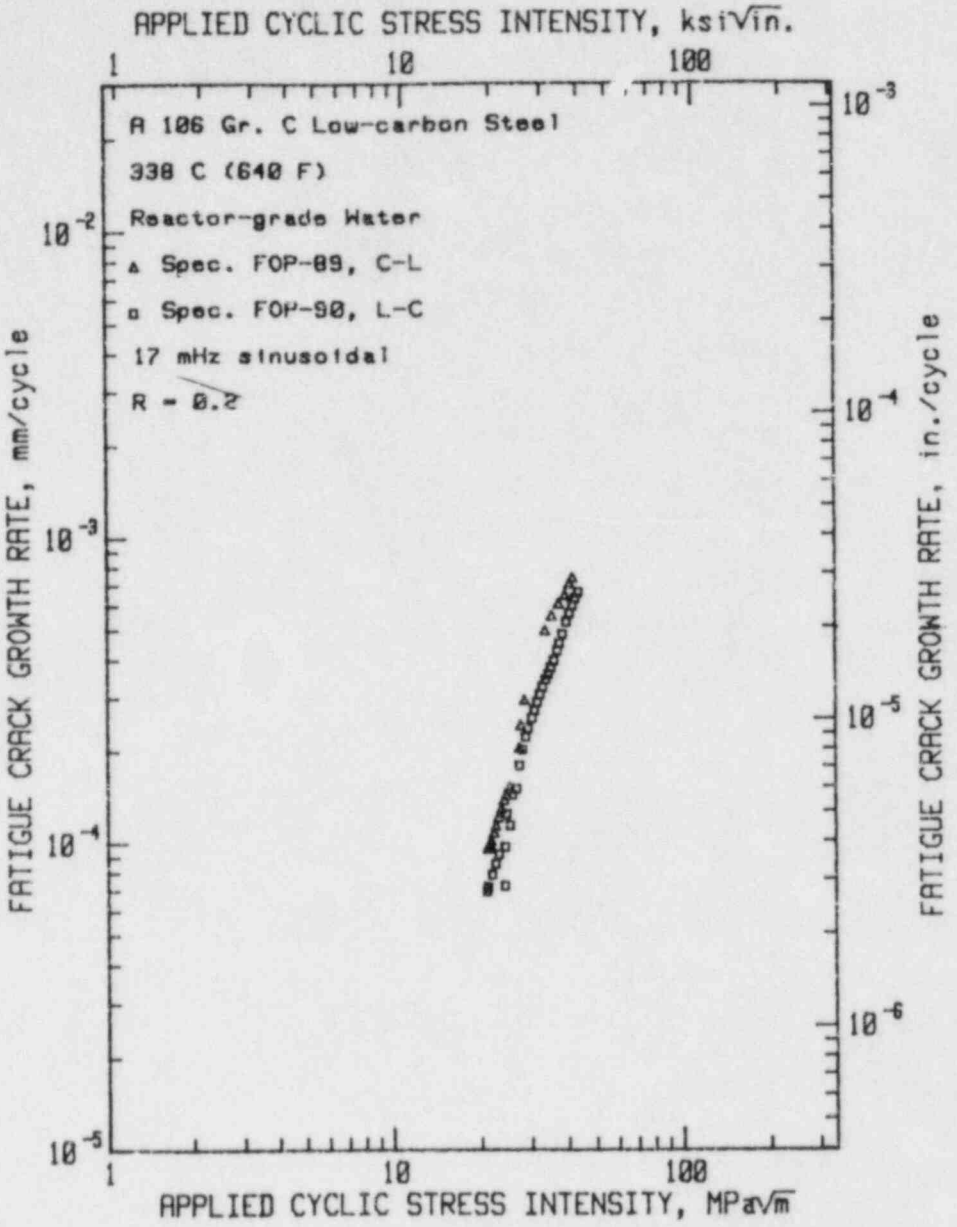

Figure 2.15 Fatigue crack growth rates vs. applied cyclic stress intensity factor for A 106 Gr. C piping steel. Test temperature was 338°C (640°F). Two orientations were tested, with little difference in the growth rates between the two, although growth rates are slightly higher than at 288°C.

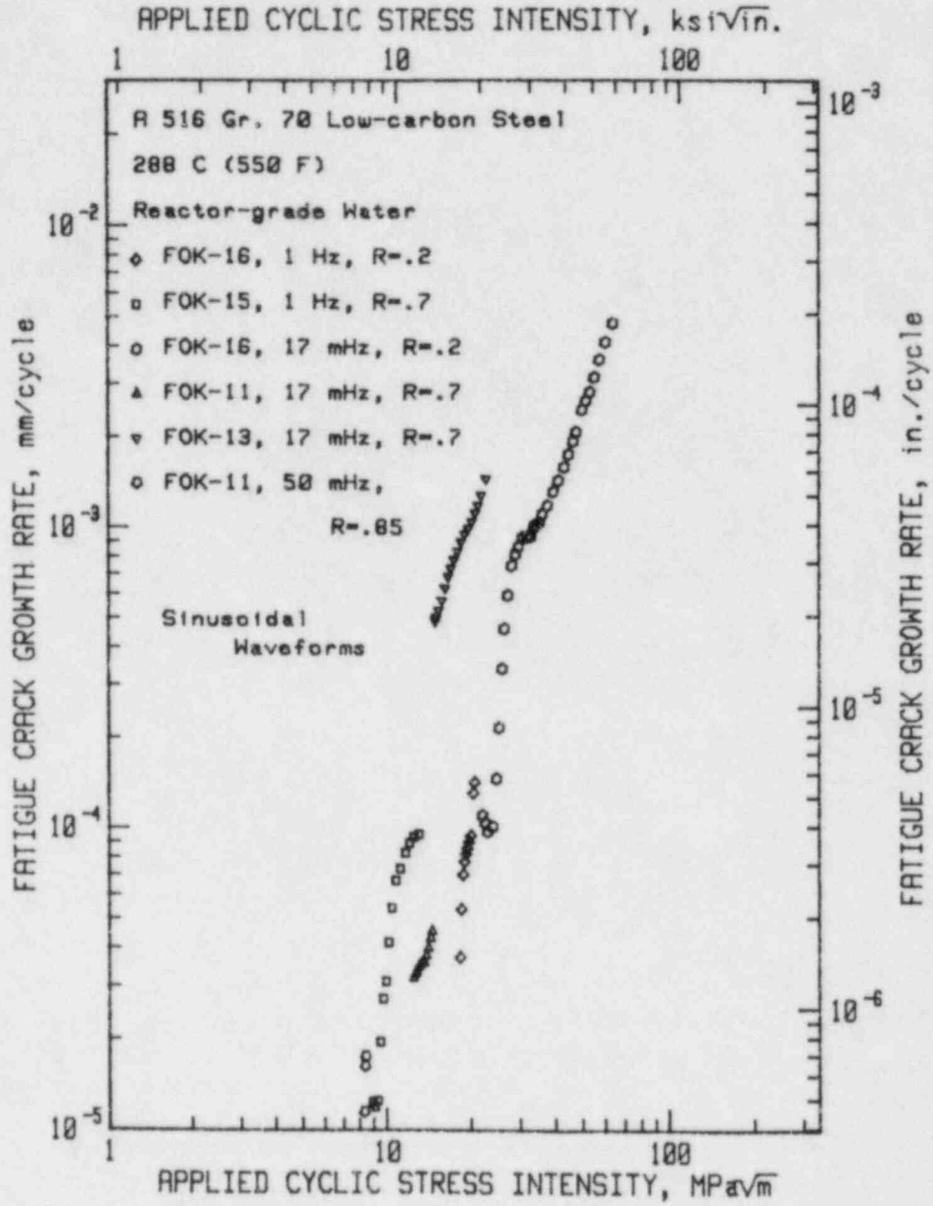

Figure 2.16 Fatigue crack growth rates vs. applied cyclic stress intensity factor for A 516 Gr. 70 piping steel. Data are shown for tests at two load ratios, 0.2 and 0.7, and frequencies of 1 Hz and 17 mHz.

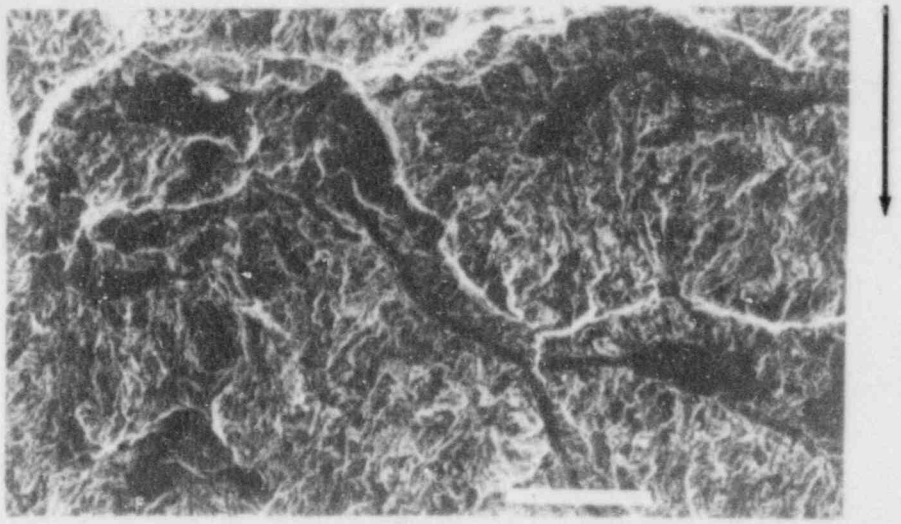

Figure 2.17 Fractographic features of environmentally-assisted fatigue crack growth in the S-T orientation in A 516 Gr. 70. Note that the crack changes plane in order to intersect a manganese sulfide inclusion, which is presumably a weak feature of the structure. The subsequent dissolution of the MnS may also contribute to the degree of environmental assistance.

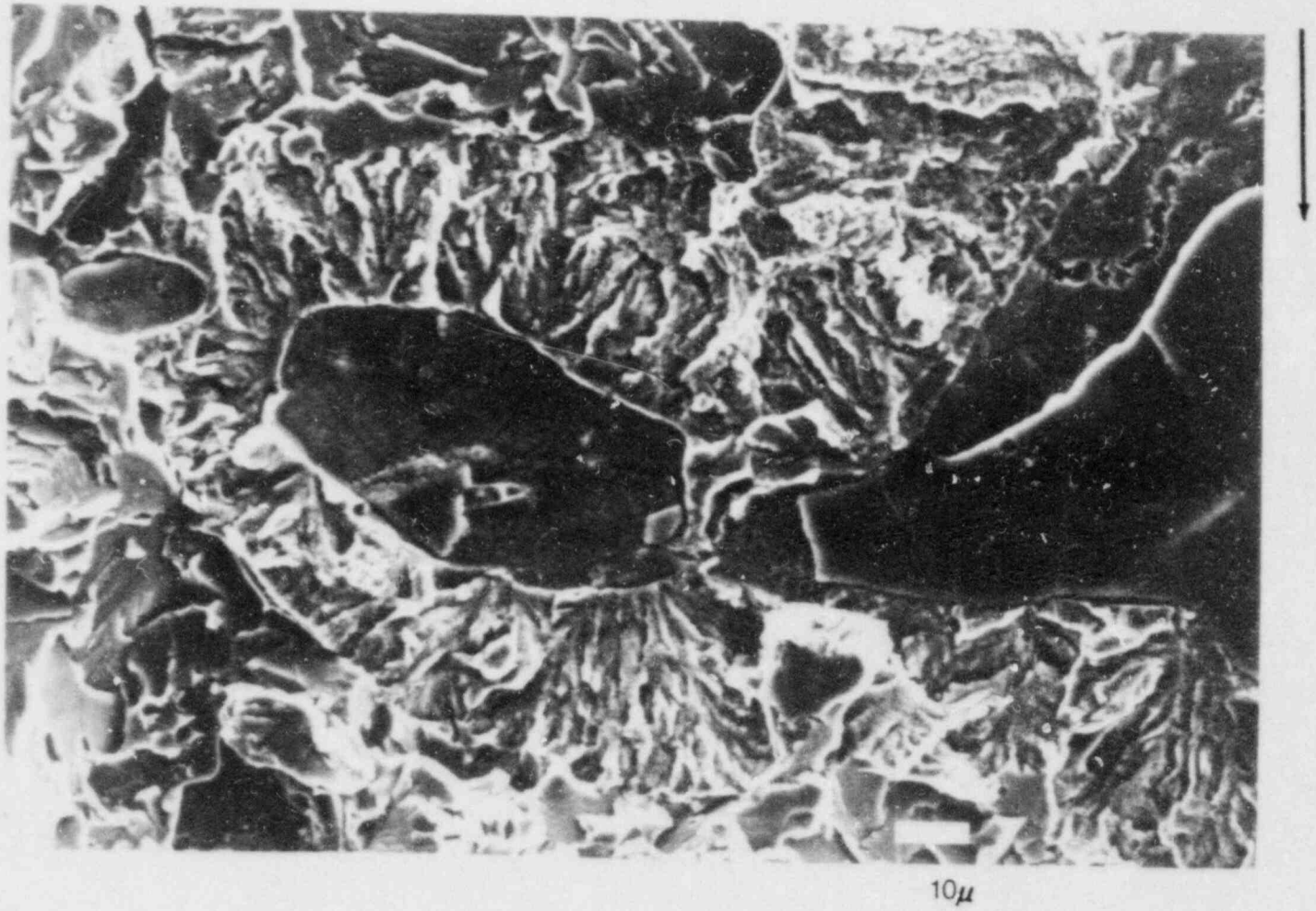

Figure 2.18 Fractographic features of environmentally-assisted fatigue crack growth in the S-T orientation in A 516 Gr. 70 steel. This view shows the definition of the final crack front, which was opened by chilling and fracturing below the brittle transition temperature. Note that the fatigue crack has followed the projection of the MnS inclusion and spread out laterally from the boundary of the inclusion. This is one way in which a crack front develops a rather irregular shape.

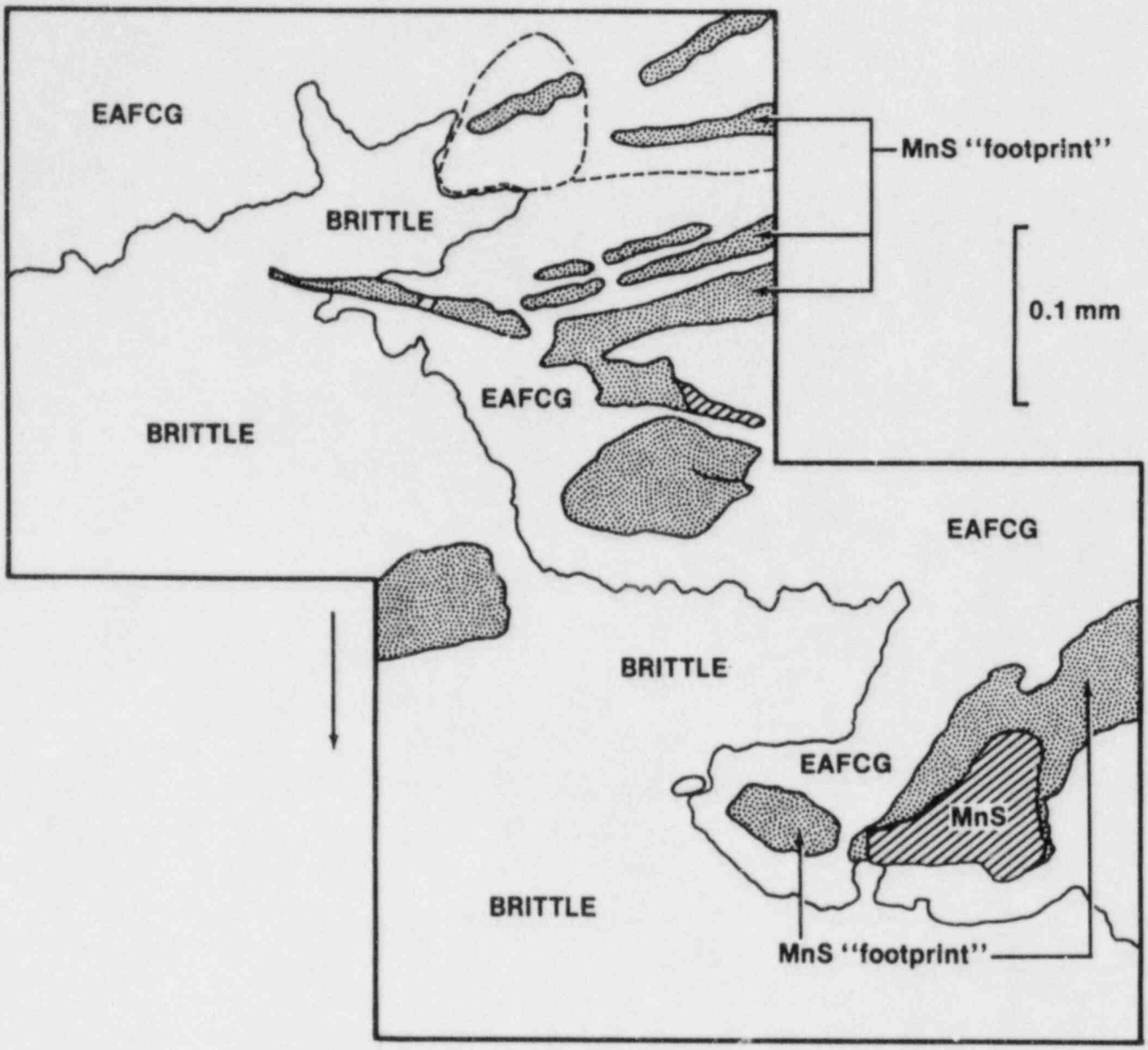

Figure 2.19 A schematic of the crack front morphology in Fig. 2.18. The areas denoted "EAFCG" are regions of environmentally-assisted fatigue crack growth. The areas marked "BRITTLE" are from the post-test, low-temperature fracture. The MnS "footprint" regions are the former residence of manganese sulfide inclusions which have dissolved in the high-temperature water.

3.0 RADIATION SENSITIVITY AND POSTIRRADIATION PROPERTIES RECOVERY

3.1 Assessment of Postirradiation Heat Treatment as a Method for Alleviating Radiation-Induced Embrittlement

J. R. Hawthorne

3.1.1 Background

Steels and weld deposits forming reactor pressure vessels are required by Title 10 of the Code of Federal Regulations (10 CFR Part 50) and the ASME Code to exhibit a certain minimum fracture resistance throughout vessel life. Specifically, the Charpy-V (C_v) upper shelf level of vessel materials must be at least 68 J for unrestricted vessel operation. For those cases where properties are reduced by radiation to below minimum values, postirradiation heat treatment for the restoration of vessel safety margins is one option available for continuation of vessel service. The method is under active consideration both in the U.S.A. and in Europe, and earlier was applied successfully to the Army SM-1A reactor vessel which operated at 232°C. Service temperatures for commercial PWR vessels in contrast range from ~ 260 to 302°C.

The present investigation represents a continuation of studies initiated in 1982 for the experimental definition of the general reembrittlement path which follows annealing at 399°C and the exploration of the potential for weld-to-weld variability in reirradiation sensitivity. This study, identified as IAR Phase 2, builds on an investigation of irradiation (I)- anneal (IA)- reirradiation (IAR) effects conducted in 1980-81 which showed that the IAR method could reduce cumulative irradiation effects (Refs. 24 and 25). This earlier study employed high copper, high nickel content welds from commercial reactor vessels (nozzle cut outs). High copper welds are of particular interest because of their high radiation embrittlement sensitivity at typical U.S.A. reactor service temperatures (~ 288°C) and subsequent concerns for the resultant degradation in pressurized thermal shock (PTS) resistance and the reduction in upper shelf toughness. The present set of investigations is being carried forth with a new set of high copper content welds produced by the submerged-arc process using Linde 80 and Linde 0091 welding fluxes. The fluxes, respectively, yield relatively low and high as-fabricated C_v upper shelf energy levels.

The Phase 1 results, while very positive in terms of showing a benefit gained, have raised questions on the exact path of reembrittlement after annealing (Fig. 3.1) and the possibilities for metallurgical influences on reembrittlement behavior. Implementation of the method and the NRC's assessment of proposed startup/shutdown pressure temperature limits for postanneal vessel operations will depend in great measure on clarification of these uncertainties.

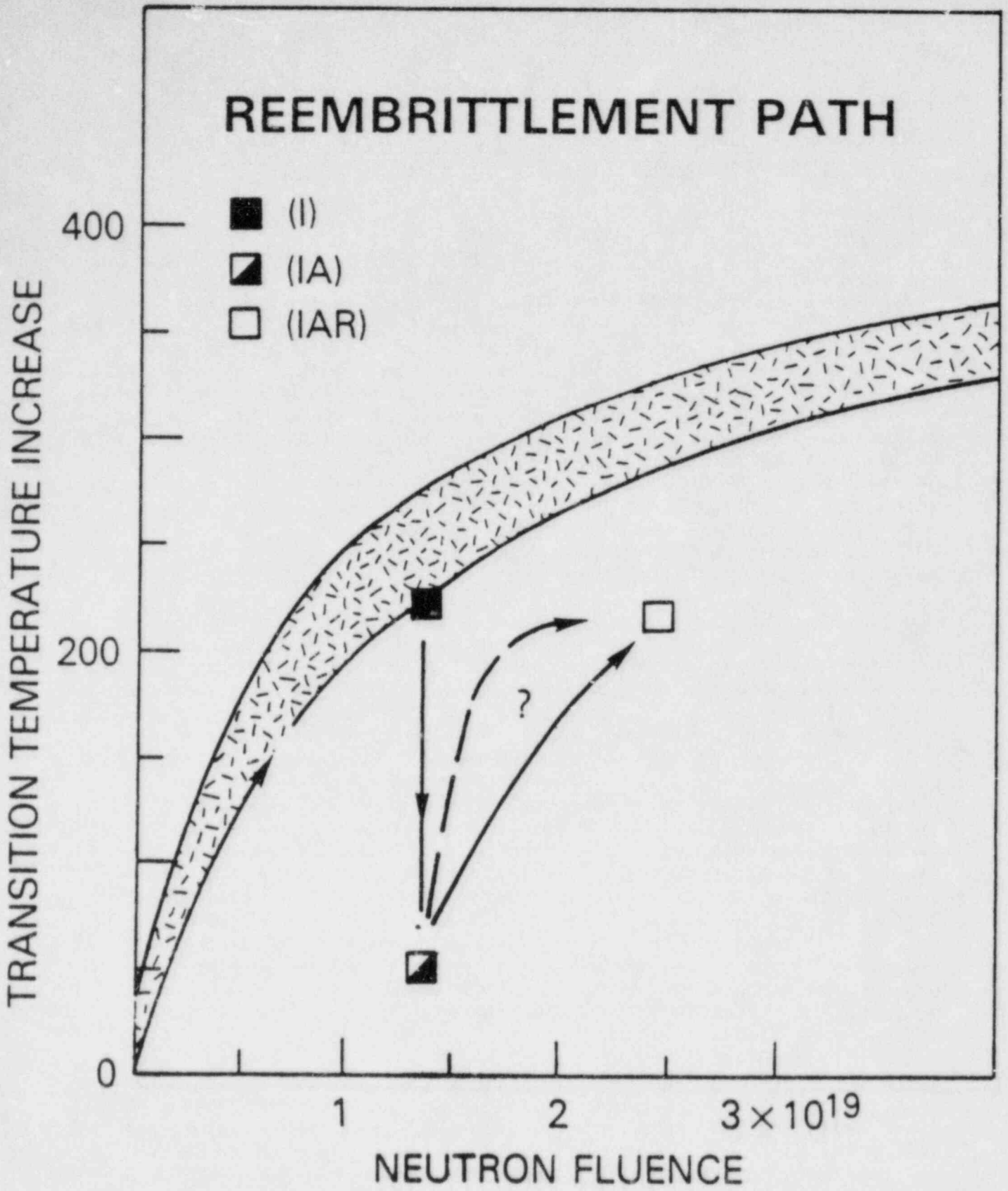

Figure 3.1 Illustration showing the uncertainty over the reembrittlement path with reirradiation.

3.1.2 Materials

For reference, specifications for the welds made thus far for the Phase 2 investigations are summarized in Table 3.1. Two welds, each 1800-mm long, were produced using Linde 80 flux; one weld 1000-mm long was made with the Linde 0091 flux. The fabrication of additional welds is planned. All welding was accomplished with a single melt of filler metal and single lots of the two welding fluxes. Completed welds received a 621°C-24 h stress-relief anneal prior to sectioning for specimens.

Table 3.1 Welding Specifications for IAR Phase 2 Welds

Base Plate:	210-mm thick A 533-B Class 1 Steel
Filler Type:	High Mn-Mo-Ni
Process:	Submerged arc, single electrode
Electrode:	Heat 3P8393, 3.2-mm diameter copper coated
Flux:	Linde 80 (Lot 0418, control 8556) or Linde 0091 (Lot 0204, control 3756)
Heat Input:	80-95 kJ/inch (range)

As-welded notch ductility and strength properties are listed in Table 3.2. Photomacrographs of full-thickness cross sections of two of the welds after etching are shown in Figs. 3.2 and 3.3. Properties of the "sister" welds (W8A and W8B) show good agreement, indicating good weld reproducibility when the same flux lot was used. As expected, a higher transition temperature and a lower upper shelf level was observed for the Linde 80 weld compared to the Linde 0091 weld. The 80 J (60 ft-lb) upper shelf of the former permits its classification as a "low shelf" weld, thereby satisfying one objective of weld preplanning and fabrication.

3.1.3 Irradiation Test Plan

The plan of experiment irradiations for Phase 2 is illustrated in Fig. 3.4. At each of the points indicated, C_v properties would be established. In addition, compact tension specimen tests were planned for the three points marked by the subscript, CT. The intent here was to test the correlation of fracture toughness and notch ductility changes produced by the various conditions. Each of the CT specimen irradiation assemblies contained 12 specimens of the Linde 80 weld (code W8A) and 12 specimens of the Linde 0091 weld (code W9A). This number was sufficient for properties definition over the full temperature range (transition and upper shelf regimes).

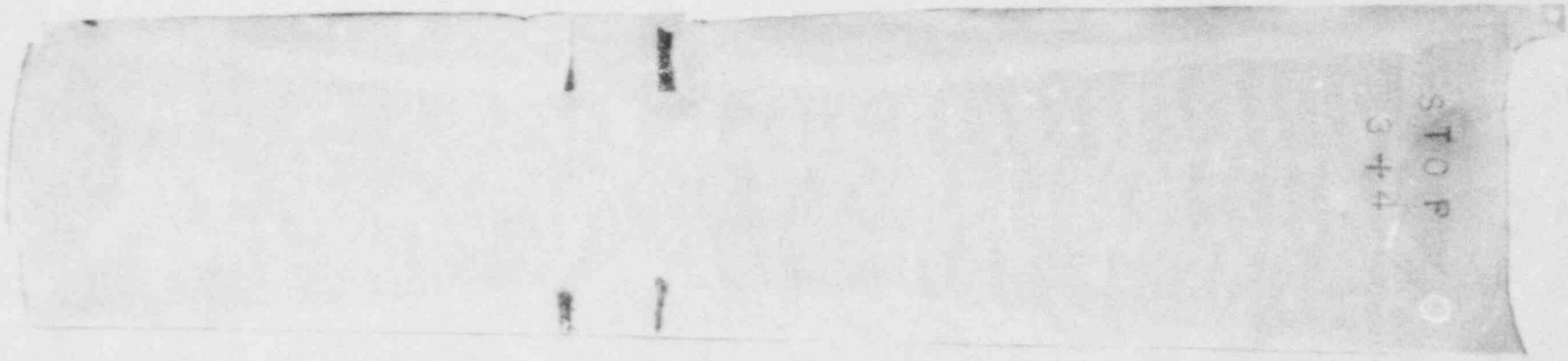

Figure 3.2 Photomacrograph of code W8A submerged-arc weld deposit (Linde 80). Material shown is a run-out-tab cross section.

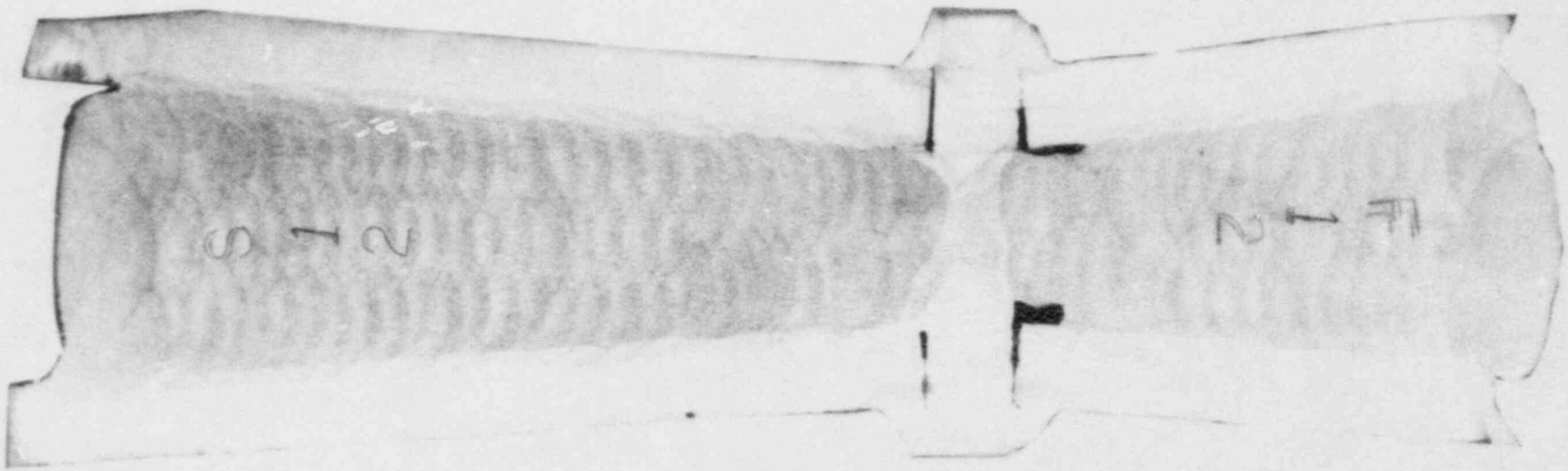

Figure 3.3 Photomacrograph of code W9A submerged-arc weld deposit (Linde 0091).

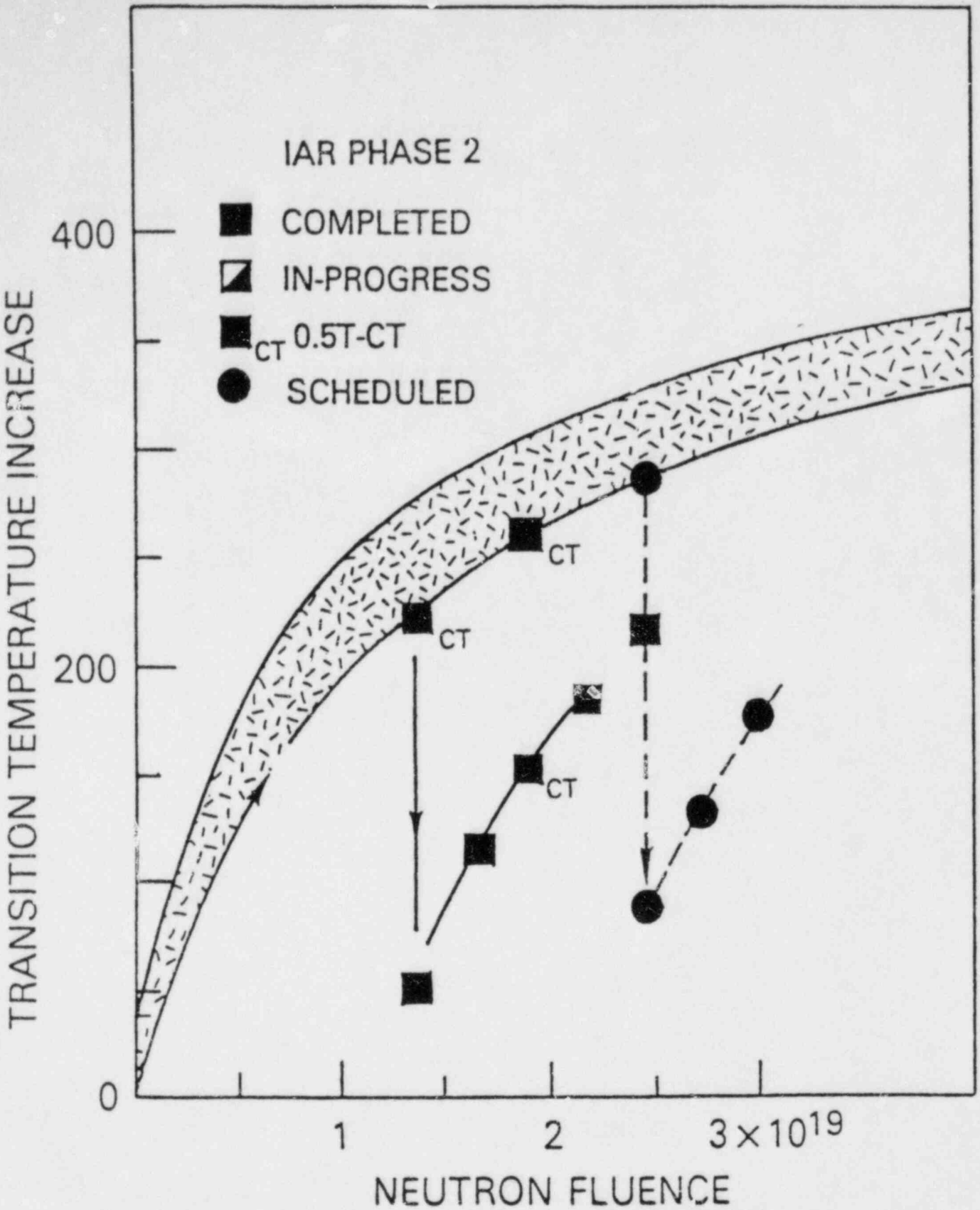

Figure 3.4 Plan of IAR Phase 2 program irradiation tests. Charpy-V properties are being developed experimentally for each point indicated. The points marked "CT" show where fracture toughness determinations are also being developed.

Table 3.2 As-Welded Properties of IAR Phase 2 Welds

	Weld W8A	Weld W8B	Weld W9A
Flux Type	Linde 80	Linde 80	Linde 0091
Heat Input	85 kJ/inch	93.5 kJ/inch	93.5 kJ/inch
% Cu (deposit)	0.42	0.37	0.38
% Ni (deposit)	0.67	0.66	0.62
Yield Strength	498 MPa	489 MPa	574 MPa
Tensile Strength	617 MPa	612 MPa	656 MPa
C_v 41 J	-23°C	-18°C	-62°C
C_v 68 J	49°C	38°C	-46°C
C_v USE (range)	79-87 J	79-84 J	153-159 J

3.1.4 Status of Irradiation Experiments and Testing

All reactor experiments and postirradiation tests planned for target fluences up to and including 2×10^{19} n/cm^2 E > 1 MeV (I, IA and IAR conditions) were completed this year. Experiment irradiations are in progress at the NSTF/UBR reactor for the remaining C_v test points. The latter will extend the data base to ~ 2.5×10^{19} n/cm^2 and will permit an assessment of reembrittlement path vs. first cycle fluence level for 399°C annealing as illustrated in Fig. 3.4. Forward plans for 1984 also include studies of IAR behavior with a lower, first cycle fluence and with a higher temperature (454°C) heat treatment.

3.1.5 Experimental Results

As noted in Fig. 3.4 reirradiation properties have been established at fluence intervals of about 0.25×10^{19} n/cm^2 to a total (reirradiation) fluence of 1.0×10^{19} n/cm^2. Reference properties for the I condition have been established at ~ 1.0, 1.5 and 2.0×10^{19} n/cm^2.

Figures 3.5 and 3.6 present C_v data for the welds in the unirradiated, the first cycle irradiated (I) and the first cycle annealed (IA) conditions. In general, low data scatter is evident which aided the determination of 41 J transition and upper shelf energy properties. Comparisons of unirradiated and as-irradiated condition properties with those observed for welds used in the IAR Phase I program show a close similarity. For example, the transition temperature elevations in Figs. 3.5 and 3.6 compare well with the 117°C and 119°C elevations found for the Phase 1 welds (codes V84 and V86) after the first cycle

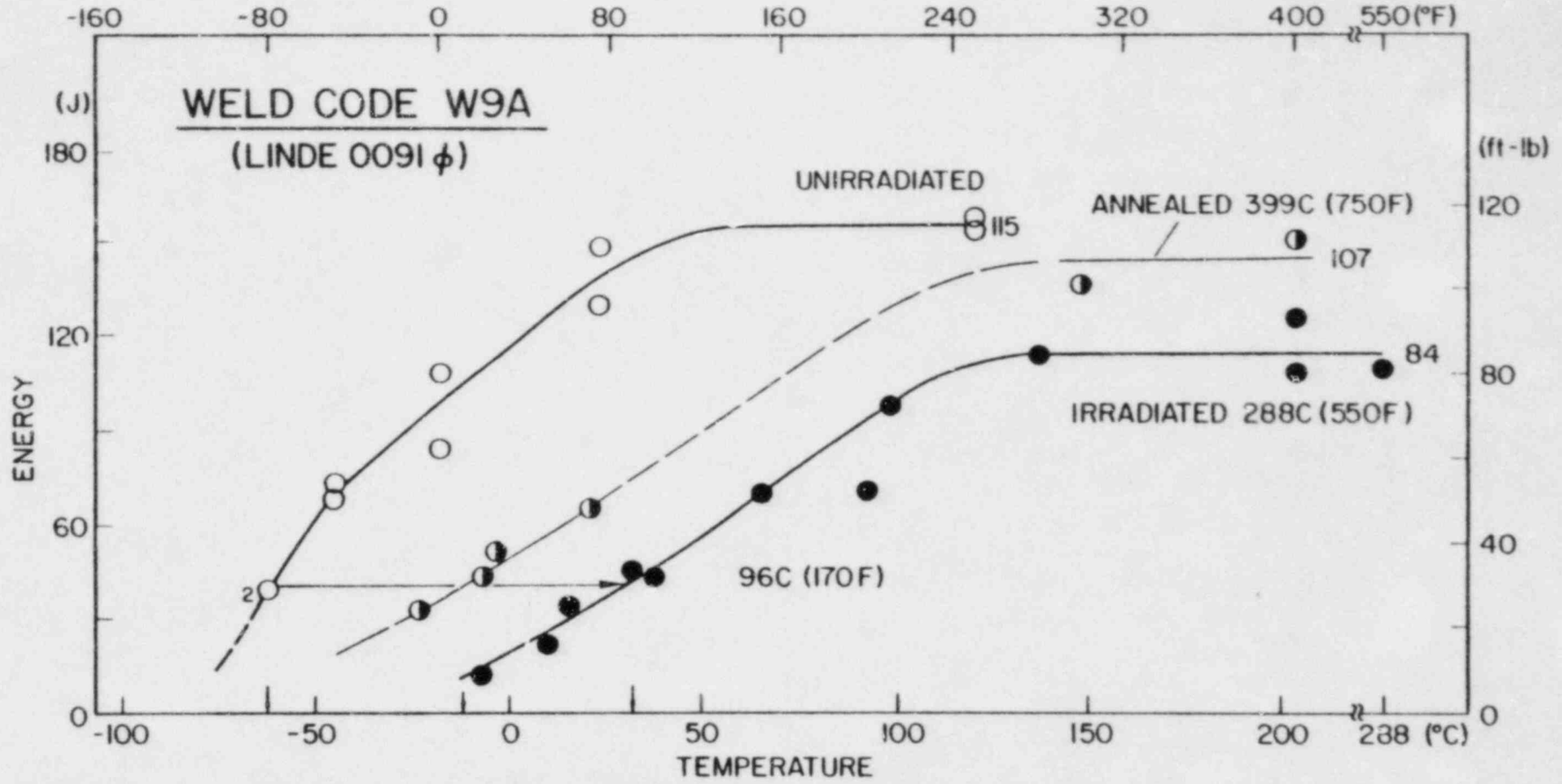

Figure 3.5 Notch ductility of weld code W9A before and after irradiation and after postirradiation annealing.

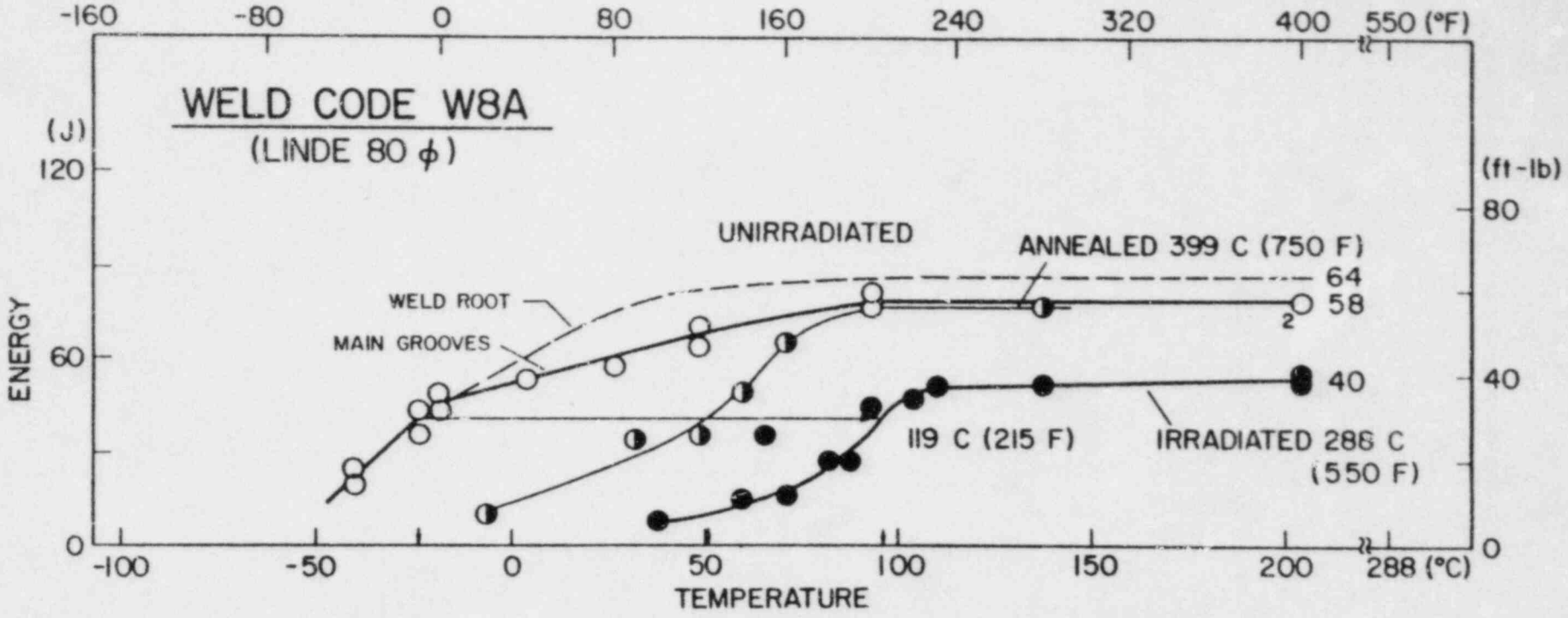

Figure 3.6 Notch ductility of weld code W8A before and after irradiation and after postirradiation annealing.

of exposure (Ref. 24). An important difference, however, is seen in the degree of transition temperature recovery by annealing. In the present case, the recovery is on the order of 35 to 45% whereas 70% recovery was observed with the same heat treatment in Phase 1 (see example, Fig. 3.7). Accordingly, a potential for large differences in recovery with 399°C annealing exists among welds. Flux type does not appear to be a causative factor since welds W8A and W9A exhibited the same (~ 42°C) recovery.

Figures 3.8 and 3.9 summarize observations made to date on the notch ductility behavior of the welds with I vs. IAR treatments. Somewhat surprising is the relatively rapid reembrittlement of the welds after annealing. A fluence of only ~ 0.25 x 10^{19} n/cm^2 mitigated a large portion of the annealing benefit. The results for a reirradiation fluence of ~ 0.75 x 10^{19} n/cm^2, nevertheless, reinforce the earlier Phase 1 findings. That is, at this fluence level, the reembrittlement with IAR was not more than the embrittlement induced by the first cycle of irradiation. Of special interest, the data trend for the weld W8A (Linde 80 flux) is suggestive of an embrittlement plateau which, if verified by ongoing tests, could have a major impact on future annealing decisions.

Judicious use of specimens from each reactor capsule permitted a reservation of some specimens for exploratory postirradiation annealing (or post-reirradiation annealing) tests at 454°C. Figures 3.10 and 3.11 present and compare the results against the 399°C-168 h annealing data from the various capsules. The data indicate that, for both welds, notch ductility recovery is independent of the prior irradiation history (I or IAR). Note also that 454°C-168 h annealing did not produce full transition temperature recovery for either weld.

Prior MEA assessments of the effectiveness of 454°C-168 h annealing for plate materials (Ref. 26) revealed that percentage recovery with 454°C annealing is material dependent. Further investigation into the metallurgical cause(s) of this variability and exploration of the dependence of such influences on heat treatment parameters are planned.

3.2 Impurity Element-Alloy Element Interactions in Radiation Embrittlement Sensitivity

J. R. Hawthorne

3.2.1 Background

It has been established that synergisms can (and do) exist between steel alloying and copper impurities in radiation sensitivity development. A prime example is the modification (enhancement) of the detrimental effect of copper on radiation resistance by nickel when nickel alloying is greater than 0.4% Ni (Ref. 27). The confirmation of this synergism was one reason given for NRC's recent draft revision of Regulatory Guide 1.99 (Ref. 28). In addition, the confirmation has raised the issue of possible interactions between copper impurities and other alloying elements such as manganese, molybdenum and

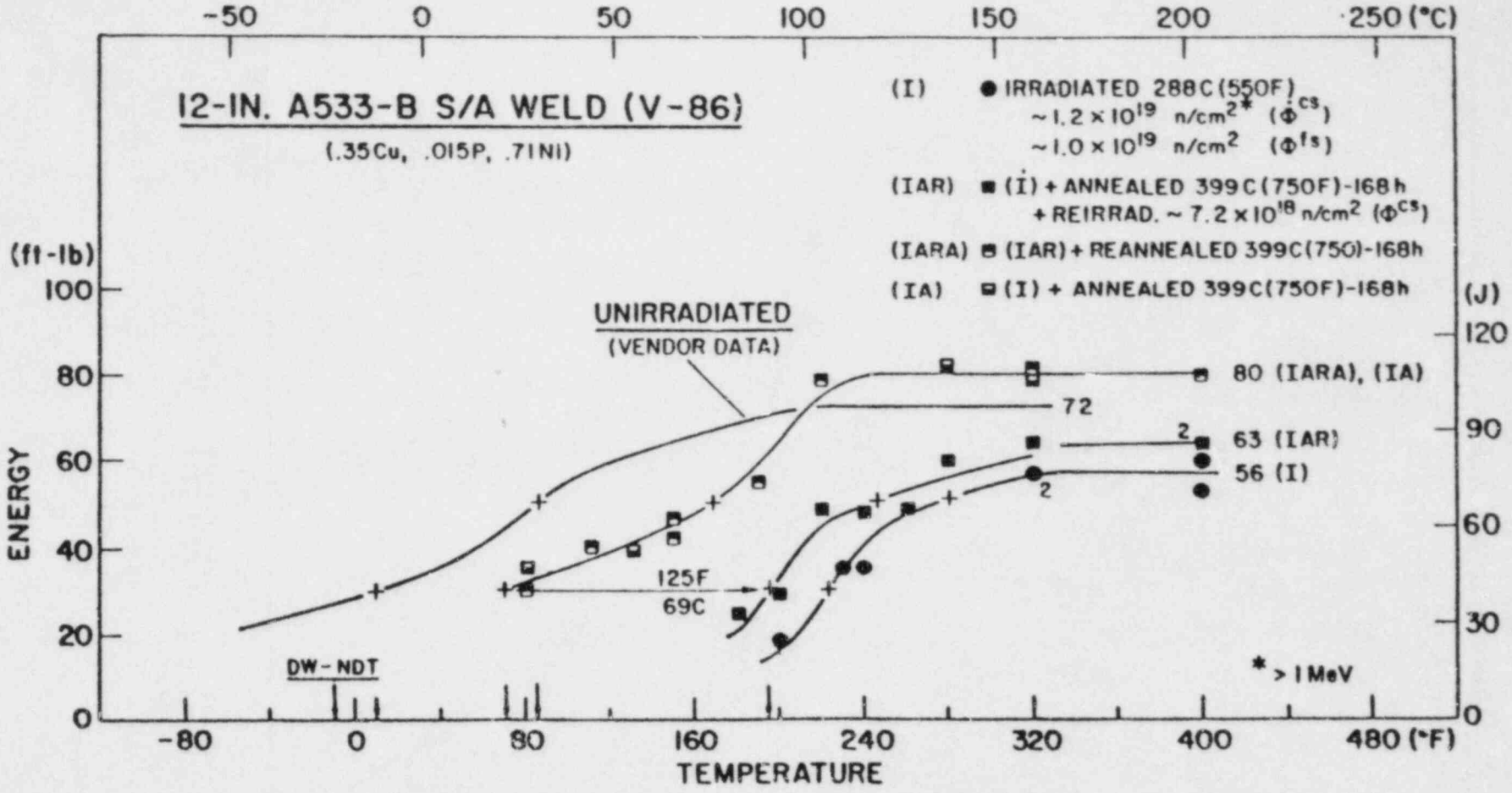

Figure 3.7 Notch ductility of weld code V86 (Phase 1 study) after irradiation, intermediate annealing and reirradiation. Limited results for reannealing are also shown.

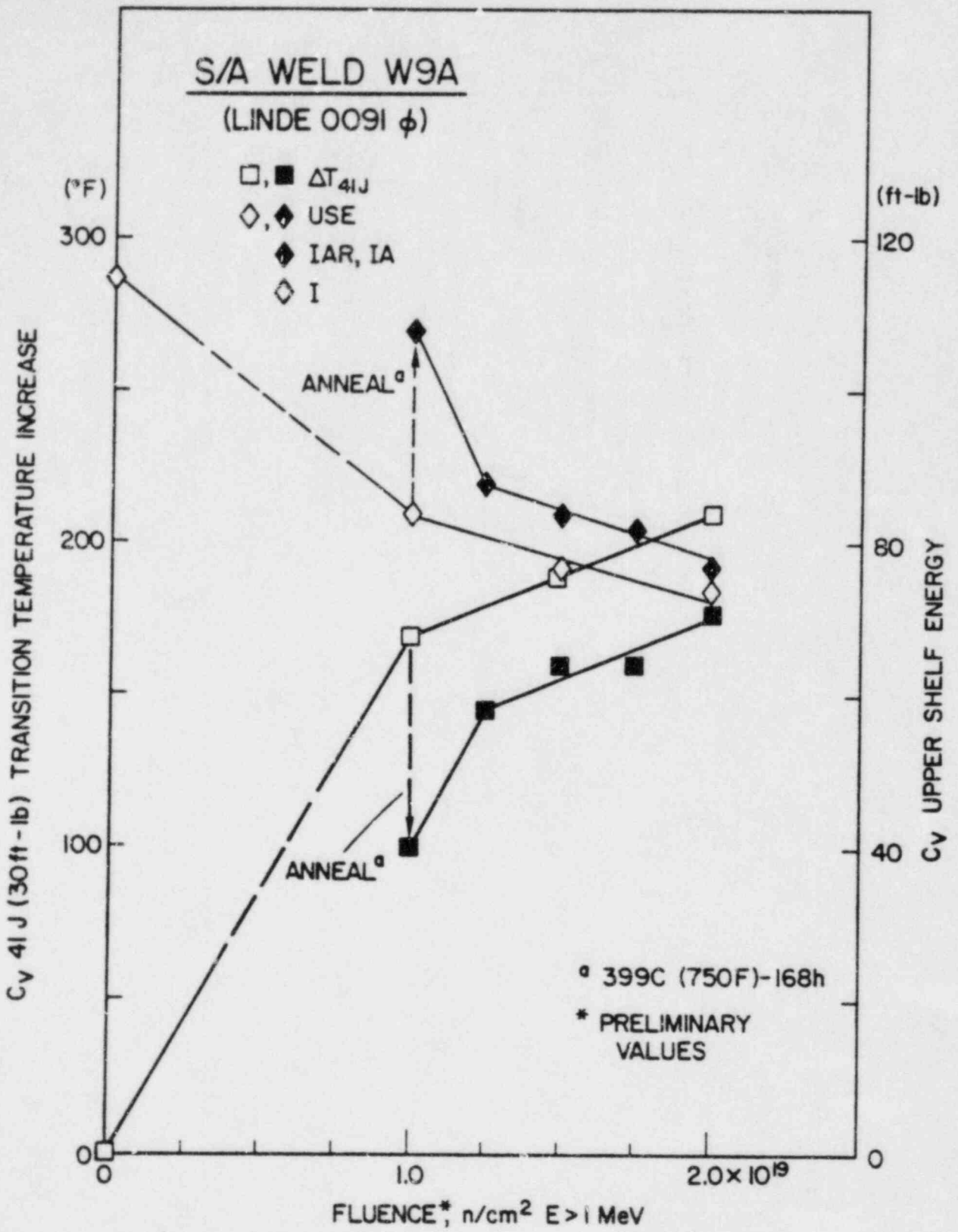

Figure 3.8 Summary of notch ductility observations for weld code W9A (I and IAR conditions).

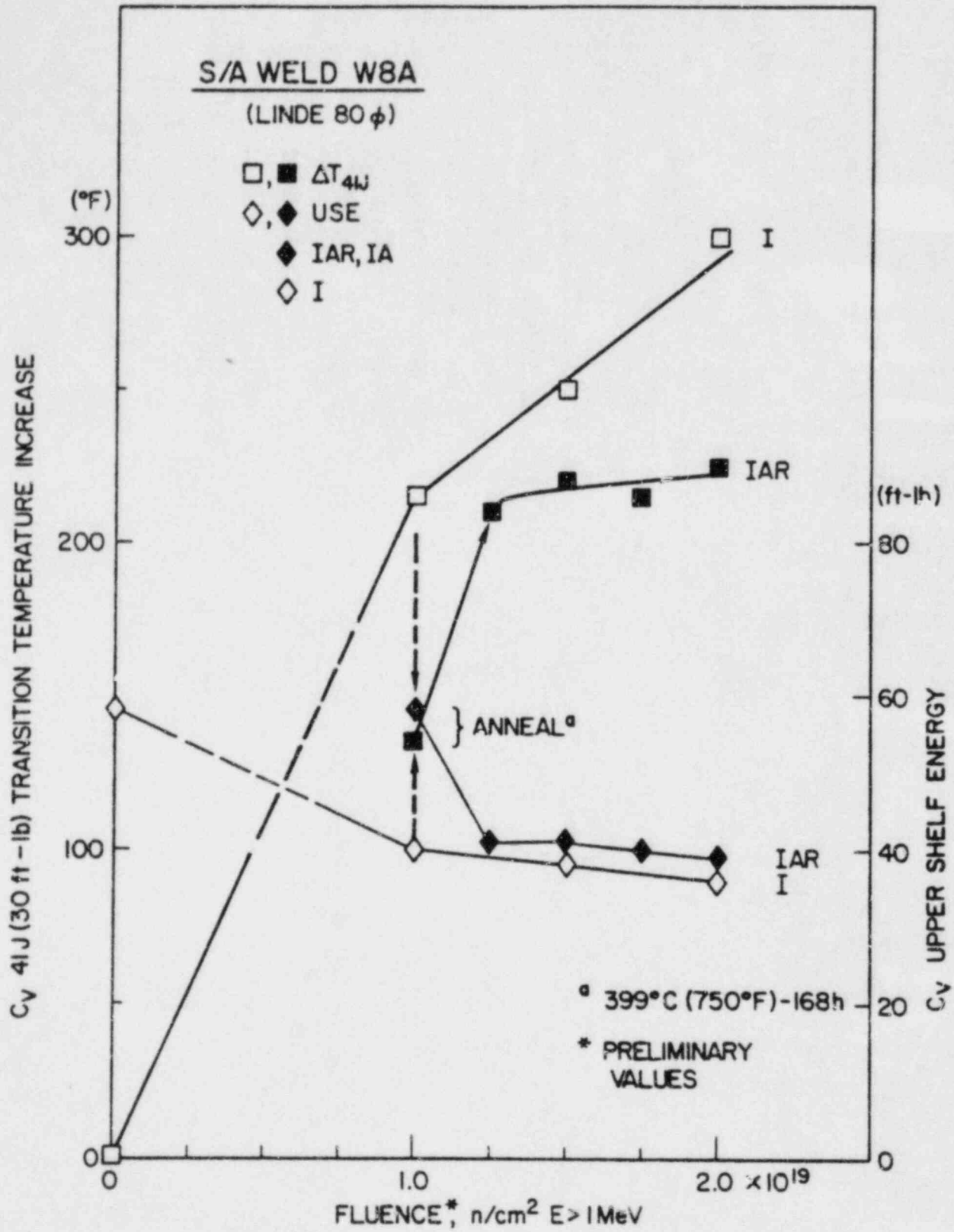

Figure 3.9 Summary of notch ductility observations for weld code W8A (I and IAR conditions).

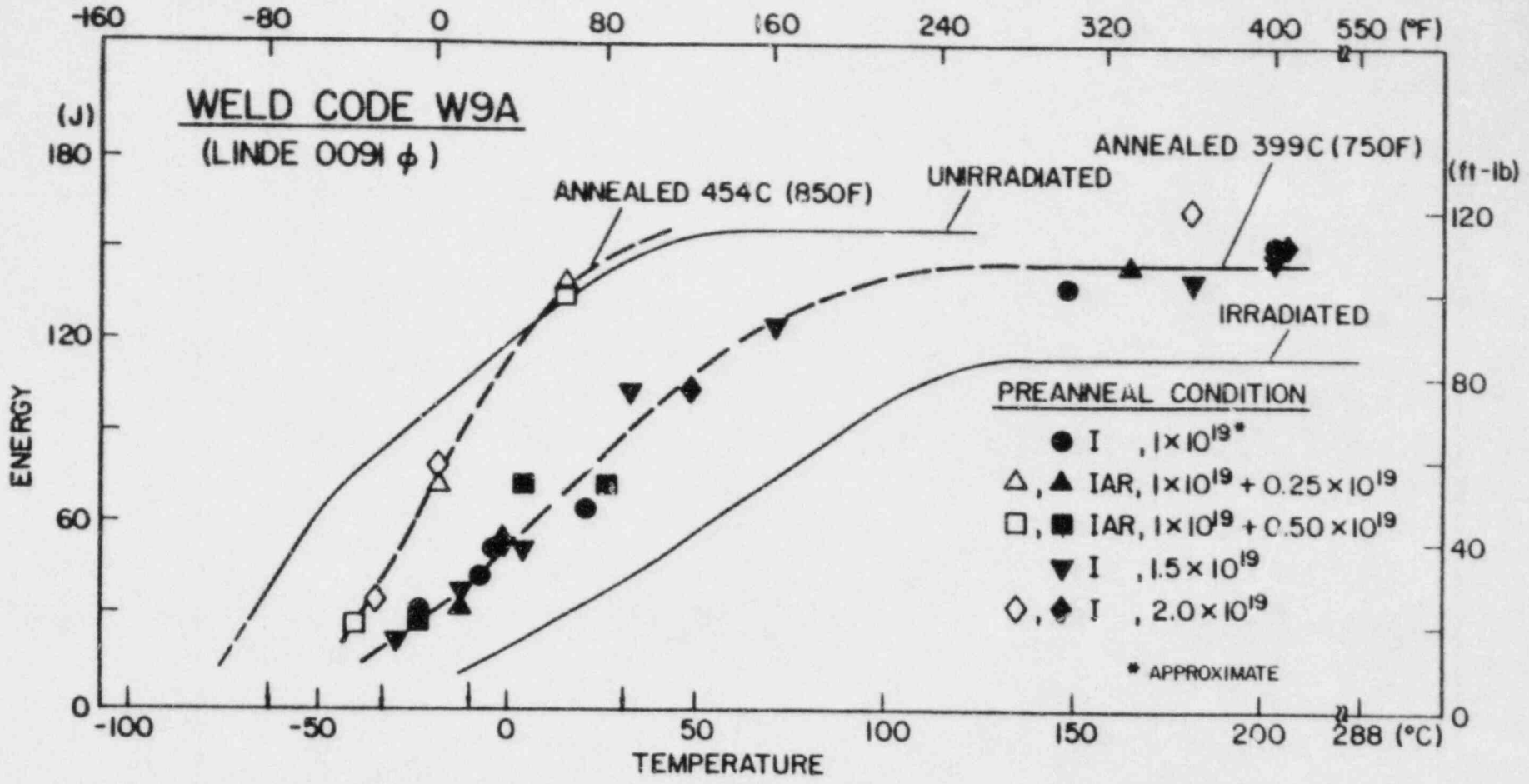

Figure 3.10 Observations on effectiveness of 399°C and 454°C annealing for weld code W9A. Results for several I and IAR experiments are shown.

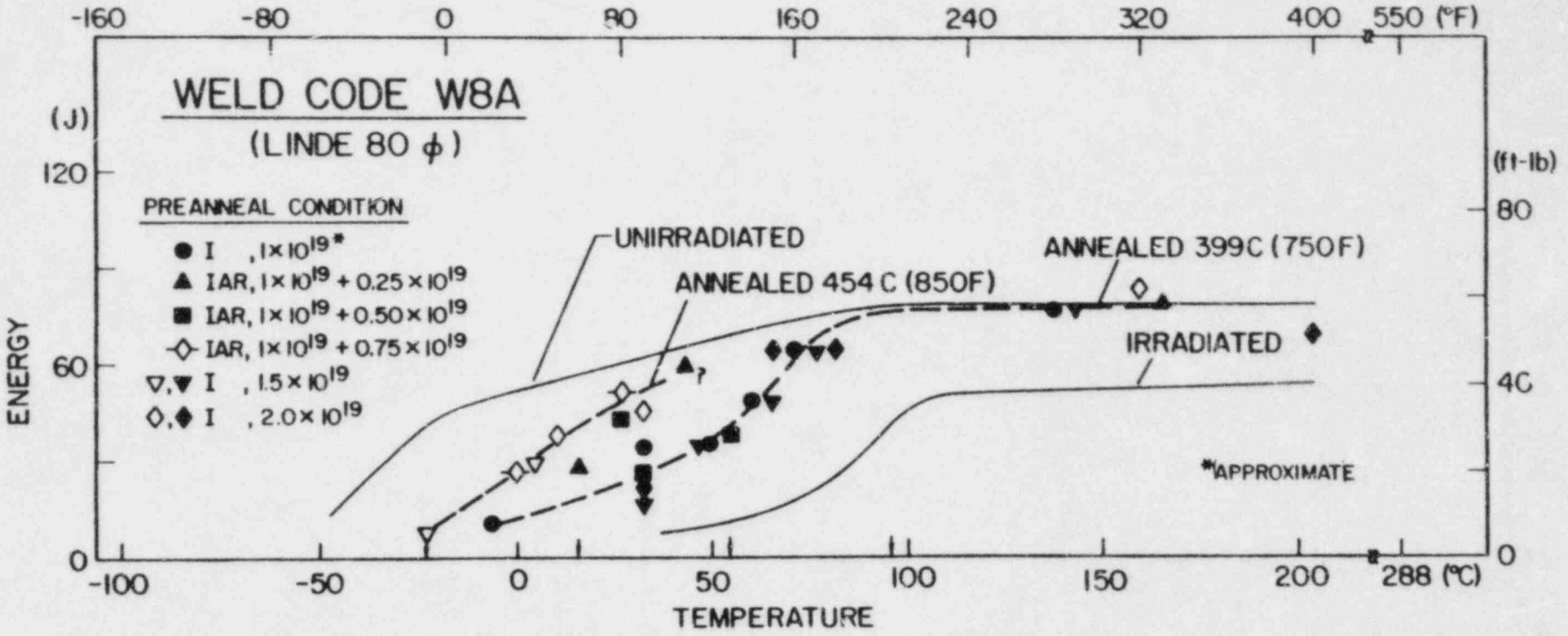

Figure 3.11 Observations on effectiveness of 399°C and 454°C annealing for weld code W8A. Results for several I and IAR experiments are shown.

chromium. Interactions between alloying and phosphorus content also are now suspicious. Phosphorus is known to influence radiation sensitivity but by a mechanism different from that of copper (Ref. 29). The present task was undertaken to explore both possibilities. Dual aims are to provide key information for further refinement of Regulatory Guide 1.99 and for gaining a better understanding of certain power reactor surveillance data.

In 1983, a series of seven (4-way split) laboratory melts of steel were cast and processed to plates as a means of obtaining statistical combinations of specific impurity elements and/or alloying elements. Table 3.3 lists the individual plate compositions by source melt number. The matrix focuses on binary and tertiary element combinations identified by data bank reviews as having high correlations with radiation sensitivity level. The primary base composition for melting was ASTM A 302-B or A 533-B. Ingots were rolled to 15-mm gage plates which, in turn, were heat treated to microstructures typical of 150-mm or thicker plates at the quarter-thickness location. Other details of melt processing and a summary of preirradiation tensile strengths of the plates are given in Reference 30.

3.2.2 Material Irradiation

The study is based on comparisons of notch ductility and tensile strength changes produced by a fluence of $\sim 2.0 \times 10^{19}$ n/cm^2 at 288°C. Irradiations were scheduled for an in-core position of the UBR reactor and were to be accomplished using a controlled temperature capsule design. Space availability within the capsule allows the exposure of eight C_v specimens sets (eight plates) simultaneously; accordingly, the materials were divided into four groups for notch ductility investigations as indicated in Table 3.4. The capsule design, on the other hand, permits the full complement of tensile specimens (28 plates) to be irradiated at one time.

To date, three of four planned irradiations have been performed. Also, postirradiation tests have been completed for the materials in groups 1 and 2. Neutron exposures were established from iron, nickel, niobium, cobalt-aluminum and silver-aluminum wires included within the specimen arrays. The fourth irradiation experiment will include ^{238}U fission detectors for fluence determinations as well. Results from these detectors can be extrapolated to the previously completed irradiations since only one fuel lattice position (B4) is being used for the series.

Table 3.3 Chemical Compositions of Plates from Laboratory (4-Way Split) Melts of Steel (A 302-B or A 522-B Base Composition)

Melt No.	Plate/ Cast No.	Chemical Composition (Weight-%)												
		C	Mn	P	S	Si	Cu	Ni	Cr	Mo	As	Sn	N	B
1	66A	0.24	1.30	0.018	0.018	0.21	0.16	< 0.002	< 0.003	0.52	-----	< 0.004	0.010	0.0005
	66B						0.16		0.25					
	66C						0.32		0.25					
	66D						0.32		0.52					
2	67A	0.23	1.31	0.003	0.018	0.20	0.002	0.70	< 0.003	0.51	-----	< 0.004	0.009	0.0004
	67B			0.015								< 0.004		
	67C			0.025								< 0.004		
	67D			0.025								0.024		
3	68A	0.23	1.31	0.003	0.017	0.22	0.30	0.70	< 0.003	0.52	-----	0.004	0.010	0.0006
	68B			0.016								0.004		
	68C			0.028								0.004		
	68D			0.028								0.023		
4	69A	0.23	1.23	0.016	0.018	0.24	0.19	0.30	< 0.003	0.53	< 0.010	< 0.004	0.010	0.0005
	69B							0.30			< 0.010	0.021		
	69C							0.70			0.010	0.021		
	69D							0.70			0.033	0.021		
5	70A	0.23	0.88	0.004	0.018	0.22	0.18	0.005	< 0.003	0.37	-----	< 0.004	0.008	0.0005
	70B						0.18			0.66				
	70C						0.33			0.66				
	70D		1.62				0.33			0.66				
6	71A	0.24	0.87	0.003	0.019	0.21	0.18	< 0.002	< 0.003	0.36	-----	< 0.004	0.009	0.0006
	71B		1.63				0.18			0.36				
	71C		1.63				0.32			0.36				
	71D		1.63				0.32			0.67				
7	72A	0.23	1.31	0.020	0.019	0.21	0.33	0.25	< 0.003	0.52	< 0.010	< 0.004	0.009	0.0004
	72B							0.71	< 0.003		< 0.010			
	72C							0.71	0.50		< 0.010			
	72D							0.71	0.50		0.035			

Table 3.4 Grouping of Plates for C_v Specimen Irradiation Experiments

Group	Melts*	Composition Variations Depicted
1	67	High Ni, Low Cu; Variable P, Sn
	68	High Ni, High Cu; Variable P, Sn
2	69	Intermediate Cu, P; Variable Ni, Sn, As
	72	High Cu, Intermediate P; Variable Ni, Cr, As
3	70	Low Mo; Variable Cu
		High Cu; Variable Mn
		Low Cu; Variable Mo
	71	High Mn; Variable Cu
		High Cu; Variable Mo
		Low Cu; Variable Mn
4	66	Variable Cr, Variable Cu

* Plates A, B, C, D

3.2.3 Experimental Results

Plates from group 1 (melts 67 and 68) jointly represent variations in copper, phosphorus and tin content. C_v specimens from these materials were irradiated at 288°C to 2.5×10^{19} n/cm^2 and provided the results shown in Fig. 3.12. The data indicate clearly that phosphorus has an influence on radiation sensitivity but its contribution is dependent on the copper content. The detrimental influence of phosphorus on radiation sensitivity is most pronounced when the copper content is low. The new results help explain some of the inconsistencies reported in computer treatments of irradiation data banks for the phosphorus effect.

Figure 3.13 compares the results for plates from melt 67 against prior findings for plates from a low nickel content, laboratory split melt, i.e., A 302-B steel. About equal sensitizing effects from a 0.015% phosphorus content are observed which suggests that the level of the phosphorus contribution is not nickel content dependent.

Analysis of the data of Fig. 3.12 also indicates that differences in tin content do not influence radiation sensitivity, at least for the case of a high (0.025%) phosphorus content. The companion case of tin content variability in low phosphorus steels remains to be explored. A tin content contribution cannot be ruled out in view of the findings for melt 72 below. The evidence of a noncontribution in general is consistent with observations made in an assessment of tin, arsenic and antimony effects in NiCrMoV forging steels (Ref. 31). Forgings with a low phosphorus content (0.006% P) were found to be highly radiation resistant, irrespective of the level of the three cited elements. On

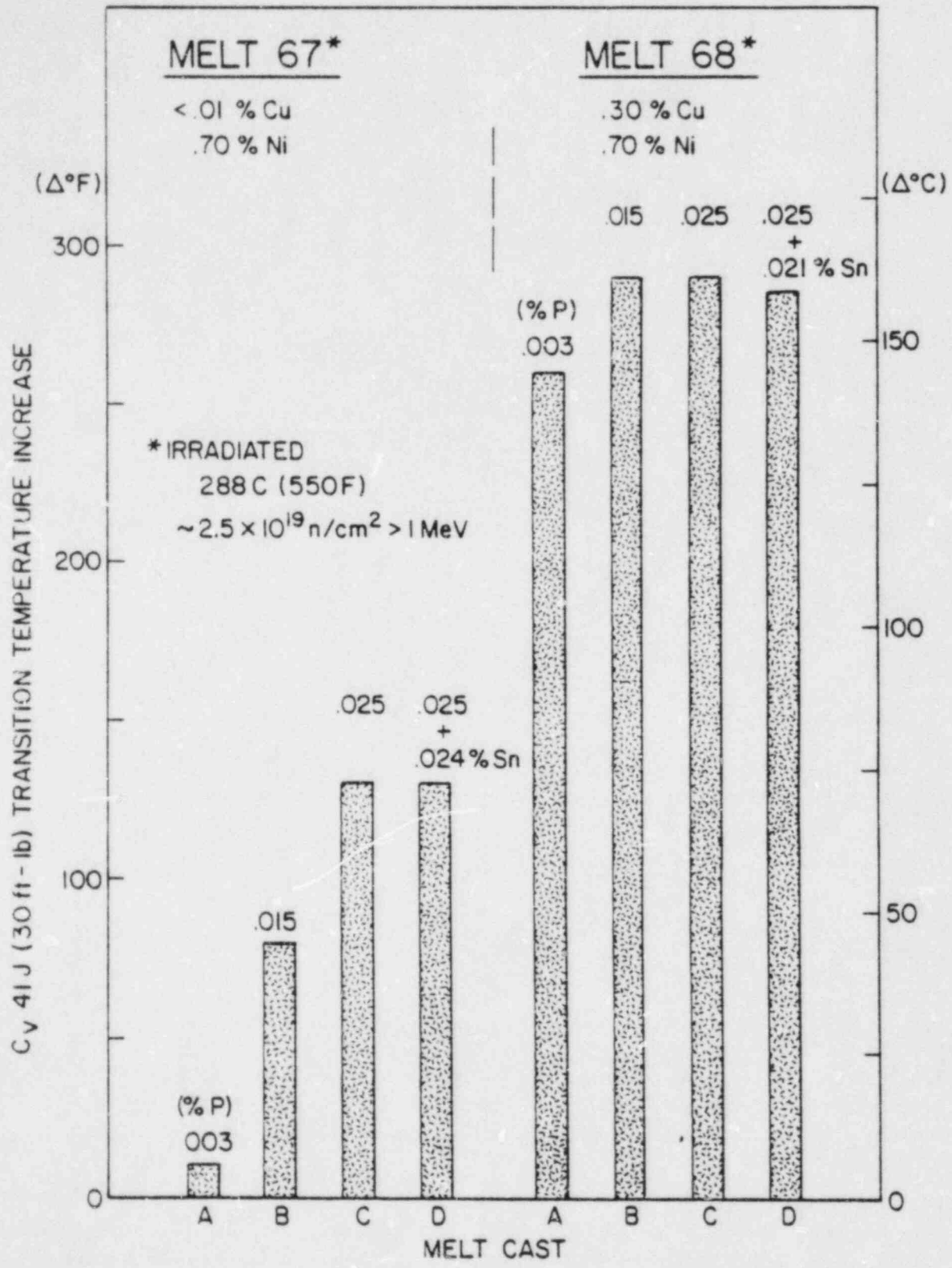

Figure 3.12 C_v 41 J transition temperature increases observed for plates from melts 67 and 68.

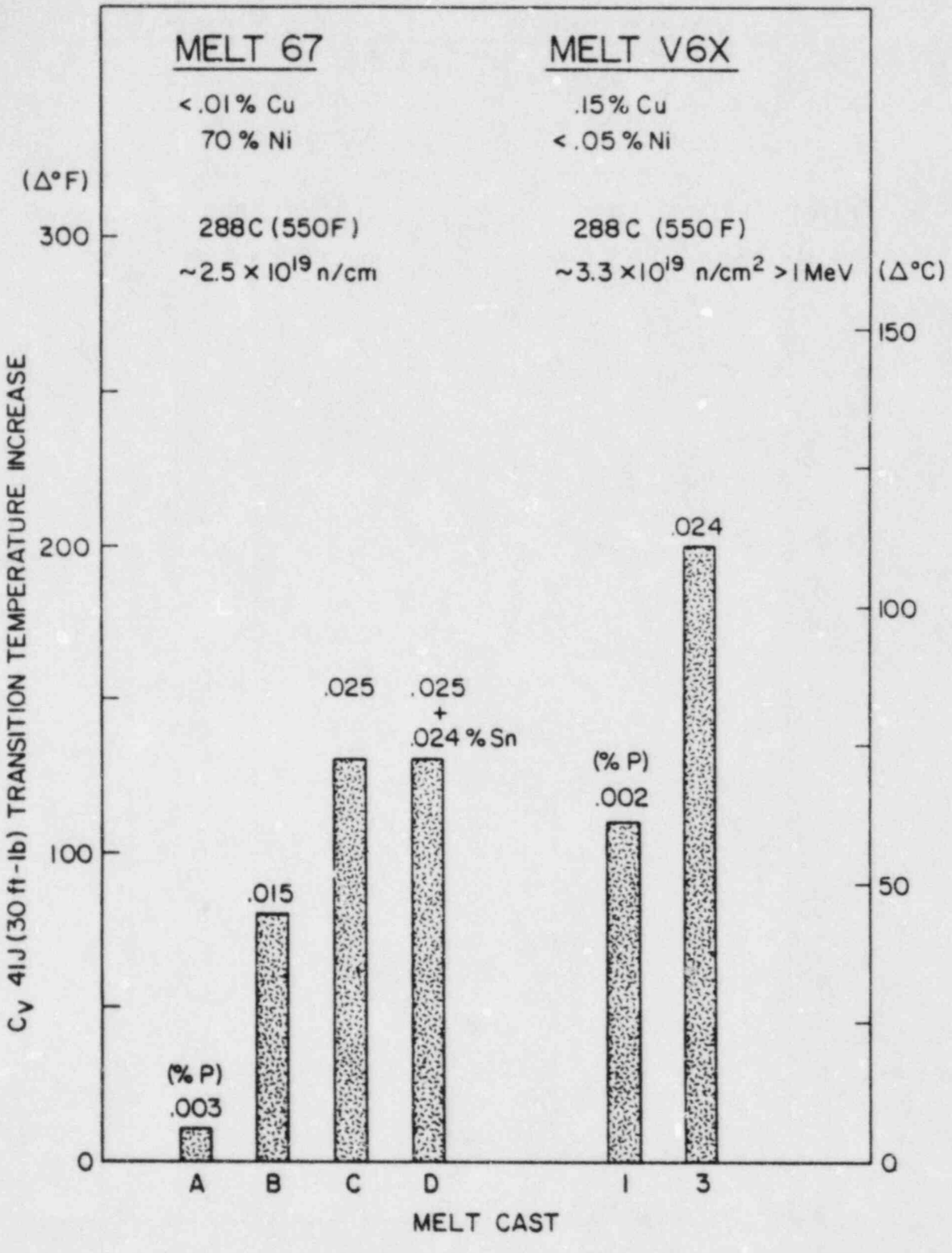

Figure 3.13 C_v 41 J transition temperature increases observed for plates from melt 67 (A 533-B steel) and plates from melt V6X (A 302-B steel).

the other hand, forgings having a high phosphorus content (0.016 to 0.018% P) showed significant embrittlement after 3.1×10^{19} n/cm^2 at 288°C. Of additional interest to the present study, tin contents on the order of 100 to 140 ppm appeared to reduce the level of the phosphorus contribution in NiCrMoV.

Postirradiation data developed for plates forming group 2 are reported in Table 3.5. Phosphorus contents of these plates are 0.016 or 0.018% P. Data for plate 69A vs. 69B indicate a small sensitizing effect of a 0.021% tin content. The effect is most evident in the respective upper shelf energy reduction values. The addition of 0.035% arsenic to the melts, on the other hand, produced no change in radiation resistance. Likewise, the 0.50% chromium addition to melt 72 did not change its apparent sensitivity level. Addition of copper to this melt, followed by nickel, did produce the expected effects. (The nickel addition made to melt 69 did not elevate radiation sensitivity because of the lower copper content.)

Companion data for plates comprising group 3 are expected in late 1984. The task is scheduled for completion in 1985.

3.3 Studies of Neutron Exposure Rate Effects on Reactor Vessel Steels

J. R. Hawthorne

3.3.1 Background

A series of closely controlled experiments has been undertaken to test the significance of high vs. low neutron exposure rates to the magnitude of radiation effects to pressure vessel steel properties, including notch ductility, fracture toughness and tensile properties. The experiments were undertaken to resolve the base question of the level of representation afforded by test reactor irradiation assessments of materials for the power reactor service case. The study was prompted by comparisons of data suggesting that differences in steel embrittlement levels and/or embrittlement trends can arise from neutron flux level effects, time-at-temperature effects, or from tendencies toward embrittlement saturation when flux levels are low and exposure times are years in duration.

The experimental approach involves the 288°C irradiation of four reference materials produced commercially (plates and weld deposits) under three flux conditions: $\sim 7\text{-}8 \times 10^{10}$, $4\text{-}5 \times 10^{11}$, and $7\text{-}8 \times 10^{12}$ n/cm^2-sec^{-1}. The two extremes of the exposure rates are considered representative of power vs. test reactor irradiation conditions. To obtain optimum control over irradiation temperature and fluence conditions, a water-cooled test reactor (UBR) was chosen for the irradiation vehicle. Three locations within the reactor provide the requisite flux levels: a location within the fuel core, a location at the core edge and a location away from the core in the reflector region (see Fig. 3.14). The plan is to obtain an exposure of 0.5×10^{19} n/cm^2 in each location and, in addition, fluence exposures of 1×10^{19} and 2×10^{19} in the core edge and in-core locations.

Table 3.5 Charpy-V Notch Ductility of Plates from Melts 69 and 72 Before and After 288°C Irradiation

Melt/ Plate[a]	Composition (Weight-%)					C_v 41 J Temperature						C_v USE		
						Preirrad.		Postirrad.		Change				
	Cu	Ni	Sn	As	Cr	°C	°F	°C	°F	Δ°C	Δ°F	Pre. J	Post. J	Change ΔJ
69A	0.19	0.30	-----[b]	-----[c]	----[b]	-15	5	79	175	94	170	157	122	35
69B	0.19	0.30	0.021	-----	----	-15	5	93	200	108	195	157	104	53
69C	0.19	0.70	0.021	-----	----	-12	10	96	205	108	195	155	106	49
69D	0.19	0.70	0.021	0.033	----	-12	10	102	215	114	205	145	103	42
72A	0.33	0.25	-----[b]	-----[c]	----[b]	-7	20	116	240	123	220	144	92	52
72B	0.33	0.71	-----	-----	----	-7	20	138	280	145	260	144	84	60
72C	0.33	0.71	-----	-----	0.50	-23	-10	118	245	141	255	145	85	60
72D	0.33	0.71	-----	0.035	0.50	-12	10	132	270	144	260	140	85	55

[a] 0.016 or 0.020% P
[b] < 0.004% Sn or Cr
[c] < 0.010% As

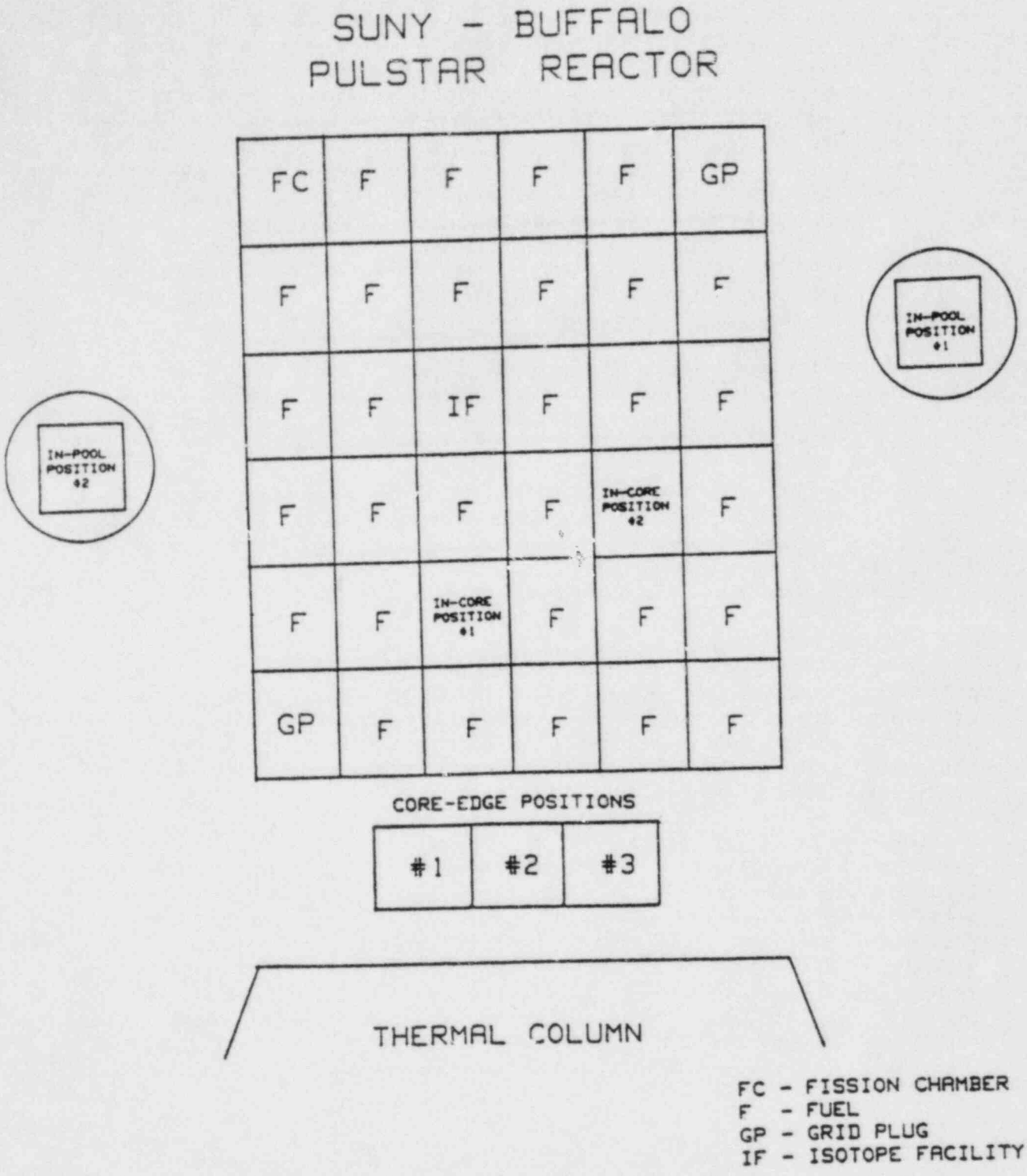

Figure 3.14 Schematic illustration of irradiation locations in the UBR chosen for exposure rate effects study.

3.3.2 Progress

Preparations for irradiation, including construction of the special core-edge and reflector region experiment holders and fabrication of instrumentation consoles were completed in early 1983. Ambient flux levels at preselected positions were qualified, using dummy irradiation capsules containing iron, nickel and cobalt-aluminum and silver-aluminum flux wires. A spectrum calculation, now available for the in-core locations, will be extended to out-of-core locations before completion of the capsule irradiation series. Additional flux verification tests, using fission detector sets, are also planned.

Early in 1983, the first of two planned irradiation assemblies was loaded into the reflector facility. Also, three assemblies representing the total complement for intermediate flux tests, were inserted into the core edge facilities. Irradiation exposures for all four assemblies were still in progress at year's end. The anticipated in-reactor residence time for the lowest flux experiment is 3.5 years. The exposure of one core-edge experiment was approximately 75% complete at the end of 1983.

Commencement of in-core irradiations (highest flux level) was not scheduled for 1983. In this case, the irradiations are to begin after the core-edge experiments are discharged and their fluences verified from internal dosimetry. Close matching of fluence conditions (in-core vs. core-edge) will be permitted in this manner.

The temperature control method employed for the core-edge capsules is the same as that used routinely by MEA for in-core experiments. The method involves double encapsulation of the specimen holder with thin stainless steel envelopes and pneumatic pressurization of the annulus. The variable gas gap thus formed can increase or decrease the gamma heating loss from the specimens on demand. No electrical resistance heaters are used with this control scheme.

Preliminary tests of gamma heating levels in the reflector region showed that a supplemental heat source would be required to obtain the irradiation temperature at this location. The final design for this position features a dry "standpipe" equipped with replaceable internal resistance heaters. The heaters are deenergized during periods of extended (days) reactor outages. Periodic rotation of the specimen capsule for fluence balancing is permitted by the overall design. At this writing, two capsule rotations on separate occasions have been performed (successfully). Construction of a second facility was undertaken, but was not completed in time for use in 1983.

3.4 Mechanical Properties Determinations for PSF Simulated Surveillance and Through-Wall Specimen Capsules

J. R. Hawthorne, B. H. Menke and A. L. Hiser

3.4.1 Background

One objective of the Light Water Reactor - Pressure Vessel (LWR-PV) Surveillance Dosimetry Improvement Program of the NRC is the development of key information for the accurate projection of radiation-induced mechanical properties changes in reactor vessel walls. The total effort represents a multilaboratory program with international participation. MEA was given responsibility for the development and analysis of mechanical properties data required for the study.

The projection of in-depth property changes occurring in service is not a simple, straightforward task because the neutron energy spectrum incident to a vessel is both modified and attenuated as it passes through the vessel wall. Aside from this, property change predictions require both an understanding of the damaging portion of the neutron energy spectrum and the trend of property degradation with total neutron exposure, i.e., fluence (n/cm^2). The correlation of property change with fluence is a nonlinear function and is highly influenced by steel metallurgy, especially composition. Therefore, the task of mechanical properties prediction reduces to three key components: proper and accurate definition of the neutron field, accurate projection of field attenuation and proper estimation of steel response to the local field.

A fourth consideration is the method of in-service monitoring. Vessel property changes typically are monitored using surveillance specimen irradiations internal to the vessel but outside of the fuel core. Extrapolation of spectrum conditions at surveillance capsules and the relationship of mechanical property change data obtained from surveillance specimens to locations inside the vessel wall are aspects of the problem addressed by the LWR-PVI Surveillance Dosimetry Improvement Program.

A pressure vessel mock-up facility was used by the program for through-wall neutron dosimetry investigations and through-wall neutron exposures of metallurgical specimens. These were to yield physics-dosimetry-metallurgy correlations for projecting in-wall properties. The facility, known as the Pool-Side Facility (PSF), is located at the Oak Ridge Research Reactor (ORR). It simulates a relatively large segment of a reactor thermal shield and vessel wall and permits irradiation of specimens in sealed capsules under closely controlled temperature conditions at simulated surveillance and through-wall locations (Fig. 3.15). The wall thickness is 22.5 cm; that of the shield is 5.9 cm. To date, five capsules have been irradiated at 288°C. Two (designated SSC-1 and SSC-2) represent surveillance capsules taken from a pressurized water reactor plant after about 15 years and 30 years of operation, i.e., at plant midlife and at plant end-of-life. The remaining three capsules (Wall 1, 2, 3) represent vessel surface (0T), quarter-wall thickness (1/4T) and half-wall

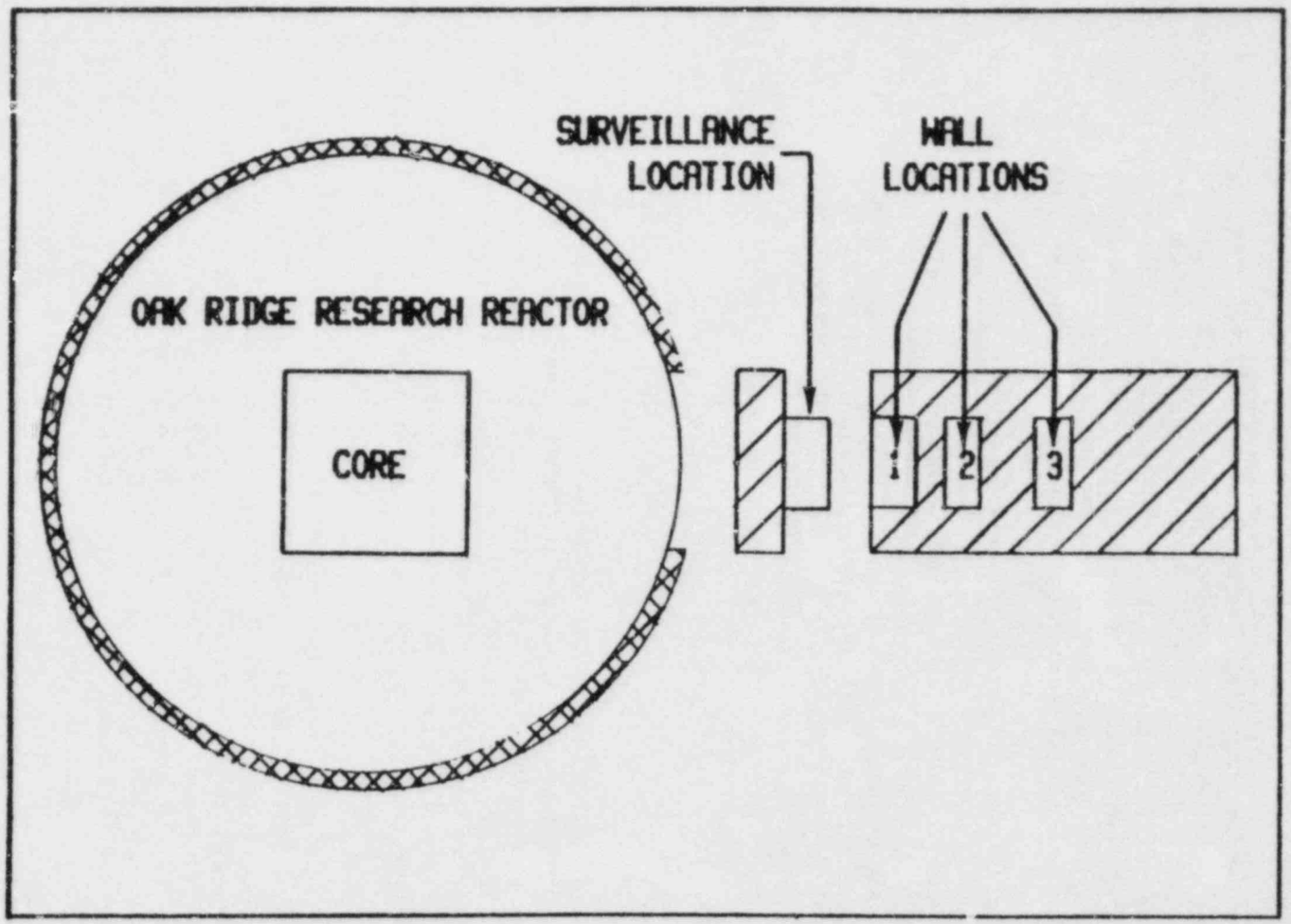

Figure 3.15 Schematic illustration of the PSF Facility showing the locations of the specimen capsules in simulated surveillance and through-wall irradiation locations.

thickness (1/2T) locations. Exposure periods and target fluences for the individual capsules are given in Table 3.6. The lead factor between surveillance and wall surface locations was about eight for the particular PSF configuration used. Additional details of the PSF facility and the bases for its particular design configuration can be found in the various annual reports of the program issued by the program manager, the Hanford Engineering Development Laboratory (HEDL) (Refs. 32, 33, 34).

Table 3.6 Capsule Irradiation Conditions

Capsule No.	PSF Location	Irradiation Time (Hours at Power)	MW Hours Exposure	Target Neutron Fluence (n/cm^2, E > 1 MeV)
SSC-1	Thermal Shield	1,291	32,000	3×10^{19}
SSC-2	Thermal Shield	2,845	64,700	$\sim 6 \times 10^{19}$
Wall-1	Simulator (Surface, 0T)	18,748	430,000*	$\sim 6 \times 10^{19}$
Wall-2	Simulator (Quarter T)	18,748	430,000	$\sim 3 \times 10^{19}$
Wall-3	Simulator (Half T)	18,748	430,000	$\sim 1.5 \times 10^{19}$

* Approximate

3.4.2 Materials

Six materials were selected for irradiation. These are identified by type, supplier, heat treatment condition and initial strength level in Table 3.7. Table 3.8 lists the material compositions. The A 302-B plate (code F23) has seen extensive use in reactor vessel surveillance applications and in test reactor studies. The A 533-B plate (code 3PS, 3PT or 3PU) was applied earlier as a reference material in the International Atomic Energy Agency's coordinated program on the behavior of advanced reactor pressure vessel steels under neutron irradiation. The respective plates are considered representative of early vessel manufacture and more recent vessel fabrication. The submerged-arc weld, code EC, also has been studied extensively. Accordingly, a significant amount of irradiation embrittlement data was on hand for at least three of the six materials at the beginning of the program.

In Table 3.7, it is noted that the materials differ considerably in their respective contents of copper and nickel and were expected to present broad differences in radiation embrittlement sensitivity.

Table 3.7 Materials

Material	Heat Code	Supplier	Thickness (mm)	Yield[a] Strength (MPa)	Heat Treatment
A 533-B (HSST Plate 03)	3PS, 3PT, 3PU	NRL	305	454	843 to 899°C - 4 h, water quenched 649 to 677°C - 4 h, air cooled 607 to 636°C - 20 h, furnace cooled
A 302-B (ASTM Reference Plate)	F23	NRL	152	482	899°C - 6 h, water quenched 649°C - 6 h, air cooled
Submerged-Arc Weld (Single Vee type, A 533-B Base Plate)	R	Rolls Royce & Assoc., Ltd.	160	489	920°C ± 15°C - 6 h, water spray quenched 600°C - 6 h, air cooled 600°C - 36 h, air cooled 650°C - 6 h, air cooled
Submerged-Arc Weld (Single Vee type, A 533-B Base Plate)	EC	EPRI	235	456	621°C ± 28°C - 50 h, furnace cooled
22NiMoCr37 Forging	K	KFA	295	407	Not reported to MEA or ORNL
A 508-3 Forging	MO	MOL	238	462	900-955°C - 12.8 h, air cooled 630-665°C - 14 h, furnace cooled 610°C ± 10°C - 24 h, furnace cooled

[a] Ambient temperature strength

Table 3.8 Chemical Compositions (Wt-%)

Material	Code	C	Si	Mn	P	S	Cr	Mo	Ni	Al	Cu	Sn	Ti	V
A 533-B (HSST Plate 03)	3PS, 3PT, 3PU	0.20	0.25	1.26	0.011	0.018	0.10	0.45	0.56	----	0.12	-----	-----	-----
A 302-B (ASTM Ref. Plate)	F23	0.24	0.23	1.34	0.011	0.023	0.11	0.51	0.18	0.04	0.20	0.037	0.015	0.001
A 533-B S/A Weld	R	0.05	0.45	1.54	0.009	0.008	0.12	0.34	1.58	0.01	0.23	0.006	0.003	0.01
A 533-B S/A Weld	EC	0.11	0.52	1.57	0.007	0.011	0.02	0.48	0.64	0.008	0.24	0.004	<0.01	0.005
22NiMoCr37 Forging	K	0.18	0.16	0.72	0.009	0.004	0.45	0.63	0.96	0.031	0.12	-----	----	-----
A 508-3	MO	0.20	0.28	1.43	0.008	0.008	----	0.53	0.75	0.031	0.05	-----	----	<0.01

Phosphorus content differences, on the other hand, are small; accordingly, this element could not be a factor in materials variability.

Standard Charpy-V (C_v) and 4.52-mm diameter tension (T) specimens were used for making notch ductility and tensile strength determinations for all six materials. In addition, 0.5T-CT and 1T-CT compact tension specimens were taken from the two reference plates (A 302-B and A 533-B) for fracture toughness studies. A typical capsule loading is shown in Fig. 3.16. Samples from the A 533-B plate and the 22NiMoCr37 forging were oriented for transverse (TL, weak) direction testing; those of the A 302-B plate and the A 508-3 forging were oriented for longitudinal (LT, strong) direction tests. Weld metal specimens were taken with the long axis spanning the width of the weld joint.

3.4.3 Fracture Toughness Testing

A program objective was to obtain E 399 valid K_{Ic} data wherever possible. Due to the relatively small specimen sizes, valid data could be expected only at the very low toughness end of the transition region. A modified single specimen compliance (SSC) test procedure was therefore used. To meet E 399 requirements for tests in the transition temperature region, no unloadings of the specimen were made until the load-deflection record violated E 399 requirements, i.e., exceeded the 5% secant line by a factor of 1.1. After reaching this point, the test was completed using the normal SSC technique. Test records were first analyzed for K_{Ic} validity according to E 399 procedures. Then, analysis by the MEA procedure for J_{Ic} was performed. Only a few tests produced valid K_{Ic} results. For the remainder, an initiation toughness, termed K_{Jc}, was computed from J_{Ic} as follows:

$$K_{Jc} = [EJ_{Ic}/ (1-\gamma^2)]^{1/2} \qquad (1)$$

where γ is Poisson's ratio, taken to be 0.3. All J_{Ic} values were valid by ASTM E 813; however, values of K_{Jc} computed from the equation were not interpreted as K_{Ic}. Instead, an estimate of K_{Ic} was obtained by means of the "β_{Ic} correction" attributed to Irwin (Ref. 14).

3.4.4 Fluence Determinations

Capsule construction, irradiation and disassembly operations were conducted by the ORNL for the NRC. Primary responsibility for neutron dosimetry and fluence determinations is shared by ORNL and HEDL. Fluences given in this report are tentative values subject to confirmation by these laboratories.

It should be noted that the exposure time of capsule SSC-1 was adjusted to provide a fluence matching that of Wall-2 capsule which was in the quarter-wall thickness position. Similarly, the exposure time of capsule SSC-2 was adjusted to match its fluence against that of the Wall-1 capsule located at the wall inner surface. The Wall-1, Wall-2

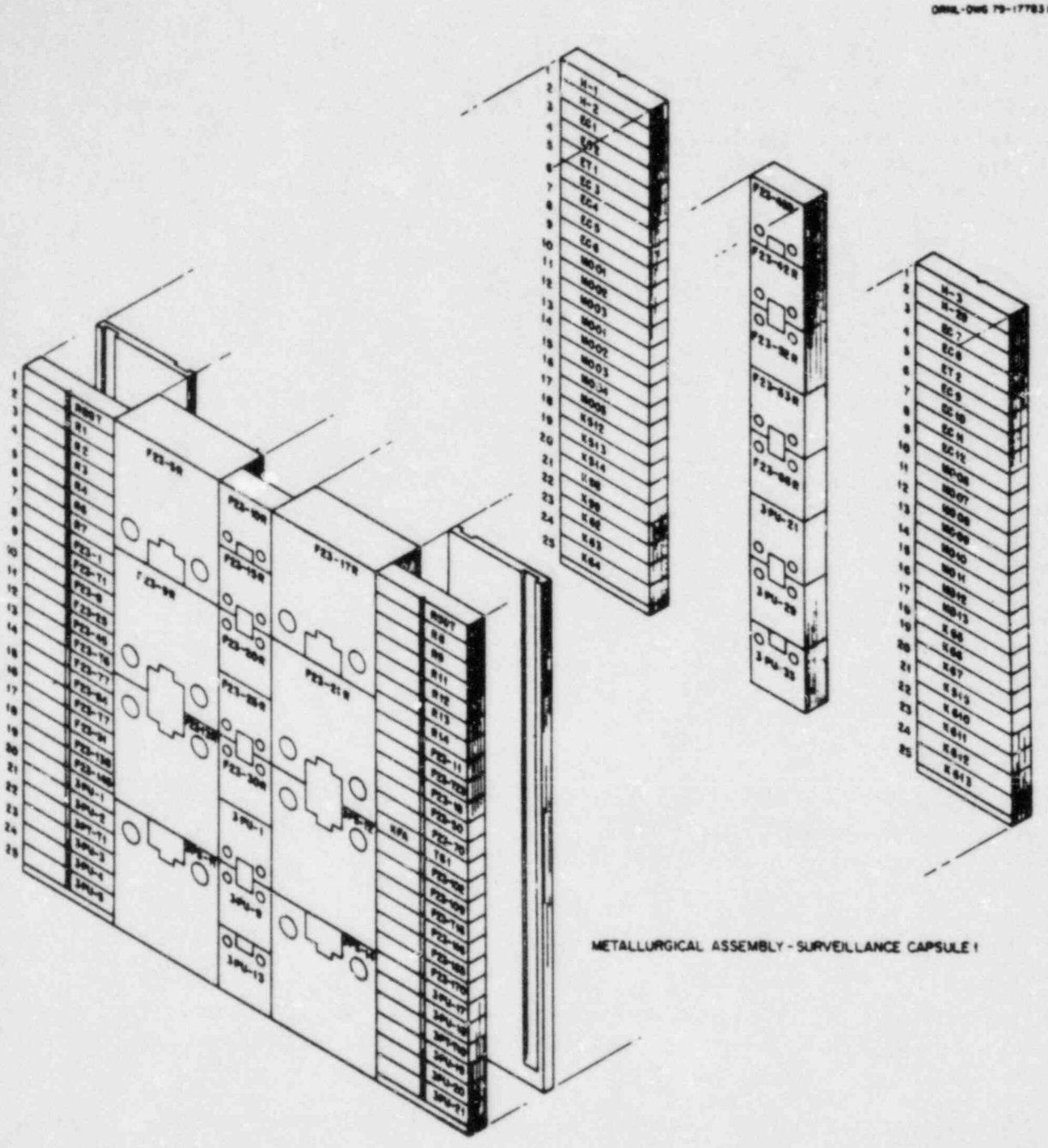

Figure 3.16 C_V, CT and tension test specimen locations in the simulated surveillance capsule SSC-1 (courtesy ORNL). Tension test specimens are identified by the letter T in the specimen number.

and Wall-3 capsules were irradiated simultaneously and were exposed for the same time period. In turn, the spread in fluences between these capsules accurately reflects normal flux attenuation conditions through a vessel thickness.

3.4.5 Experimental Results

A full discussion of the experimental results obtained by MEA would far exceed allowable space limitations here. Accordingly, only key observations are summarized using a data table (Table 3.9) and data summary figures (Figs. 3.17 to 3.22). The reader is referred to References 35 and 36 for complete information and detailed analyses of the experimental results.

Primary conclusions and observations drawn from the C_v and tensile test results for the materials, except for code R, were as follows:

1. The surveillance capsule data indicated reasonably well the irradiation effect to the wall surface and quarter-wall thickness locations (Fig. 3.17). With one exception, the C_v surveillance results proved conservative where significant (> 10°C) differences were observed; predictions of the 41 J transition temperature were within 20°C. The exception pertains to capsule SSC-1 results for the forging code K which underpredict the in-wall transition temperature elevation by 17°C.

2. The in-wall toughness gradient produced by irradiation, indexed to the transition temperature, was small (Table 3.9, Fig. 3.17). The difference in 41 J temperature between wall surface and midthickness locations ranged between 31°C (A 302-B plate) and 11°C (forging code M0). The average difference for all materials, including the weld code R, was 25°C.

3. In parallel with (2), the doubling of fluence to the materials produced only a small, additional 41 J temperature elevation in the surveillance capsule irradiations (SSC-2 vs. SSC-1).

4. The postirradiation 41 J temperature elevation was in close agreement with the 68 J and 0.89 mm transition temperature elevations (within 14°C in most cases).

5. Irradiation sensitivity levels of the materials are in accord with initial predictions based on material copper and nickel contents (Fig. 3.18).

6. Tensile test findings support the notch ductility trend determinations (Fig. 3.19).

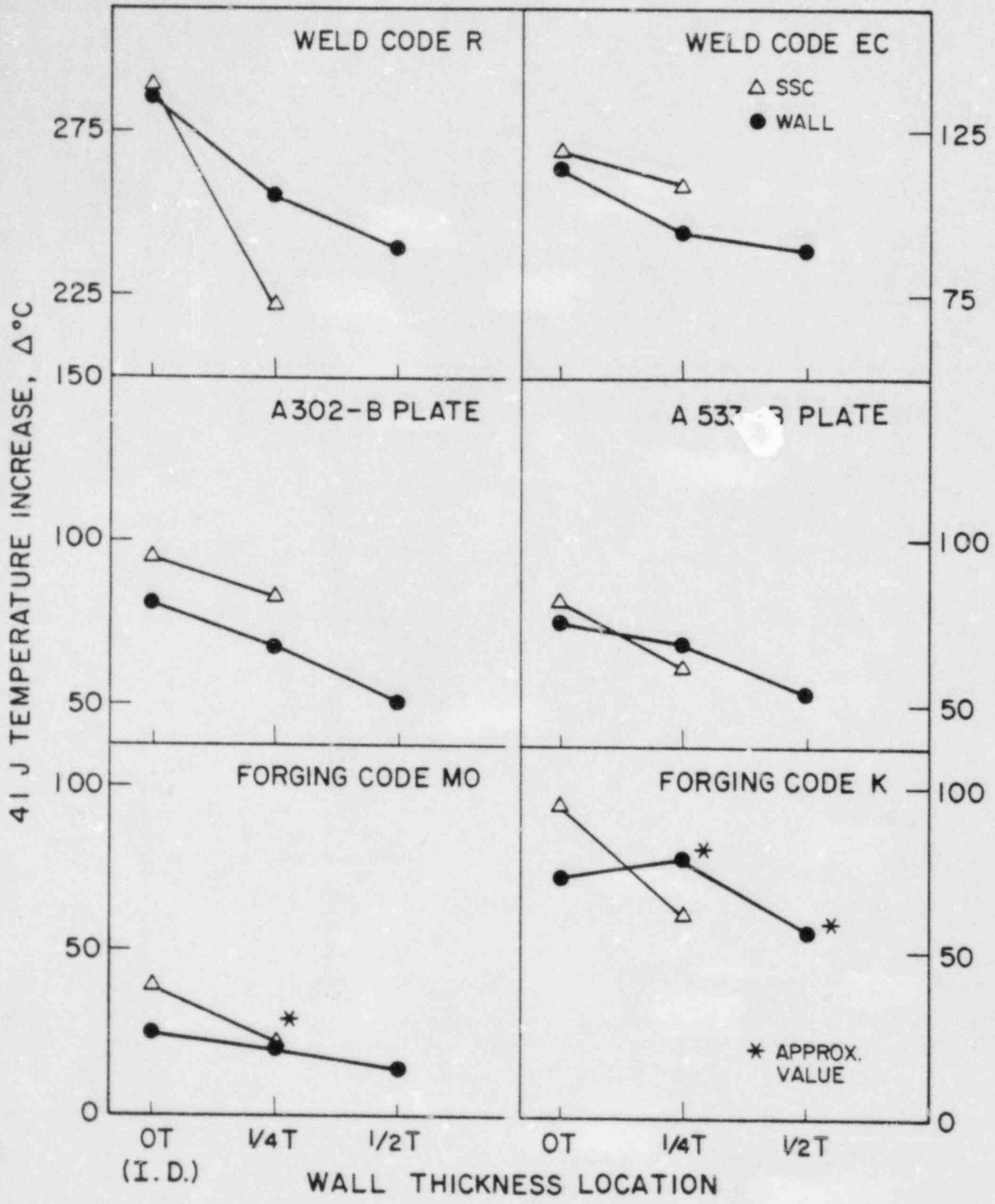

Figure 3.17 Comparison of C_v data from simulated surveillance capsules vs. in-wall capsules (open triangle vs. filled circle points). With two exceptions, the surveillance capsule data either predict well or overpredict the transition temperature elevation for the wall location.

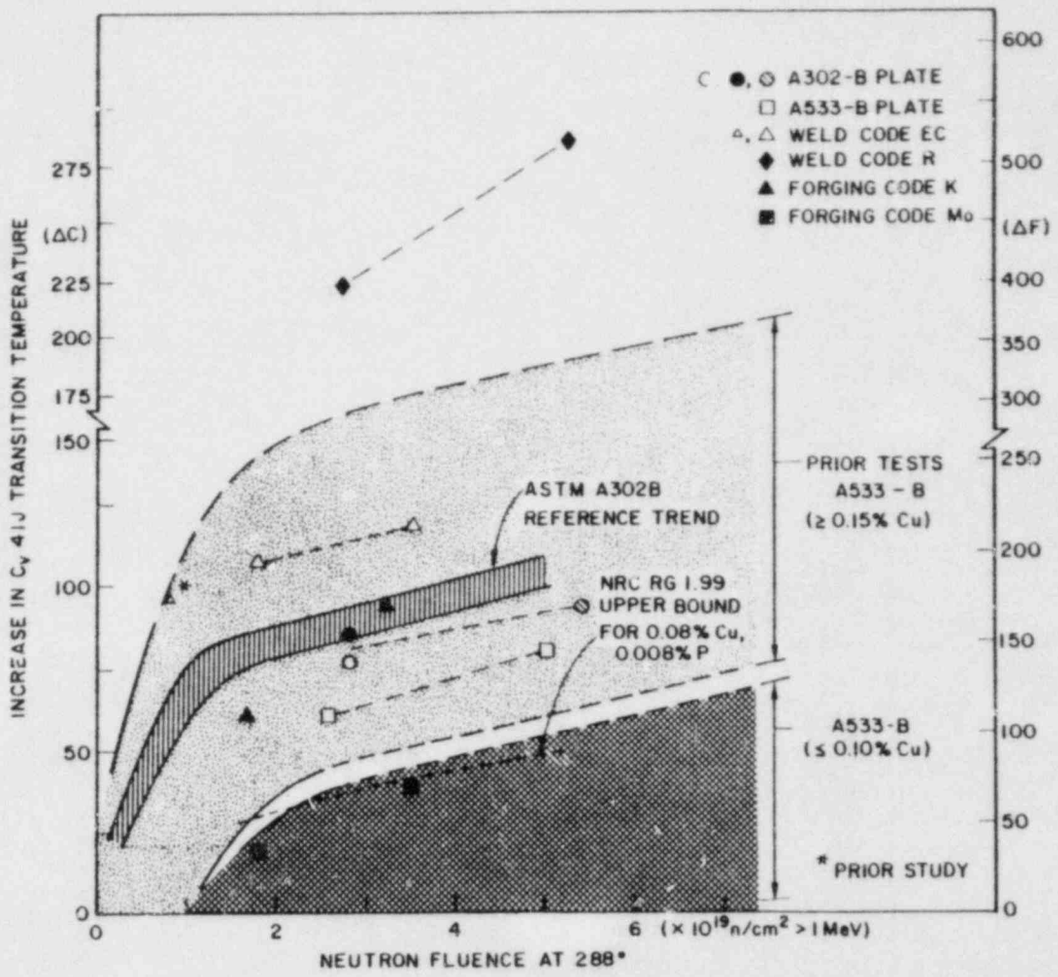

Figure 3.18 Data from the capsules SSC-1 and SSC-2 compared against trends of C_v 41 J transition temperature change with irradiation observed with in-core, test reactor experiments. The trend band, marked ASTM A 302-B Reference Trend was established with several independent experiments using code F23 material; good agreement at both fluence levels is indicated. Observations for the remaining five materials show good agreement with projections based on % Cu (and % Ni) content.

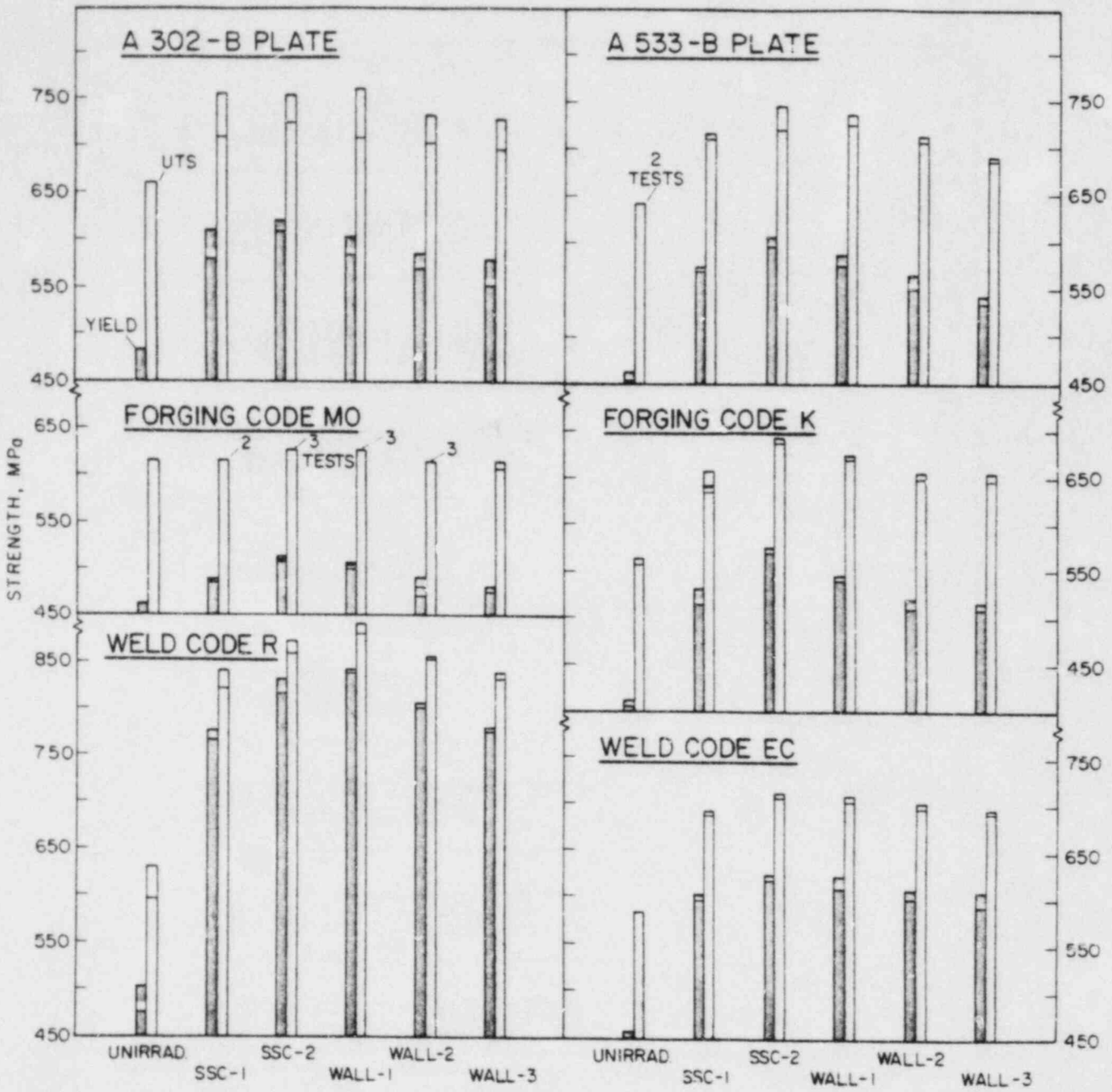

Figure 3.19 Variation in tensile properties of the materials between irradiation capsules for ambient temperature tests.

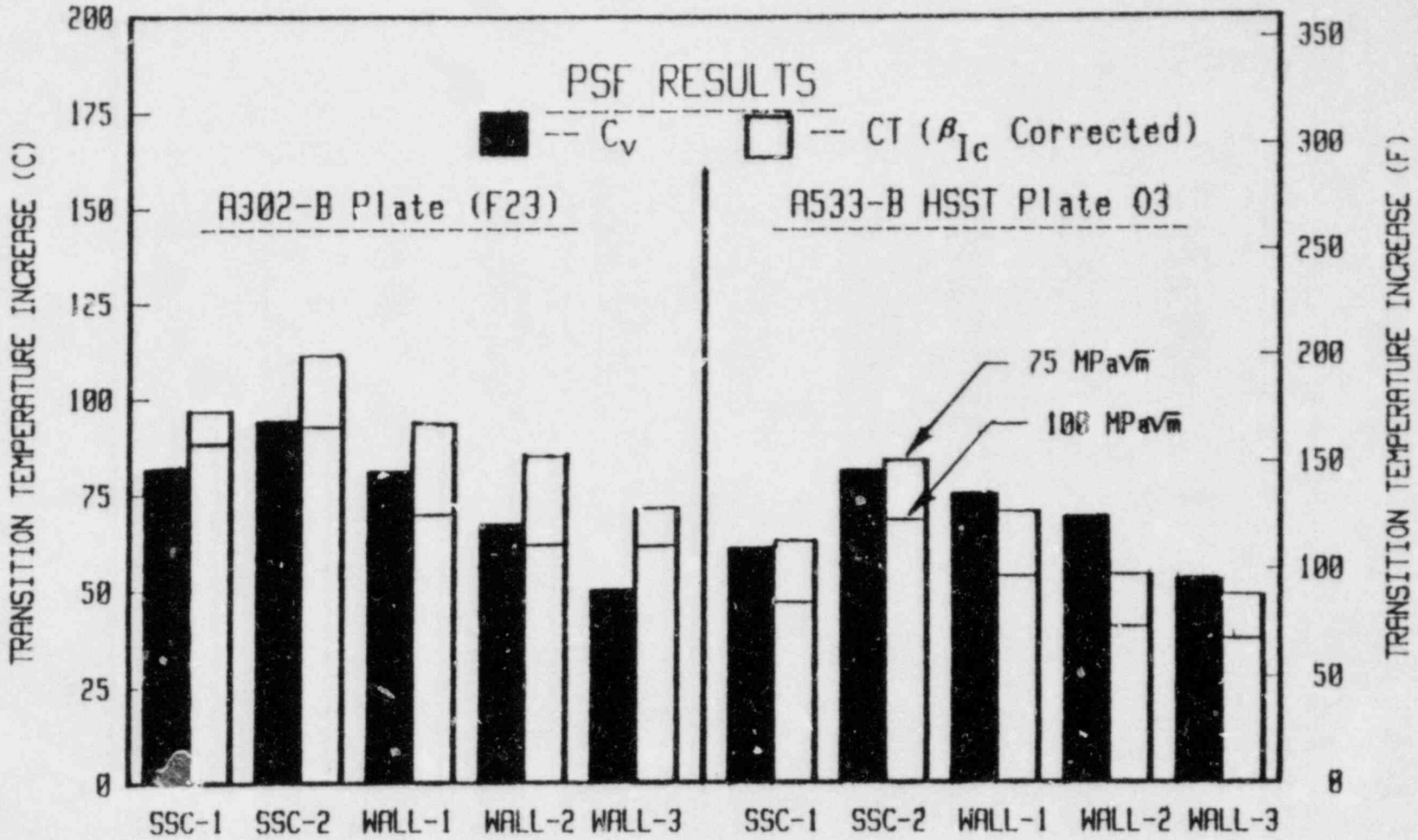

Figure 3.20 Comparison of 41 J (C_v) and $K_{\beta c}$ (CT) transition temperature elevations.

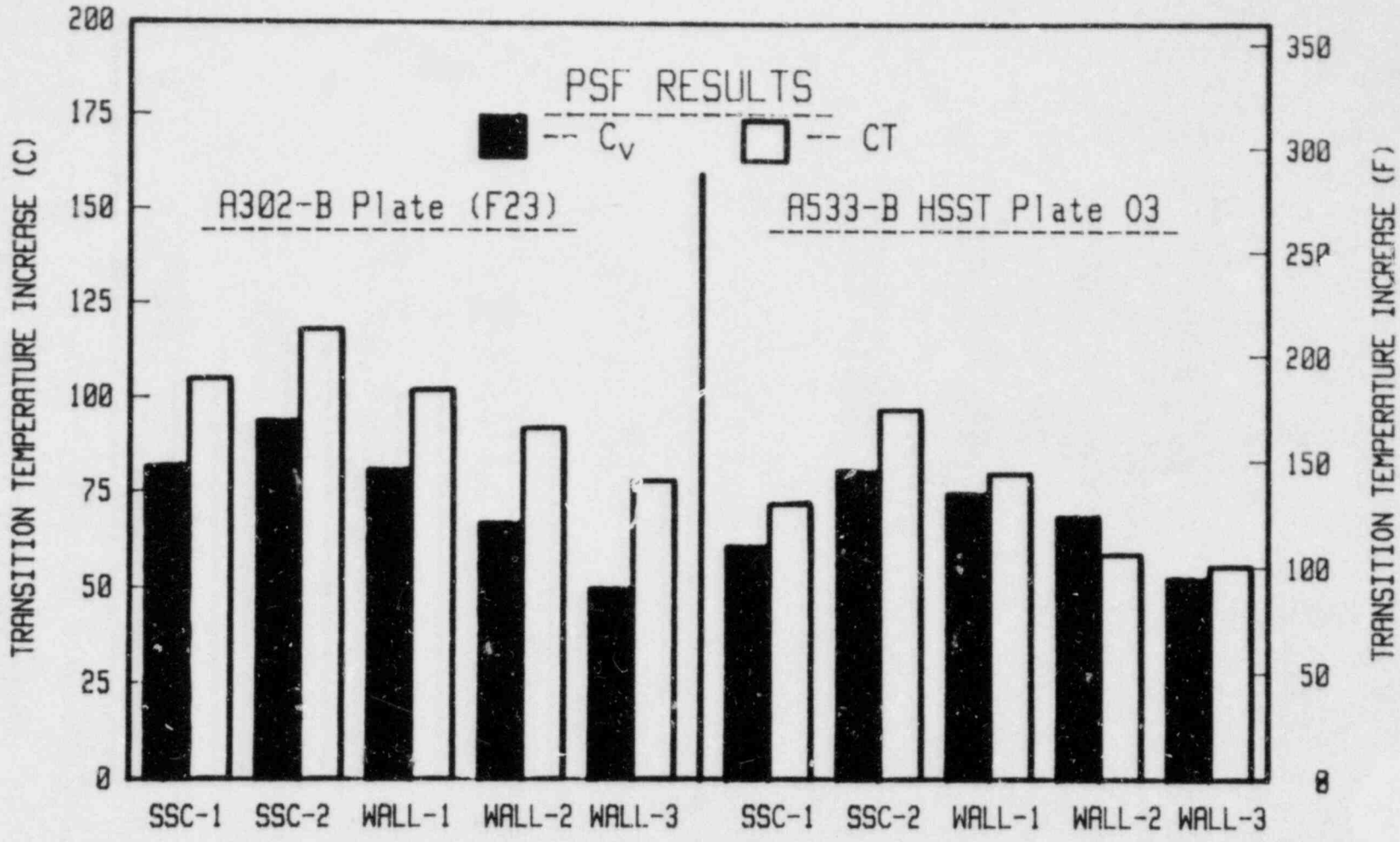

Figure 3.21 Comparison of 41 J (C_v) and 100 MPa$\sqrt{m}$ (CT) transition temperature elevations (before βc correction).

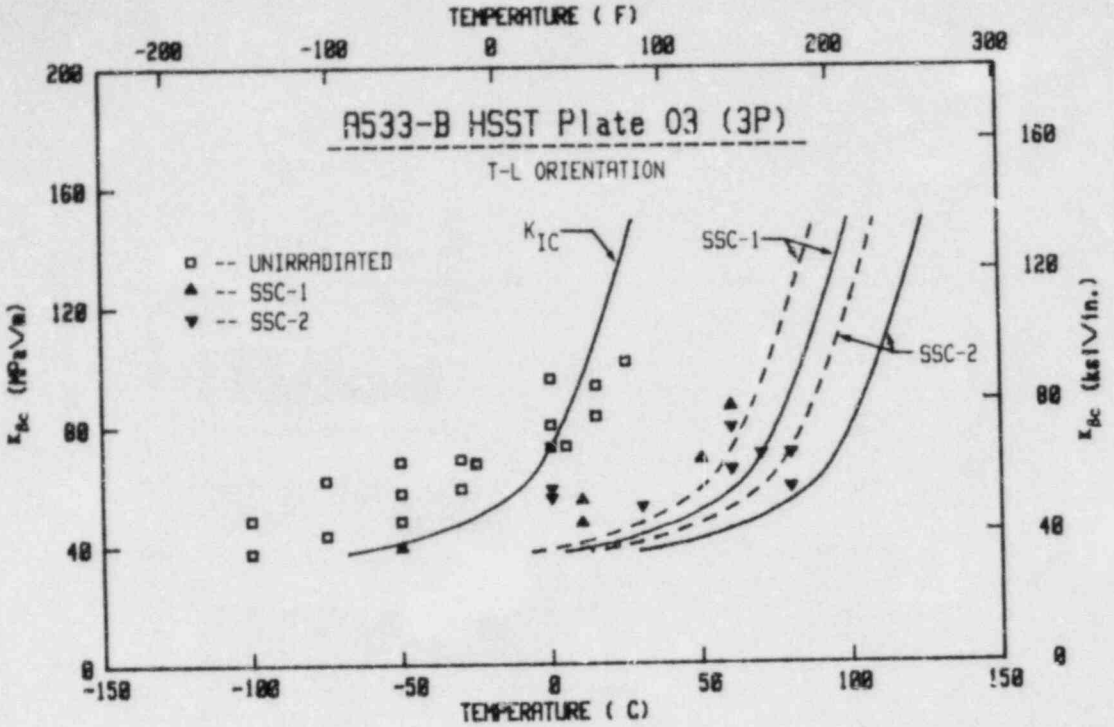

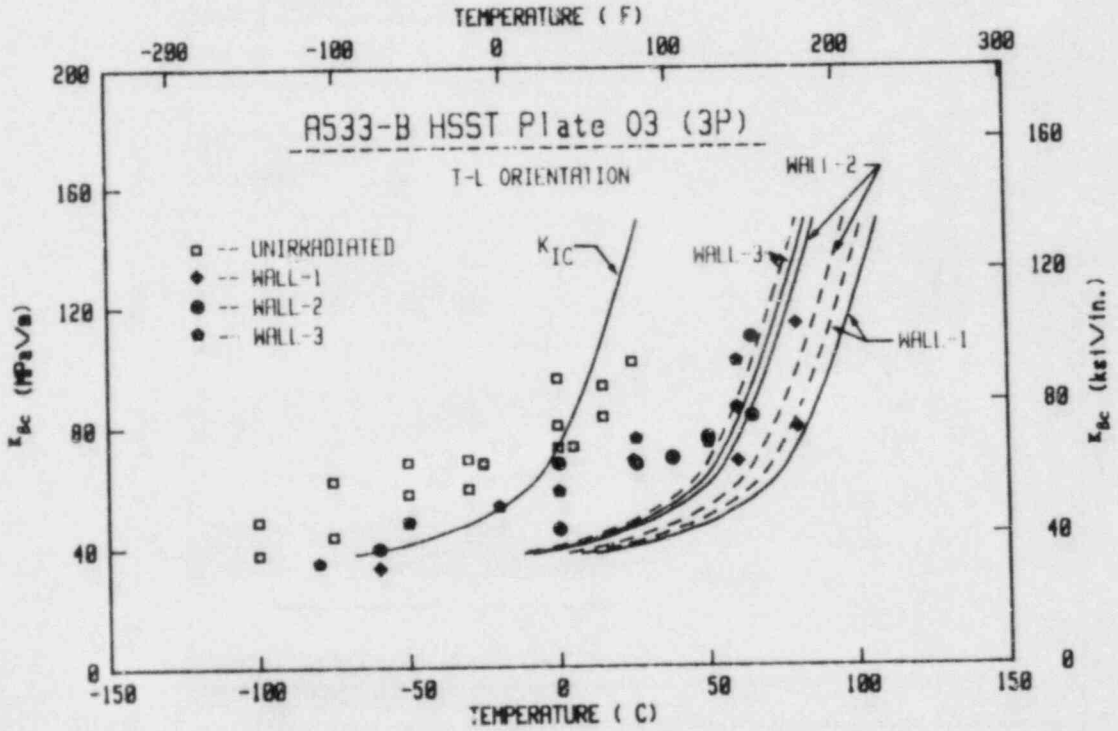

Figure 3.22 $K_{\beta c}$ data for the A 533-B reference plate. The ASME K_{Ic} curve for the irradiated condition has been shifted by amounts equal to that of Charpy (41 J, dashed lines) and compact (K_{Jc}, 100 MPa$\sqrt{m}$, solid lines) specimen data from the various capsules.

Table 3.9 Observations on 41 J Temperature Increase for Capsules Wall-1 and Wall-3

Material	41 J Temperature Increase, Δ°C		
	Capsule Wall-1 (A)	Capsule Wall-3 (B)	Difference, °C (A-B)
A 302-B Plate (Code F23)	81	50	31
A 533-B Plate (Codes 3PT, 3PU)	75	53	22
Forging (Code K)	72	~ 56	~ 16
Forging (Code MO)	25	14	11
Weld (Code EC)	114	89	25
Weld (Code R)	286	239	47

Additional observations pertaining to the weld code R and the A 302-B plate were:

7. High radiation embrittlement sensitivity was characteristic of the weld code R which contained 0.23% Cu and 1.58% Ni (Table 3.14, Fig. 3.18). The unusually high level of sensitivity suggests contributions by two or more embrittlement mechanisms, in addition to the normal irradiation effect. An independent contribution of Ni to radiation sensitivity development and a time-at-temperature effect are currently suspect.

8. Capsule SSC-1 results for weld code R significantly underpredicted in-wall behavior. A time-at-temperature effect would explain this finding.

9. The postirradiation 41 J temperature elevation for the weld code R underpredicted the 68 J and 0.89 mm transition temperature elevations by as much as 36°C. Differences were due to a pronounced modification of the shape of the brittle/ductile transition curve by irradiation.

10. Postirradiation C_v data for the A 302-B plate exhibited an anomalous difference traceable to specimen thickness location in the original plate. The anomaly was most evident in the upper shelf temperature regime and with data from capsule SSC-1. Good properties uniformity was observed in preirradiation (reference) condition data, however.

Primary conclusions and observations drawn from fracture toughness tests of the A 302-B and A 533-B reference plates were:

11. The surveillance capsule CT specimen test results indicated reasonably well the irradiation effects to wall surface and quarter-wall thickness locations (Figs. 3.20 and 3.21). Likewise, the in-wall toughness gradient produced by irradiation, indexed to the (measured) K_{Jc} 100 MPa$\sqrt{m}$ temperature, was small (24°C, both materials).

12. Adjustment of the ASME Section III, Appendix G, toughness curve by the radiation-induced elevation of the C_v 41 J temperature was conservative when compared against experimentally derived, $K_{\beta c}$ data.

13. Adjustment of the ASME Section XI, Appendix A, lower bound K_{Ic} toughness curve for A 533-B steel by the 41 J and 100 MPa$\sqrt{m}$ temperature elevations, proved unconservative in some cases when compared against experimentally derived $K_{\beta c}$ data for the A 533-B reference plate (Fig. 3.22). The maximum disparity, however, was only 15°C.

14. The $K_{\beta c}$ elevations tended to be less than the 41 J temperature elevation. The $K_{\beta c}$ 100 MPa$\sqrt{m}$ temperature elevations were ~ 23°C less than the K_{Jc} elevations at that same level (Fig. 3.20 vs. Fig. 3.21).

15. Results for the 0.5T-CT and 1T-CT specimens did not show a significant effect of specimen size on the temperature location of the toughness transition.

REFERENCES

1. R. E. Johnson, ed., "Resolution of Reactor Vessel Materials Toughness Issue, Task Action Plan A-11," USNRC Report NUREG/CR-0744, Sept. 1981.

2. P. C. Paris, H. Tada, A. Zahoor and H. A. Ernst, "The Theory of Instability of the Tearing Mode of Elastic-Plastic Crack Growth," in Elastic-Plastic Fracture, ASTM STP 668, American Society for Testing and Materials, Mar. 1979, pp. 5-36.

3. A. L. Hiser, F. J. Loss and B. H. Menke, "J-R Curve Characterization of Irradiated Low Upper Shelf Welds," USNRC Report NUREG/CR-3506, April 1984.

4. P. Albrecht, et al., "Tentative Test Procedure for Determining the Plane Strain J_I-R Curve," Journal of Testing and Evaluation, Vol. 10, No. 6, Nov. 1982, pp. 245-251.

5. A. L. Hiser and F. J. Loss, "Alternative Procedures for J-R Curve Determination," USNRC Report NUREG/CR-3402, July 1983.

6. J. R. Hawthorne, et al, "Evaluation and Prediction of Neutron Embrittlement in Reactor Pressure Vessel Materials," EPRI NP-2782, Electric Power Research Institute, Dec. 1982.

7. A. L. Hiser and D. B. Fishman, "J-R Curve Data Base Analysis of Reactor Pressure Vessel Steels," Electric Power Research Institute, Palo Alto, Calif., to be published.

8. H. A. Ernst, "Material Resistance and Instability Beyond J-Controlled Growth," Scientific Paper 81-107-JINTF-P6, Westinghouse R&D Center, Dec. 3, 1981.

9. C. A. Baldwin, "Neutron Spectral Characterization Calculations for the 4th Nuclear Regulatory Heavy Section Steel Technology 1T-CT Irradiation Experiments," USNRC Report NUREG/CR-3311, ORNL/TM-8782, Oak Ridge National Laboratory, June 1983.

10. F. W. Stallman, et al., "Neutron Spectral Characterization Calculations of the 4th Nuclear Regulatory Commission Heavy Section Steel Technology 1T-CT Irradiation Experiments: Dosimetry and Uncertainty Analysis," USNRC Report NUREG/CR-3333, ORNL/TM-8798, Oak Ridge National Laboratory, June 1983.

11. "Structural Integrity of Water Reactor Pressure Boundary Components, Quarterly Progress Report for the Period April-June 1979," F. J. Loss, ed., USNRC Report NUREG/CR-0943, NRL Memorandum Report 4064, Naval Research Laboratory, 28 Sept. 1979.

12. "Structural Integrity of Water Reactor Pressure Boundary Components, Annual Report, Fiscal Year 1979," F. J. Loss, ed., USNRC Report NUREG/CR-1128, NRL Memorandum Report 4122, Naval Research Laboratory, 30 Sept. 1979.

13. R. G. Berggren, et al., "An Analysis of Charpy V-Notch Impact Toughness of Irradiated A 533 Grade B Class 1 Plate and Four Submerged-Arc Welds," presented at the 12th International Symposium on the Effects of Radiation on Materials, Williamsburg, VA, 18 June 1984.

14. G. R. Irwin, "Fracture Mode Transition for a Crack Transversing a Plate," Journal of Basic Engineering, Vol. 82(2), 1960, pp. 417-425.

15. J. G. Merkle, "An Examination of the Size Effects of Data Scatter Observed in Small Specimen Cleavage Fracture Toughness Testing," USNRC Report NUREG/CR-3672, ORNL/TM-9088, Oak Ridge National Laboratory, April 1984.

16. W. H. Cullen, et al., "The Temperature Dependence of Fatigue Crack Growth Rates of A 351-CF8A Cast Stainless Steel in LWR Environment", USNRC Report NUREG/CR-3546, April 1984.

17. W. H. Cullen, K. Torronen and M. Kemppainen, "Effects of Temperature on Crack Growth of A 508-2 Steel in LWR Environment, USNRC Report NUREG/CR-3230, April 1983.

18. J. D. Atkinson, S. T. Cole and J. E. Forrest, "Corrosion Fatigue Mechanisms in Ferritic Pressure Vessel Steels Exposed to Simulated PWR Environments," Vol. 2, Proceedings of Specialists Meeting on Subcritical Growth, 13-15 May, 1981, International Atomic Energy Agency, USNRC Proceeding NUREG/CP-0044, May 1983, pp. 173-197.

19. W. H. Cullen, et al., "The Temperature Dependence and Environmental Enhancement Mechanism of Fatigue Crack Growth Rates of A 351-CF8A Cast Stainless Steel in LWR Environment," in Proceedings of Specialists' Meeting on Corrosion and Stress Corrosion of Steel Pressure Boundary Components and Steam Turbines, 22-24 November 1983, International Atomic Energy Agency, 1984, pp. 165-194.

20. W. H. Cullen, "Fatigue Crack Growth Rates of Low-Carbon and Stainless Piping Steels in LWR Environments," to be published as a USNRC Report.

21. W. H. Cullen, "Characterization of Environmentally-Assisted Crack Growth in LWR Materials," in Structural Integrity of Water Reactor Pressure Boundary Components -- Annual Report for 1982, USNRC Report NUREG/CR-3228, April 1983.

22. T. V. Venkatasubramanian and T. J. Baker, "Role of Elongated MnS Inclusions in Hydrogen Embrittlement of High-Strength Steels," Metal Science, Vol. 16, 1982, pp. 543-554.

23. K. Torronen and M. Kemppainen, "Fractography and Mechanisms of Environmentally Enhanced Fatigue Crack Propagation of a Reactor Pressure Vessel Steel," in Corrosion Fatigue: Mechanics, Metallurgy, Electrochemistry and Engineering, ASTM STP 801, 1983, pp. 287-318.

24. J. R. Hawthorne, H. E. Watson and F. J. Loss, "Experimental Investigation of Multicycle Irradiation and Annealing Effects on Notch Ductility of A 533-B Weld Deposits," in Effects of Radiation on Materials: Tenth Conference, ASTM STP 725, American Society for Testing and Materials, 1981, pp. 63-75.

25. F. J. Loss, B. H. Menke, R. A. Gray, Jr., J. R. Hawthorne and H. E. Watson, "J-R Curve Characterization of A 533-B Weld Metal with Irradiation and Postirradiation Annealing," in Effects of Radiation on Materials: Tenth Conference, ASTM STP 725, American Society for Testing and Materials, 1981, pp. 76-91.

26. J. R. Hawthorne, "Exploratory Assessment of Postirradiation Heat Treatment Variables in Notch Ductility Recovery of A 533-B Steel," USNRC Report NUREG/CR-3229, April 1983.

27. J. R. Hawthorne, "Significance of Nickel and Copper Content to Radiation Sensitivity and Postirradiation Heat Treatment Recovery of Reactor Vessel Steels, USNRC Report NUREG/CR-2948, Nov. 1982.

28. U. S. Nuclear Regulatory Commission, Regulatory Guide 1.99, Rev. 2, "Effects of Residual Elements on Predicted Radiation Damage to Reactor Vessel Materials" (in preparation).

29. F. A. Smidt, Jr., and J. A. Sprague, "Property Changes Resulting from Impurity-Defect Interactions in Iron and Pressure Vessel Steel Alloys," in Effects of Radiation on Substructure and Mechanical Properties of Metals and Alloys, ASTM STP 529, American Society for Testing and Materials, 1973, pp. 78-91.

30. "Structural Integrity of Water Reactor Pressure Boundary Components, Annual Report for 1982," USNRC Report NUREG/CR-3228, April 1983.

31. J. R. Hawthorne, "Contributions of Selected Residual Elements to the Radiation Embrittlement Resistance of Steel Forgings," NRL Report 7526, Jan. 18, 1973.

32. W. N. McElroy, et al., "LWR Pressure Vessel Surveillance Dosimetry Improvement Program -- 1980 Annual Report," USNRC Report NUREG/CR-1747, Hanford Engineering Development Laboratory Report HEDL-TME 80-73, 1981.

33. W. N. McElroy, et al., "LWR Pressure Vessel Surveillance Dosimetry Improvement Program -- 1981 Annual Report," USNRC Report NUREG/CR-0029, Hanford Engineering Development Laboratory Report HEDL-SA-2546, 1982.

34. W. N. McElroy, et al., "LWR Pressure Vessel Surveillance Dosimetry Improvement Program — 1982 Annual Report," USNRC Report NUREG/CR-2805, Vol. 3, Hanford Engineering Development Laboratory Report HEDL-TME 82-20, Jan. 1983.

35. J. R. Hawthorne, B. H. Menke and A. L. Hiser, "Light Water Reactor Pressure Vessel Surveillance Dosimetry Improvement Program: Notch Ductility and Fracture Toughness Degradation of A 302-B and A 533-B Reference Plates from PSF Simulated Surveillance and Through-Wall Irradiation Capsules," USNRC Report NUREG/CR-3295, Vol. 1, April 1984.

36. J. R. Hawthorne and B. H. Menke, "Light Water Reactor Pressure Vessel Surveillance Dosimetry Improvement Program: Postirradiation Notch Ductility and Tensile Strength Determinations for PSF Simulated Surveillance and Through-Wall Specimen Capsules," USNRC Report NUREG/CR-3295, Vol. 2, April 1984.

NRC FORM 335 (11-81)

U.S. NUCLEAR REGULATORY COMMISSION

BIBLIOGRAPHIC DATA SHEET

1. REPORT NUMBER (Assigned by DDC)
NUREG/CR-3228 Vol. 2
MEA-2051

4. TITLE AND SUBTITLE (Add Volume No., if appropriate)
Structural Integrity of Water Reactor Pressure Boundary Components
Annual Report for 1983

2. (Leave blank)

3. RECIPIENT'S ACCESSION NO.

7. AUTHOR(S)

5. DATE REPORT COMPLETED
MONTH: August | YEAR: 1984

9. PERFORMING ORGANIZATION NAME AND MAILING ADDRESS (Include Zip Code)
Materials Engineering Associates, Inc.
9700-B George Palmer Highway
Lanham, Maryland 20706

DATE REPORT ISSUED
MONTH: September | YEAR: 1984

6. (Leave blank)

8. (Leave blank)

12. SPONSORING ORGANIZATION NAME AND MAILING ADDRESS (Include Zip Code)
Division of Engineering Technology
Office of Nuclear Regulatory Research
U. S. Nuclear Regulatory Commission
Washington, D. C. 20555

10. PROJECT/TASK/WORK UNIT NO.

11. FIN NO.
B3900

13. TYPE OF REPORT
Technical Report

PERIOD COVERED (Inclusive dates)
1 January - 31 December 1983

15. SUPPLEMENTARY NOTES

14. (Leave blank)

16. ABSTRACT (200 words or less)

The objective of this research program is to characterize materials behavior in relation to structural safety and reliability of pressure boundary components for light water reactors. Specific objectives include developing an understanding of elastic-plastic fracture and environmentally-assisted crack propagation phenomena in terms of continuum mechanics, metallurgical variables, and neutron irradiation. Emphasis is placed on identifying metallurgical factors responsible for radiation embrittlement of steels and on developing procedures for embrittlement relief, including guidelines for radiation-resistant steels. The underlying goal is the interpretation of material properties performance to establish engineering criteria for structural reliability and long-term operation. Current work is organized into three major tasks: (1) fracture mechanics investigations, (2) environmentally-assisted crack growth in high temperature, primary reactor water and (3) radiation sensitivity and postirradiation properties recovery. Research progress in these tasks for 1983 is summarized here.

17. KEY WORDS AND DOCUMENT ANALYSIS

17a. DESCRIPTORS

J Integral - R Curve; Low Upper Shelf; Elastic-Plastic Fracture; Nuclear Pressure Vessel Steels; Corrosion Fatigue; Stress Corrosion Cracking; Piping Steels; Load Ratio Effects; A 533-B Steel; Postirradiation Heat Treatment; Radiation Embrittlement; Notch Ductility; Embrittlement Relief; Annealing; Temperature Effects; Orientation Effects

17b. IDENTIFIERS/OPEN-ENDED TERMS

18. AVAILABILITY STATEMENT
Unlimited

19. SECURITY CLASS (This report)
Unclassified

21. NO. OF PAGES

20. SECURITY CLASS (This page)
Unclassified

22. PRICE
$